UNIVERSITÀ DEGLI STUDI DI MILANO

Facoltà di Scienze del Farmaco

Dipartimento di Scienze Farmacologiche e Biomolecolari

PhD program in

EXPERIMENTAL MEDICINE AND MEDICAL BIOTECHNOLOGY

PhD cohort XXX

(MED/04, MED/05, MED/13)

DEVELOPMENT AND PATHOPHYSIOLOGICAL CHARACTERIZATION OF AN IN VIVO MODEL OF IRON OVERLOAD ASSOCIATED TO INSULIN RESISTANCE AND REPRODUCTIVE IMPAIRMENT

PhD student

Dr. Chiara MACCHI

R11039 – R22

Internal supervisor:

Dr. Paolo MAGNI

Coordinator PhD program

Prof. Massimo LOCATI

Academic Year: 2016/2017

INDEX

1. LIST OF ABBREVIATIONS

AAS, atomic absorption spectrometry

ACTH, adrenocorticotropic hormone

aPV, anterior periventricular nucleus

AR, androgen receptor

ARC, arcuate nucleus

AREs, androgen response elements

BBB, blood-brain barrier

BBM, brush-border membrane

BLM, basolateral membrane

BTB, blood-testis barrier

CHOP, CAAT/enhancer binding protein (C/EBP) homologous protein

CLAMS, comprehensive laboratory animal monitoring system

CNS, central nervous system

CPS count per second

CTR, control

DCYTB, duodenal cytochrome b

DEXA, dual-energy X-ray absorptiometry

DFO, Deferoxamine

DIOS, dysmetabolic iron overload syndrome

DMH, dorsomedial hypothalamus

DMT1, divalent metal-ion transporter 1

ELISA, enzyme-linked immunosorbent assay

EMA, European Medicines Agency

ER, endoplasmic reticulum

ERK, extracellular signal-regulated kinase

FAC, ferric ammonium citrate

FBXL5, F-box and leucine rich repeat protein 5

FDA, Food and Drug Administration

FOXO1, forkhead box protein O1

FPN, ferroportin

FSH, follicle-stimulating hormone

Ft, ferritin

FtMt, mitoferritin

GH, growth hormone

Glut4, glucose transporter 4

GnRH, gonadotropin-releasing hormone

GPR54, G protein-coupled receptor 54

hCG, human chorionic gonadotropin

HCP1, heme carrier protein 1

HCV, hepatitis C virus

HFE, hemochromatosis protein

HH, hypogonadotropic hypogonadism

HJV, hemojuvelin

HOMA-IR, Homeostatic Model Assessment of Insulin Resistance

HPG axis, hypothalamic-pituitary-gonadal axis

IED, iron-enriched diet

IL6, interleukin 6

IR, insulin resistance

IREs, iron responsive elements

IRPs, iron regulatory proteins

JAK, janus kinase

JH, juvenile hemochromatosis

KISS1, kisspeptin

KNDy neurons, kisspeptin/neurokinin B/dynorphin neurons

LH, luteinizing hormone

LHRH, luteinizing hormone-releasing hormone

LIC, liver iron concentration

LIP, labile iron pool

MBH, mediobasal hypothalamus

ME, median eminence

MEK 1/2, mitogen-activated protein (MAP) kinase/ extracellular signal-regulated kinase 1/2

MetS, metabolic syndrome

MRI, magnetic resonance imaging

NAFLD, nonalcoholic fatty liver disease

NPY, neuropeptide Y

NTBI, non-transferrin bound iron

POA, preoptic area

POMC, pro-opiomelanocortin

PRL, prolactin

PVN, paraventricular nucleus

RIA, radioimmunoassay

ROS, reactive oxygen species

SCN, suprachiasmatic nucleus

SD, standard deviation

SEM, standard error of the mean

SHBG, sex hormone binding globulin

SOCS3, suppressor of cytokine signaling-3

SOD, superoxide dismutase

SON, supraoptic nucleus

SQUID, superconducting quantum interference device

StAR, steroidogenic acute regulatory

STAT3, signal transducer and activator of transcription 3

STEAP3, six-transmembrane epithelial antigen of prostate

T2DM, type 2 diabetes mellitus

T, testosterone

Tf, transferrin

TfR, transferrin receptor

TNFα, tumor necrosis factor α

TSH, thyroid stimulating hormone

UPR, unfolded protein response

UROD, uroporphyrinogen decarboxylase

UTRs, untranslated regions

VMH, ventromedial hypothalamus

XBP-1, X-box binding protein-1

2. ABSTRACT

Introduction. Iron is an essential micronutrient required for fundamental biochemical activities, such as oxygen and energy metabolism, mitochondrial function and brain development. However, it may catalyze the formation of highly reactive hydroxyl radicals, leading to oxidative stress, lipid peroxidation, and DNA damage with, finally, cell and tissue damages. Given its potential high toxicity, a condition of iron overload can promote multiple organ damages, associated to acute and chronic diseases. Among the several complications associated with iron overload syndromes, hypogonadism is the second most common endocrinopathy although the role of iron in its pathophysiology is still debated.

Aim. To explore in a dysmetabolic murine model, the molecular determinants of hypogonadism induced by iron overload, with a specific focus on hypothalamic derangement.

Material and methods. Male C57BL/6J mice fed standard iron concentration diet or iron-enriched diet (IED, 3% carbonyl-iron) and $HFE^{-/-}$ mice, these last resembling a murine model of human genetic hemochromatosis; cell-based models of gonadotropin-releasing hormone (GnRH) neurons (GN-11 and GT1-7 cell lines); radioimmunoassay (RIA); enzyme-linked immunosorbent assay (ELISA); histological analysis and immunostaining; image processing and quantitation; atomic absorption spectrometry; ATPlite^{TM} 1step assay; Trypan Blue exclusion test; qRT-PCR; Boyden's chamber assay; Western blot analysis.

Results*. In vivo models.* IED led to a hypogonadal phenotype as shown by micro- and macroscopic alterations at the testicular level. Iron accumulation in testes and pituitary significantly reduced serum levels of testosterone (-83%) and luteinizing hormone (-86%). Although, hypothalamic iron concentration did not differ in mice fed IED compared to controls, a significant increment in GnRH gene expression (+34%) and in intensity of GnRH-neuron innervation of the median eminence (+1.5-fold) were found; similar changes were obtained in $HFE^{-/-}$ mice. Hypothalamic gene expression of tumor necrosis factor α was increased in IED mice.

Moreover, a series of metabolic impairments, such as (i) increment in glycemia and Homeostatic Model Assessment of Insulin Resistance (HOMA-IR) index and (ii) reduction in body weight and fat as well as in plasma leptin was found upon IED.

In vitro models. Treatment of GN-11 and GT1-7 cells with ferric ammonium citrate, as a source of iron, significantly increased its intracellular concentration; as such, the genes involved in iron

homeostasis were changed: transferrin receptor, -75%; ferritin H, +92%. Furthermore, GN-11 cell chemomigration was inhibited by iron overload with an apparent involvement of the extracellular signal-regulated kinase (ERK) 1/2 cell signaling pathway. Finally, iron overload induced oxidative stress in GN-11 cells.

Conclusions. In adult male mice, iron overload leads to a severe impairment of the hypothalamic-pituitary-gonadal axis possibly resulting in a hypogonadal condition, a feature possibly deriving from iron deposition in pituitary and/or gonads via extrahypothalamic mechanisms. This finding represents a further step in understanding how iron overload leads to this endocrinopathy. In this context, the use of *in vitro* GnRH neurons, which functions were impaired by iron accumulation, leaves open questions relative to the role of brain blood barrier in the protection of the central region (hypothalamus).

3. INTRODUCTION

3.1 IRON

3.1.1 IRON PHYSIOLOGY

Iron is an essential micronutrient required for fundamental biochemical activities, such as oxygen and energy metabolism, mitochondrial function, brain development and function. In vertebrates, iron acts as an essential co-factor for many proteins and enzymes involved in central cellular processes such as respiration, metabolite biosynthesis, DNA synthesis and repair, protein synthesis, ribosome biogenesis, and oxygen transport [1]. The human body contains ~3–5 g of iron and most of them are present as heme protein complexes. These latter are involved in numerous biological functions, like oxygen binding and transport. This family includes hemoglobin of erythroid cells, which accounts for more than 2 g of iron, and myoglobin of muscles, containing ~300 mg of iron [2]. In hemoglobin, iron is stabilized in the Fe^{2+} oxidation state and directly binds and releases oxygen in circulating erythrocytes. Also in myoglobin, a protein responsible for oxygen storage and transport from erythrocytes to muscle cellular mitochondria, iron is present in the ferrous state. Other hemeproteins, containing smaller amounts of iron, are involved in oxygen metabolism (catalases, peroxidases), cellular respiration and electron transport (cytochromes). Iron can also be found in non-heme proteins, such as transferrin (Tf, protein that transports iron throughout the body), and ferritin (Ft, intracellular iron storage protein). In these forms, iron plays a role in fundamental cellular processes such as DNA synthesis and repair (ribonucleotide reductase), cell proliferation and differentiation, gene regulation, drug metabolism, and steroid synthesis [2, 3].

3.1.2 IRON TOXICITY

From a chemical point of view, iron is the 26^{th} element of the periodic table with a molecular weight of 55.85. It is a *d*-block transition metal and it can assume several oxidation states. The most common species are the divalent ferrous (Fe^{2+}) and the trivalent ferric (Fe^{3+}) iron, by which it takes part in oxidation/reduction reactions. This chemical property of iron, underling its ability to donate and accept electrons is essential for this metal functions. However, the highly reactive “free” iron reacts with reactive oxygen species (ROS), physiologically produced during aerobic respiration and enzymatic reactions, leading to the generation of hydroxyl radicals

(Fenton chemistry). These, in turn, trigger oxidative stress, lipid peroxidation, and DNA damage with the final result of cell and tissue damage, making iron a highly toxic metal.

$Fe^{3+} + O_2^{\cdot -} \rightarrow Fe^{2+} + O_2$

$Fe^{2+} + H_2O_2 \rightarrow Fe^{3+} + OH^- + OH^{\cdot}$

Fenton reaction

The highly reactive “free” iron, in particular, represents a minor fraction of the total cellular iron (~3–5%) and it constitutes the labile iron pool (LIP), which includes both Fe^{2+} and Fe^{3+}. The metal within the LIP is thought to be in steady state equilibrium and is proposed to bind different low molecular weight chelates, such as organic anions (phosphates, citrates, carboxylates) and poly-functional ligands (polypeptides, siderophores) [2].

3.1.3 IRON METABOLISM

In healthy individuals, the total amount of body iron is maintained within the range of 4-5 g by a strict control of its absorption, mobilization, storage and recycling.

3.1.3.1 Bioavailability

It is important to highlight that iron stores are not directly related to the capacity of the small intestine to absorb the metal, because the amount of bioavailable iron is often the limiting factor [4].

Dietary iron bioavailability is high from refined Western diets, which contain meat, poultry, fish, abundant sources of ascorbic acid and low amount of phytic acid from whole grains and legumes and are associated to limited drinking of coffee and tea with meals. Dietary heme, in particular, has a higher bioavailability compared with non-heme iron in the predominantly alkaline conditions found in the lumen of the small intestine [5].

Heme iron absorption is efficient and largely uninfluenced by other dietary constituents. Conversely, nonheme (and largely ferric) iron, found in both meat and plant foods, is highly insoluble, and its bioavailability is influenced by many dietary components. Among them, factors commonly found in plants, such as phytate, oxalate, polyphenols, and tannins are able to decrease its absorption. Moreover, the chronic use of proton pump inhibitors for gastric acid reflux, Helicobacter pylori infection, and inflammatory conditions (e.g., celiac disease) also

decrease nonheme iron absorption. In fact, gastric acid and ascorbic acid promote reduction and solubilization of dietary ferric iron, thus making the absorption more efficient [3, 4].

3.1.3.2 Absorption

Due to its toxicity, the metabolic balance of iron is tightly controlled, mediating the absorption of sufficient amounts of the metal, essential for physiological functions, but avoiding an excessive accumulation that can be hazardous for cells and tissues. Since, unlike most essential nutrients, no active excretory mechanisms exist for iron in humans, the balance of this metal is controlled almost exclusively by absorption [6].

In adults, the iron stock is about 3 g in men and 2.5 g in women. A regular diet contains 6 mg of iron per 1,000 calories. In normal conditions, around 10% of iron is absorbed (~1 mg/die) at the duodenal level. This amount can increase in particular conditions, like during pregnancy, breastfeeding, anemias, in response to tissue hypoxia or when erythropoiesis is stimulated [4].

As above stated, dietary iron is present as heme and non-heme forms. Heme iron is predominantly derived from hemoglobin and myoglobin in meats. In the duodenum, the uptake of luminal heme occurs as a metalloporphyrin. It is degraded by the enzyme heme oxygenase to yield ferrous iron which then enters into enterocytes, along with iron absorbed as inorganic (*i.e.*, non-heme) iron. The heme carrier protein 1 (HCP1) has been suggested to be a potential candidate to transport intestinal heme. Thus, iron exits the enterocyte via the basolateral transporter ferroportin-1 (FPN1) [7, 8].

Relative to the non-heme iron, it exists predominantly in the ferric form, which must be reduced before being transported into duodenal enterocytes. This process occurs at the brush-border membrane (BBM), where a ferric reductase, the duodenal cytochrome b (DCYTB), reduces iron to Fe^{2+}. Interestingly, DCYTB facilitates the reduction of ferric iron via electron transfer from intracellular ascorbate, providing one potential mechanism by which vitamin C enhances iron absorption. DCYTB is strongly upregulated in duodenal enterocytes during iron deficiency and acute hypoxia [4]. Subsequent to reduction of dietary ferric iron, ferrous iron is transported across the BBM of enterocytes into the mucosal cell, via divalent metal-ion transporter 1 (DMT1; encoded by the *SLC11A2* gene). DMT1 is a transmembrane protein mediating proton-coupled and ferrous iron uptake; it is so called because it DMT1 transports other divalent cations, including manganese and cobalt [4].

After ferrous iron is transported across the BBM into enterocytes, it is likely chelated by small molecular weight organic acids (*e.g.*, citrate), amino acids, or intracellular proteins. When body iron demand is low, iron can be stored in Ft, an intracellular iron storage protein complex consisting of heavy (H) and light (L) chain subunits forming a hollow sphere accepting up to 4,500 iron atoms. L-Ft is predominant in iron storing tissues, whereas H-Ft is preferentially expressed in cells that take up and release iron rapidly [2]. Given the role of iron in ROS formation, induction of Ft synthesis is induced not only by iron but also by oxidative stress conditions. Most of the iron stored in Ft is likely lost via subsequent exfoliation of intestinal epithelial cells.

Ferrous iron exits enterocytes crossing the basolateral membrane (BLM) via FPN1-mediated transport. FPN1 (encoded by the *SLC40A1* gene) is the only ferrous iron export protein identified to date in mammals. Subsequently, iron can be transported throughout the body bound to the protein Tf. Notably, Tf requires iron to be in the ferric form. Therefore, exported Fe^{2+} is rapidly oxidized to Fe^{3+} by a membrane-anchored, multicopper-containing ferroxidases (hephaestin) to be taken up by apotransferrin (free Tf) and distributed via the circulation throughout the body as Fe-Tf complexes [4, 8] [Fig. 1].

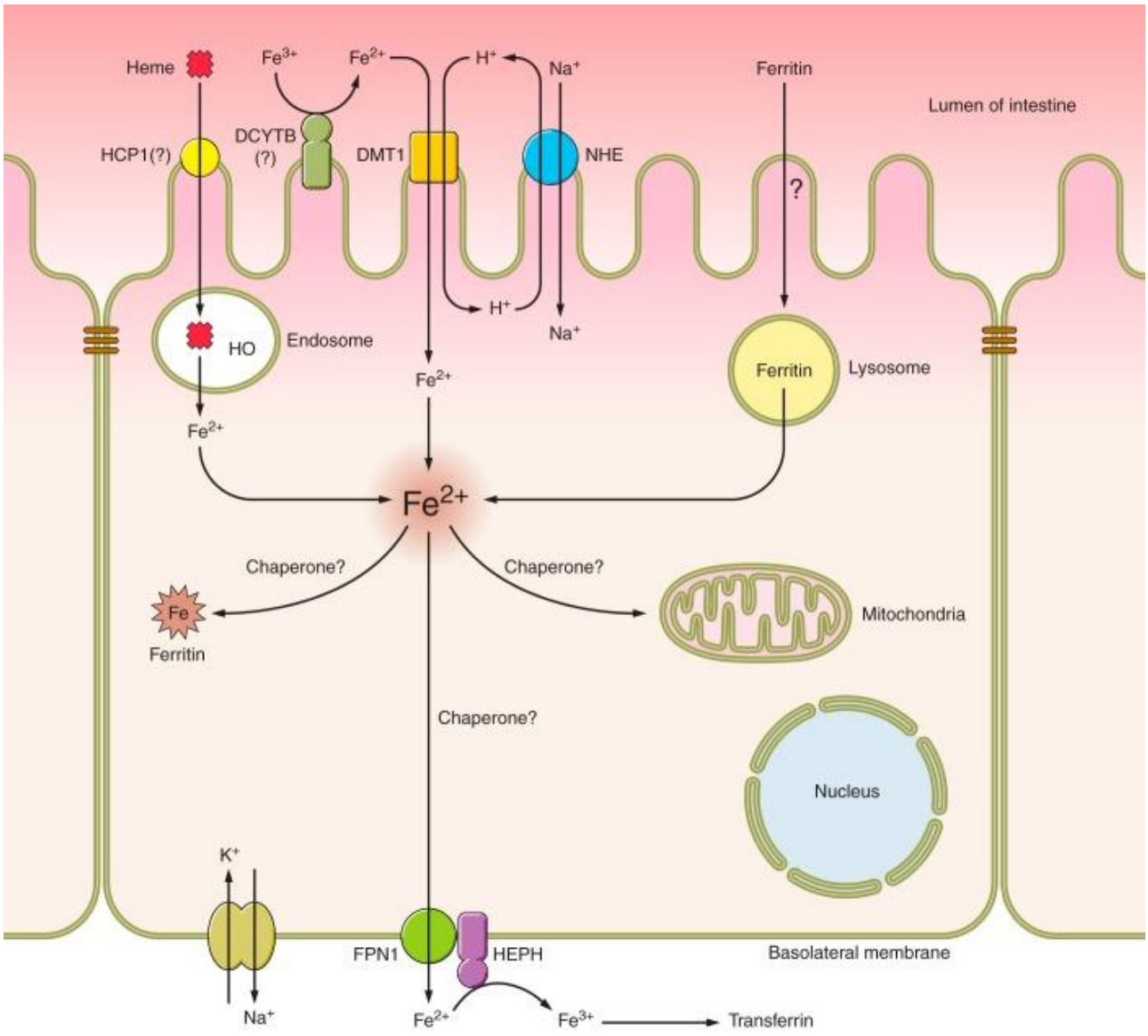

Gulec S. et al. Am J Physiol Gastrointest Liver Physiol. 2014; 307(4):G397-409 [4].

Fig. 1. *Mechanisms of iron absorption in the duodenum. Iron may be derived from heme or it may occur as free non-heme iron. Heme iron transport is probably mediated by endocytosis of heme followed by iron liberation from heme within endosomes by heme oxygenase (HO). Non-heme ferric iron must be reduced, by duodenal cytochrome b (DCYTB), and subsequently transported into cells via divalent metal-ion transporter 1 (DMT1). Iron destined for export traverses the basolateral membrane (BLM) via ferroportin 1 (FPN1). The exit of ferrous iron is functionally coupled with iron oxidation via hephaestin (HEPH). Ultimately, ferric iron binds to Tf in the interstitial fluids or in the vasculature and is distributed throughout the body.*

3.1.3.2.1 Regulation of intestinal iron absorption

The major regulator of systemic iron homeostasis is hepcidin, a 25-amino acid peptide produced by the hepatocytes but expressed, at low levels, also in macrophages and in cells from non-hepatic tissues (such as heart, brain, pancreas, stomach, lung, kidney, adipose tissue, retina). Nevertheless, only hepatic hepcidin appears to regulate systemic iron trafficking [8, 9].

Hepcidin functions. Hepcidin functions are to block intestinal iron absorption and to inhibit iron release from stores.

Hepcidin's mechanism of action. Since its discovery in 2001, numerous studies have been conducted to understand the mechanism of action of this peptide. Hepcidin acts as a negative regulator of iron uptake by binding FPN1 on the plasma membrane of enterocytes, macrophages, hepatocytes and other cells, promoting its Jak2-mediated tyrosine phosphorylation and internalization and subsequent lysosomal degradation. Accordingly, low hepcidin states are characterized by high levels of FPN as well as high iron export to extracellular fluid and plasma. In contrast, high circulating hepcidin concentrations lead to a reduction of FPN levels at the membrane level, with the consequent decreased iron export to plasma [10]. However, several authors have found that this internalization mechanism was not observed in the intestine. Indeed, in the duodenum, hepcidin was found to act rather on DMT1, leading to its internalization and proteasomal degradation [8].

Hepcidin synthesis. Hepcidin synthesis is regulated by different signals including circulating iron concentration, erythropoiesis, and inflammation. Iron-dependent induction of hepcidin serves to prevent excessive dietary iron absorption from enterocytes when body iron levels increase. When the levels of this metal are high, hepcidin is significantly upregulated, limiting further iron absorption and thus reflecting a regulatory response against iron overload. In contrast, iron deficiency significantly reduced hepcidin synthesis, allowing more iron to enter plasma. This regulation is complex and involves different hemochromatotic proteins. In particular, increased hepcidin gene transcription related to iron levels, involves the hemojuvelin/bone morphogenetic/SMAD (HJV/BMP/SMAD) pathway, which is activated following BMP6 over-expression. In addition, hereditary hemochromatosis protein (HFE) and the Tf receptor 2 (TfR2), both expressed on the hepatocyte cell membranes, also participate, under conditions of iron excess, in the induction of hepcidin expression [11]. Hepcidin inhibition, in response to iron deficiency, can also be mediated by the reduction of BMP6 expression, which decreases the

BMPR/HJV/SMAD signaling pathway. Besides being responsive to iron, hepcidin synthesis is strongly increased by inflammation through the interleukin 6 (IL6) / Signal transducer and activator of transcription 3 (STAT3) pathway, contributing to limited iron bioavailability for invading microorganisms, malignant cells or oxidative stress during chronic inflammation [8, 11]. In addition, hepcidin can be regulated also according to the erythropoietic requirement for iron. Indeed, during active erythropoiesis hepcidin production is suppressed, making more iron available for hemoglobin synthesis [12]. Factors reducing hepcidin expression include hypoxia. In this context, serum iron and Tf saturation are increased, allowing intense erythropoiesis to compensate for tissue hypoxia [13].

3.1.3.3 Transport

Exported Fe^{3+} is captured by Tf, the plasma iron carrier, and transported to bone marrow erythroblasts and other cells in peripheral tissues. Tf is an 80-kDa glycoprotein, synthesized and secreted mainly by the liver, which maintains iron in a redox inert state and delivers it to tissues. Varying amounts are also produced in lymph nodes, thymus, spleen, salivary glands, bone marrow and testis. Tf contains two high affinity (kD = 10^{-23} M) ferric binding sites, and is only partially (30%) saturated with iron under physiological conditions. The concentration of diferric Tf in plasma is ~5 µmol/L, corresponding to approximately one tenth of total circulating Tf. The high abundance of unsaturated apo-Tf allows an efficient buffering of increased plasma iron levels and prevents the build-up of non-transferrin bound iron (NTBI). This latter is taken up by tissue parenchymal cells and promotes oxidative injury. Under physiological conditions, NTBI is undetectable, but it is generated in iron overload states, such as in hereditary hemochromatosis, where Tf gradually becomes fully saturated with iron and loses its buffering capacity, or in atransferrinemia [2]. The uptake of Tf-iron through Tf receptor 1 (TfR1) is the main source of iron for most cells. The iron status of Tf influences its affinity for TfR1, with diferric Tf having the greatest affinity, monoferric Tf intermediate and apo Tf the lowest. Tf-iron binds to TfR1 on the cell surface and the complex undergoes endocytosis via clathrin-coated pits. A proton pump acidifies the endosome resulting in the release of Fe^{3+}, which is subsequently reduced to Fe^{2+} by six-transmembrane epithelial antigen of prostate (STEAP3) and transported across the endosomal membrane to the cytosol by DMT1. Apo-Tf is recycled back to the cell surface and released from TfR1 to plasma to repeat another cycle [2, 14].

After reduction of ferric iron by the STEAP3 protein, iron is transferred to the cytosol, where it is transported to intracellular sites either for local use or for storage, bound to Ft. The mechanism of iron transport through the cytosol is not well understood. Presumably, iron binds to dedicated iron chaperones, such as poly (rC)-binding proteins mediating its storage in Ft, its use for synthesis of heme as well as iron-sulfur clusters in the mitochondrion [1, 8].

3.1.3.4 Storage

More than 70% of body iron (3-5 g) is present within hemoglobin of red cells. In fact, the plasma compartment contains only 2–3 mg of iron, bound to Tf. When erythrocytes are degraded by macrophages, their iron content is returned to plasma Tf. Degradation of senescent red blood cells by splenic macrophages accounts for 90% of total iron recycling, the remaining 10% comes from the diet. The iron-Tf is mostly destined for erythrocyte production in the bone marrow. Other cells contain and require much less iron, and some of them are able to utilize non-transferrin bound iron as well. In the average adult male, significant fractions of body iron are distributed within tissue macrophages (∼5%) and hepatocytes (∼20%). In these sites, iron is stored in cytoplasmic Ft and is readily mobilized during periods of high iron demand. However, in general, the amount stored is much lower in women of reproductive age, due to blood losses from menstruation and parturition [9, 12, 15] [Fig. 2].

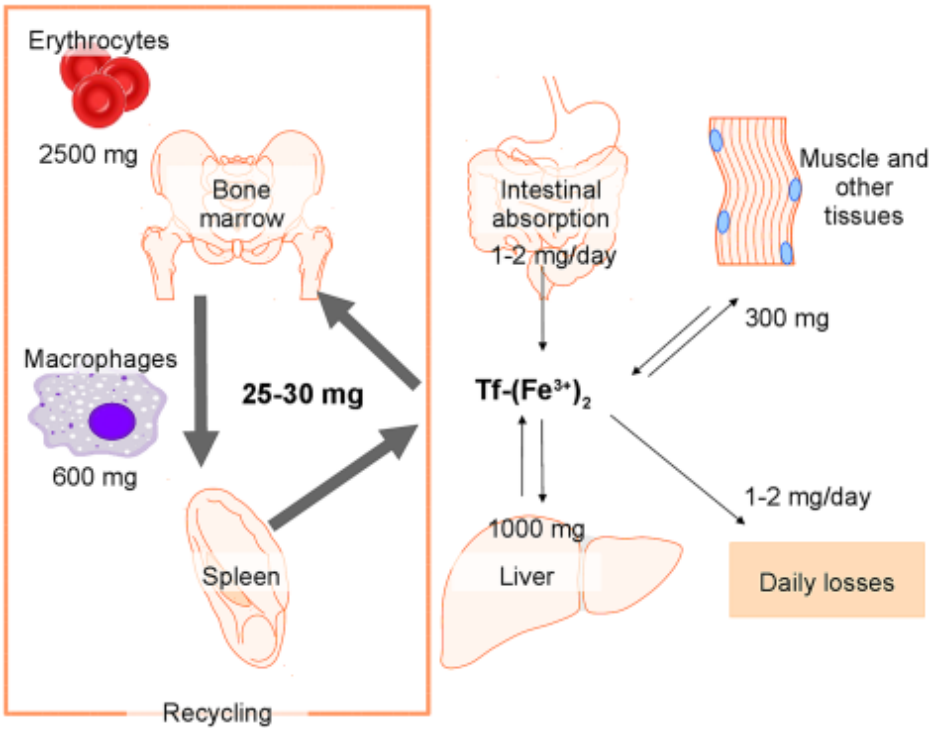

Papanikolaou G. et al. IUBMB Life. 2017; 69(6):399-413 [9].

Fig. 2. *Distribution of iron in humans.*

3.1.3.4.1 Intracellular regulation of iron

Inside the cell, iron balance is controlled by post-transcriptional mechanisms involving the Iron Regulatory Proteins (IRPs) and the Iron Responsive Elements (IREs). IRPs are capable of binding to IREs located in untranslated regions (UTRs) of mRNAs encoding iron-regulated proteins. When IRPs are active, they interact with the IRE and limit the expression of proteins having an IRE in its 5'UTR, whereas they stabilize mRNA displaying IRE motifs in 3'UTR. In particular, the DMT1 transcript contains an IRE in its 3' UTR, TfR1 mRNA contains multiple IREs within its long 3' UTR, while the mRNAs encoding H- and L-ferritin and the FPN1 transcript contain a single IRE in their 5' UTRs [2, 4, 15]. Thus, when intracellular iron is low, IRPs are maintained in their active form, leading to the stabilization of TfR1 and DMT1 mRNAs and the inhibition of FPN1 and Ft mRNAs translation. This response results in an increment of intracellular iron availability by both increment of cellular iron uptake and decrease of iron storage and release. On the contrary, when iron is abundant, the decrease in IRP activity leads to a decrease in DMT1 and TfR1 mRNA expression and in the translation of FPN1 and Ft mRNAs. This minimizes further internalization of iron and promotes the storage of excessive intracellular iron into Ft [2, 14].

As a further explanation of how the regulation of intracellular iron occurs, it is important to highlight that the cytosolic proteins that specifically recognize and bind IREs are IRP1 and IRP2. IRP1 acts as a sensor of iron levels within the cell and as a regulator of cellular iron homeostasis. Indeed, as an apoform, it is able to bind IRE, but it can also assemble a [4Fe–4S] cluster and become the cytosolic counterpart of mitochondrial aconitase, the enzyme that converts citrate to isocitrate in the tricarboxylic acid cycle. Under high iron conditions, the cluster is assembled and IRP1 functions as cytosolic aconitase. In this case, the iron-sulfur cluster keeps IRP1 in a closed conformation precluding access of IREs. Conversely, when iron levels are low, no cluster is formed and IRP1 acquires IRE-binding activity. IRP2 is highly homologous to IRP1 but lacks aconitase activity, probably because of its inability to assemble a [4Fe–4S] cluster [2, 16]. In iron-replete cells, IRP2 undergoes iron-dependent proteasomal degradation via the ubiquitin ligase F-box and leucine rich repeat protein 5 (FBXL5), while in iron deficiency FBXL5 is degraded and IRP2 accumulated [9].

3.1.3.5 Excretion

Iron excretion is not actively controlled and skin desquamation is the major mechanism, so far, described accounting for about 1–2 mg per day less than 0.1% of the 3–4 g of total iron in the human body; iron must be replaced from dietary sources to maintain its balance. Adolescent girls and premenopausal women excrete considerable amounts of iron through menstruation. Non-menstrual iron losses occur also through desquamation of epithelial cells in the intestine, through bile, urine and minor bleeding. Importantly, the losses of iron cannot substantially increase through physiologic mechanisms, even if iron intake and stores become excessive [8, 15].

3.1.4 Mitochondria and iron

Mitochondria are the major site of iron utilization. They harbor several abundant iron-dependent proteins that play essential roles in the respiratory chain (complexes I–IV), the citric acid cycle (aconitase) and the biosynthesis of amino acids and vitamins (e.g., lipoate synthase). They are also central sites for the synthesis of iron-containing co-factors, as well as of heme and iron sulfur clusters [1]. Moreover, mitochondria are key players in the regulation of cellular iron homeostasis and they actively communicate the status of mitochondrial iron availability to the cytosolic iron-regulatory systems, in order to balance cellular iron uptake and storage to

intracellular demands. Mitochondrial handling of iron is complex and even more delicate than in the rest of the cell because mitochondria are an important source of ROS. Mitochondrial iron trafficking mirrors cellular iron metabolism, but the exact mechanism by which it occurs remains elusive and not all the carriers involved are known. Iron must cross both outer and inner mitochondrial membranes to reach the site of heme synthesis, the matrix [2]. Mitochondrial outer membrane facilitators of iron import were identified by computational screening, which yielded several members of the SLC family, as well as a non-SLC transporter. Interestingly, members of the SLC family also facilitate iron import across the mitochondrial inner membrane. Most notable are SLC25A37 or Mitoferrin-1 and SLC25A38 or Mitoferrin-2, which are important for mitochondrial iron import into erythroid and non-erythroid cells, respectively [2]. Moving the attention from iron transport to its storage, mitochondria are characterized by the presence of a specific iron storage protein, the mitochondrial Ft or mitoferritin (FtMt), which is also able to change cellular iron distribution by attracting iron from the cytosol to mitochondria [2, 14]. Also in this organelle, FtMt plays a role in the protection against iron toxicity. In contrast to cytosolic Ft, the expression of FtMt is restricted to few tissues. Indeed, it is particularly expressed in mitochondria-rich tissues, such as the heart, skeletal muscle and osteoclasts [14].

3.2 IRON OVERLOAD

Given its potential high toxicity, an excessive iron accumulation in specific tissues, cellular and subcellular sites can promote a vast array of acute and chronic illness. This condition is defined as “iron overload” and can promote the development of organ damage as well as an increased mortality. The pathogenesis of this disease is not always clear. Indeed, this syndrome can occur as a consequence of mutations in genes involved in iron metabolism, or it may be secondary to acquired conditions, such as hazardous alcohol consumption and metabolic diseases, among others [17, 18]. Accordingly, iron overload syndromes can be divided into two groups: Inherited or Primary iron overload and Secondary iron overload syndromes, as described in Table 1 and Table 2, respectively [18].

Table 1 – Inherited iron overload syndromes
HFE-related hemochromatosis (Type 1)
C282Y/C282Y
C282Y/H63D
Other *HFE* mutations
Non-*HFE* related hemochromatosis
Juvenile Hemochromatosis (Type 2)
Type 2A – Hemojuvelin mutations
Type 2B – Hepcidin mutations
Transferrin receptor 2 hemochromatosis (Type 3)
Ferroportin diseases (Type 4)
Classical
Non classical

Table 2 – Secondary iron overload syndromes
Iron-loading anemia
Thalassemic syndromes (β Thalassemia)
Sideroblastic Anemias
Chronic Hemolytic Anemia
Apalstic Anemia
Pyruvate Kinase Deficiency
Chronic liver disease
Hepatic C infection
NAFLD
Alcholic liver disease
Porphyria Cutanea Tarda
Iatrogenic
Red blood cell transfusion
Long-term hemodialysis
Miscellaneous
Aceruloplasminemia
African iron overload
Neonatal iron overload

Modified by Siddique A. et al. Aliment Pharmacol Ther. 2012; 35(8):876-93 [18].

Table 1 and Table 2. *Primary and secondary iron overload syndromes.*

3.2.1 Primary iron overload syndromes

Hemochromatosis was first described by Armand Trousseau in 1865 as a "case of bronze diabetes and cirrhosis". Then, in 1935, Sheldon recognized the inherited nature of this disorder and the association with abnormal iron metabolism and, for this reason, this disease is now defined as "hereditary hemochromatosis". This latter is a group of inherited disorders characterized by progressive iron accumulation in tissues associated to iron-mediated injury and organ dysfunction. This pathology is characterized by an unrestricted iron efflux from enterocytes and macrophages leading to hyperferremia. The excessive circulating iron levels,

in turn, exceed the iron-binding capacity of Tf and, when the saturation of this latter is higher than 70%, NTBI appears in the circulation. NTBI is then readily taken up by hepatocytes, cardiac myocytes and other parenchymal cells. This rapid and excessive accumulation of intracellular iron causes specific tissue toxicities dependent on both the rate and the extent of iron accumulation, and triggers clinical complications. Hereditary hemochromatosis has been demonstrated to result from mutations in several genes involved in the regulation of iron homeostasis and, based on the gene causing the disease, four forms have been identified: the type 1, or HFE-related hemochromatosis, and three types of non HFE-related hemochromatosis: type 2, or juvenile hemochromatosis, type 3, or transferrin receptor 2 hemochromatosis, type 4, or ferroportin disease [19, 20].

3.2.1.1 HFE-related hemochromatosis or type 1 hemochromatosis

The most common form of hemochromatosis is associated with mutations of the *HFE* gene. *HFE*-related hemochromatosis is an autosomal recessive disorder, which usually manifests in the fourth or fifth decade. *HFE* encodes a membrane-bound major histocompatibility complex class I-like protein which binds to β2-microglobulin and this association enables it to be moved to the cell surface where it competes with Tf for binding TfR1 to modulate cellular iron uptake. It is involved in the induction of hepcidin expression under conditions of iron excess. A number of *HFE* mutations have been identified. The most common clinically relevant mutations, however, are the C282Y and H63D. The first one is a missense mutation on the short arm of chromosome 6 that causes a substitution of tyrosine for cysteine at the amino acid 282 in the HFE protein. This mutation disrupts a critical disulfide bond and impairs β2-microglobulin association and normal HFE processing. Instead, the H63D mutation is characterized by a histidine to aspartic acid substitution at amino acid 63. Generally, these mutations lead to the inability of HFE to sense increased levels of iron and to interact with TfR1, resulting in decreased hepcidin expression with the consequent impaired regulation of duodenal iron absorption and excessive delivery of iron to plasma [15, 18]. Approximately 85–90% of patients with the typical phenotype of *HFE*-related hemochromatosis are C282Y homozygotes whereas 3–5% are C282Y/H63D compound heterozygotes. The prevalence of C282Y homozygosity is 1 in 250 persons in the general population. However, iron overload features do not manifest in many C282Y homozygotes, suggesting an incomplete penetrance, the possibility that there may be other genes that act as modifiers of the *HFE*-related hemochromatosis phenotype or that

environmental or dietary factors are also important for the pathogenesis of this disease. In this context, the two main factors which can promote an increased phenotypic expression of the homozygous C282Y mutation are male gender (men are affected more frequently and more severely than women) and increased alcohol consumption [4, 18]. With regard to the H63D mutation, it has a carrier frequency of 10–20% of population of European descent and may contribute to minor increases in iron levels and rarely to iron overload in the absence of C282Y. However, only 0.5–2% of subjects with compound heterozygosity for C282/H63D develop iron overload. H63D homozygosity is unlikely to cause clinical disease in the absence of other factors, such as viral hepatitis and alcohol consumption.

In *HFE*-related hemochromatosis, widespread excess iron deposition occurs in parenchymal cells, especially in those of the liver, pancreas and heart, and can lead to organ damage and variable clinical outcomes. Among them, hepatomegaly, cirrhosis, arthropathy involving the metacarpophalangeal joints, progressive increase in skin pigmentation, diabetes mellitus, and cardiomyopathy can occur. Other common but less specific manifestations include abdominal pain, weakness, lethargy, and weight loss. Men may develop erectile dysfunction consequent to hypogonadotropic hypogonadism secondary to pituitary involvement [20].

3.2.1.2 Non HFE- related hemochromatosis

Other genetic disorders of iron metabolism result from mutations occurring outside the HFE gene.

3.2.1.2.1 Juvenile Hemochromatosis or type 2 hemochromatosis

Juvenile hemochromatosis (JH) is a rare autosomal recessive disease characterized by massive hepatocellular iron deposition as well as iron deposition in endocrine glands. Unlike classical *HFE*-related hemochromatosis, patients with JH present clinical disease early in life, usually by the third decade. This syndrome affects both genders equally and has a more rapid and severe course. Depending on the gene involved, JH is divided into two subtypes, although the clinical presentation is indistinguishable. Type 2A is due to mutations in the hemojuvelin (HJV) gene encoding protein hemojuvelin on the long arm of chromosome 1. Type 2B is due to mutation in the hepcidin gene on chromosome 19. The protein HJV, in particular, is expressed in the liver, heart and skeletal muscles, and is considered as an upstream regulator of hepcidin. Indeed, HJV

acts as a BMP co-receptor and enhances the phosphorylation of the SMADs, thereby increasing hepcidin expression. Therefore, when the HJV protein is mutated, the expression of hepcidin is inhibited and little or no hepcidin is detectable in plasma [18].

3.2.1.2.2 Transferrin receptor 2 or type 3 hemochromatosis

Type 3 hemochromatosis is a rare disorder resulting from mutations in the TfR2 gene located on the long arm of chromosome 7. It was first described in southern Italy and is inherited in an autosomal recessive fashion with an adult onset. TfR2 is mainly expressed in the liver and has a lower affinity for iron uptake compared with TfR1, but has a higher capacity to transport the complex Tf-iron to hepatocytes. As discussed above, it is involved, together with HFE protein, in the induction of hepcidin expression under conditions of iron excess. The TfR2 gene mutations impair the ability of the receptor to sense iron levels resulting in a decrease of hepcidin expression and in an increment of iron accumulation. However, in these patients, the reduction of hepcidin is not so huge and, as a result, the development of the iron overload phenotype is more gradual. Fatigue, arthralgia and cirrhosis and diabetes mellitus are the clinical manifestation of this disorder. Some individuals can present the symptoms in the second decade [4, 15, 18, 21].

3.2.1.2.3 Ferroportin disease or type 4 hemochromatosis

Type 4 hemochromatosis, also called ferroportin disease and originally identified in three families in Italy, is the second most common inherited iron overload syndrome after *HFE*-related hemochromatosis. It differs from the other types for having an autosomal dominant transmission and for not affecting hepcidin expression. Indeed, it is caused by mutations in the SLC40A gene, encoding the FPN, which result in a loss of protein function. It is characterized by hyperferritinemia, normal Tf saturation and iron accumulation in macrophages [15].

Furthermore, gain of function mutations in the SLC40A gene cause the so called “nonclassical ferroportin disease”, which can be associated with type 4 haemochromatosis. This disorder is similar to the ferroportin disease and the main signs are *(i)* increased serum Ft concentration, *(ii)* elevated Tf saturation, and *(iii)* iron accumulation in parenchymal cells [15, 18, 21].

3.2.2 Secondary iron overload syndromes

Iron overload can also be determined by secondary causes including alcohol abuse, obesity and insulin resistance, chronic hepatitis C, hemolytic and dyserythropoietic anemias and chronic transfusional therapy [22, 23]. Here some examples of secondary iron overload syndromes are presented.

3.2.2.1 Iron loading anemias

The definition “iron loading anemias” encompasses a group of inherited and acquired anemias characterized by ineffective erythropoiesis, excessive iron absorption and secondary iron overload. Two examples of these conditions are the thalassemic syndromes and the sideroblastic anemias [24].

3.2.2.1.1 β-Thalassemia

Thalassemia syndromes are a group of inherited hematological disorders which are caused by genetic defects in globin genes and are therefore characterized by the deficiency of the production of either the α- or β-globin chains. Specifically, β-thalassemia is a heterogeneous group of disorders caused by mutations occurring within one or two beta-globin genes or the immediate flanking sequences which lead to decreased or absent beta-globin production and the consequent abnormal hemoglobin formation. In β-thalassemia there is a quantitative reduction of structurally normal β globin chains in erythroid precursors. Instead, the synthesis of normal α-globin chains continues as normal, resulting in the accumulation within the erythroid precursors of an excess of unmatched α-globin. The free α-globin chains are not able to form viable tetramers and tend to form insoluble aggregates which precipitate within the developing erythroid cell at the bone marrow level with the final result of an ineffective erythropoiesis. The resulting anemia stimulates erythropoietin production, which in turn causes massive expansion of erythroid precursors, but fails to correct the anemia because the precursors undergo apoptosis [12].

Severe cases of β-thalassemia require regular blood transfusion to reduce the chronic anemia; but multiple blood transfusions together with increased hemolysis of red blood cells and increased gastrointestinal iron absorption, lead to iron overload, which is the major cause of serious morbidity and mortality in this disease. However, a severe iron overload disorder can

occur in most patients with β-thalassemia, even if they do not receive blood transfusions. In β-thalassemia, iron overload is treated with chelators, even if they have serious adverse effects and patient compliance is frequently a problem. Therefore, in recent years, new therapies are being studied. Among them, there are the allogeneic hematopoietic stem cell transplantation, the gene therapy or the induction of fetal hemoglobin. Interestingly, levels of hepcidin in β-thalassemic patients have been shown to be extremely low. This leads to a hyperabsorption of dietary iron, resulting in overloading. Therefore, hepcidin supplementation may become an alternative or an addition to the chelation therapy, at least in untransfused patients, in which hepcidin levels are normal or even increased, although still deficient considering the iron overload [12, 18, 25, 26].

3.2.2.1.2 Sideroblastic anemias

The sideroblastic anemias are a heterogeneous group of disorders characterized by anemia of varying severity and the presence of ring sideroblasts in the bone marrow. These latter are erythroblasts with an irregular accumulation of iron in mitochondria, which are clustered around the nucleus. Most of the iron deposited in ring sideroblasts is very likely present in the form of mitochondrial Ft, whereas normal erythroblasts lack this protein. The sideroblastic anemias include both inherited and acquired conditions. To date, mutations of genes involved in heme biosynthesis, Fe–S cluster biogenesis, or mitochondria biology have been reported in congenital sideroblastic anemia. Impaired function of these genes is speculated to result in an impaired utilization of iron, leading to accumulation of the metal in mitochondria. Conversely, the mechanisms by which ring sideroblasts are formed in acquired sideroblastic anemia are not fully clarified [27, 28].

3.2.2.2 Chronic liver disease

Iron can be a cofactor in chronic liver diseases, like hepatitis C virus (HCV), nonalcoholic fatty liver disease (NAFLD), alcoholic liver disease and porphyria cutanea tarda.

HCV infection is a major cause of chronic liver disease; its severity varies from asymptomatic chronic infection to cirrhosis and hepatocellular carcinoma. The mechanism by which hepatic iron overload develops in patients with chronic HCV infection remains unclear [29]. Indeed, the pathophysiology of iron overload in this disorder is likely a combination of iron release from necrotic hepatocytes, a direct effect of HCV on iron homeostasis, for example via the hepatic

overexpression of TfR1, presence of *HFE* mutations and dysregulation of hepcidin expression [18, 29].

NAFLD is considered to be the hepatic manifestation of metabolic syndrome. Approximately one third of patients show signs of impaired iron homeostasis as indicated by elevated serum Ft with normal or mildly elevated Tf saturation. Mild hepatic iron deposition is the typical histological finding in these subjects [30] and can occur in Kupffer cells as well as in hepatocytes. Mesenchymal iron deposition is more frequent than hepatocellular iron accumulation but mostly both compartments are affected [31]. Iron accumulation in NAFLD is multifactorial and is influenced by age, diet, race, HFE status and environmental factors [32]. It is mainly due to inhibition of iron mobilization from hepatocytes and Kupffer cells. Impaired iron export is related to inflammation and metabolic derangements and appear to impact iron regulators, such as hepcidin, FPN and, to a lesser degree, Tf receptor, Ft and copper [30]. Moreover, also genetic factors, such as *HFE* and beta-globin mutations can be involved [33], and a proposed mechanism to explain the hepatic iron deposition in NAFLD is an insulin-mediated cellular iron uptake through the redistribution of intracellular TfRs to the plasma membrane [29]. Indeed, metabolic alterations such as hyperinsulinemia, dysglycemia, dyslipidemia and insulin resistance worsen the clinical picture and progression of NAFLD [34].

Alcoholic liver disease is one of the major liver diseases in the developed countries and is characterized by hepatic iron overload in approximately 50% of patients [35]. According to the literature, chronic alcohol consumption in moderate to excessive amounts is associated with elevation of serum Ft concentration and Tf saturation, and can result in increased hepatic iron stores. Hepatic siderosis is frequently present with a typical mixed distribution in both hepatocytes and Kupffer cells. In these patients, low hepcidin levels are usually found along with iron deposition in macrophages. Additionally, increased intestinal iron absorption has also been documented. The mechanisms by which alcohol interferes with iron metabolism have not been fully elucidated, yet. Oxidative stress plays a key role in the pathogenesis of alcoholic liver disease and both iron and ethanol can cause oxidative stress and lipid peroxidation. Therefore, these two elements interact synergistically and exacerbate liver injury. Interestingly, in patients affected by alcoholic liver disease, alcohol consumption may cause suppression of hepcidin expression and that could represent a mechanism underling the iron accumulation in subjects affected by alcoholic liver disease [35, 36].

Porphyria cutanea tarda is a relatively rare condition caused by a decrease in uroporphyrinogen decarboxylase (UROD) activity, the fifth enzyme in the heme biosynthetic pathway. This results in an accumulation of the byproducts of heme biosynthesis, namely porphyrins. Patients have moderate to severe photosensitivity and the disease manifests in a chronic, gradually progressive manner with cutaneous vesicles, bullae, erosions, crusts, scars, particularly on the hands, after exposure to sunlight; liver disease may also be detected. Mild to moderate iron overload is almost always present, and iron depletion leads to reversal of the clinical manifestations. In particular, iron may exert a pathogenic role in different ways, such as increasing the rate of porphyrins formation, also through the ROS production, and decreasing the UROD activity. However, porphyria cutanea tarda is often induced in susceptible patients and known risk factors include UROD mutations, alcohol, smoking, hepatic tumors, estrogens and hepatitis C virus infection [36, 37].

3.2.2.3 Miscellaneous disorders

Aceruloplasminemia is a rare autosomal recessive disorder of iron metabolism which is due to a mutation in the ceruloplasmin gene. Ceruloplasmin is a plasmatic multicopper ferroxidase synthesized in the hepatocytes. It catalyzes the oxidation of ferrous iron to the ferric form, reaction that allows the metal to be released from intracellular stores and to be transported by Tf. Absence or dysfunction of ceruloplasmin leads to iron accumulation, mainly in the liver, pancreas and central nervous system. The classic triad of aceruloplasminemia is comprised of retinal degeneration, neurological symptoms and diabetes mellitus. Patients present elevated hepatic iron and serum Ft concentrations with low serum iron levels [18, 38].

African iron overload was originally described in individuals from southern and central African countries. Initially, it was attributed to consumption of food, or more significantly to large quantities of traditional beer prepared in iron-rich pots. Later, several studies hypothesized that the pathophysiology of such disease would probably be more complex and it has been suggested that African iron overload may have a genetic component. In particular, a mutation of the FPN gene SLC4OA1, restricted to Africans and African Americans, was taken into account. Moreover, alcoholic beverages could participate to the development of this disease. African iron overload is characterized by hepatic and probably, systemic iron overload. It is a frequent cause of cirrhosis and hepatocellular carcinoma and confers susceptibility to tuberculosis and other infections [18, 39, 40].

3.2.3 Treatment of iron overload

The treatment of pathological conditions associated with iron overload strongly improved with the introduction of different methods for evaluating the iron overload degree. These analyses include: the measurement of serum Ft levels, the detection of iron concentration through biopsy, the superconducting quantum interference device (SQUID) and the magnetic resonance imaging (MRI). The simplest way to quantify iron overload is to measure serum Ft level which correlates with iron stores in body. However, Ft level is variable in several non-iron overloaded conditions, including acute and chronic inflammatory disorders, infections, vitamin C deficiency, NAFLD, neoplastic disease, HCV, alcohol abuse and, for this reason, the reliability of this method is questionable [24, 41]. Liver iron concentration (LIC) is a reliable indicator of body iron concentration and can be measured by performing a liver biopsy or, noninvasively, by biomagnetic liver susceptometry through the use of SQUID [42, 43]. Another safe, noninvasive, and accurate alternative to liver biopsy is represented by MRI, which, similar to SQUID, is sensitive to the magnetic susceptibility of tissues. It can be applied, not only at the hepatic level, but also in other organs, such as pancreas, spleen, and vertebral bone marrow, providing new insights into the pathophysiology of systemic iron distribution [18, 43, 44].

Thanks to these techniques is then possible to routinely monitor body iron concentration with the consequent important possibility to adjust the therapy minimizing the potential for adverse side effects and avoiding serious complications of iron overload, such as hepatic, endocrinological and cardiac dysfunctions.

Among the most prescribed therapies, phlebotomy and chelation treatment are the most representative. Phlebotomy is a strategy including two phases, an initial induction phase to induce iron depletion followed by maintenance phase to prevent excess iron re-accumulation. However, some patients, such as those affected by β-thalassemia and hereditary hemochromatosis, cannot undergo this treatment because of their anemia. Moreover, phlebotomy can worsen hepcidin deficiency with the increased iron absorption and the need for further therapeutic phlebotomies and, also, it is not suitable for all patients because of poor vascular access and adverse physiological responses [12, 18].

Instead, iron chelators work by neutralizing unbound iron and removing excess iron from the tissues [41, 43].

Several iron chelators have been designed to excrete tissue iron by forming complexes [41].

Among them, deferoxamine, deferiprone and deferasirox are approved by the US Food and Drug Administration (FDA).

3.2.3.1 Deferoxamine

Deferoxamine (DFO, Desferal®), is a non-toxic iron chelator which is clinically approved and effective for long-term iron chelation therapy in iron overload syndromes. It is the first iron chelator used in treatment of iron toxicity and it has been the treatment of choice for iron overload for the last 40 years. It is a hexadentate chelator that can bind to all the six active sites of iron, achieving the complete inactivation of a single atom of iron at a 1:1 molar ratio. DFO can chelate iron irrespective of the metal accumulation site. Indeed, for example, it can precipitate iron present in old red blood cells leading to its excretion through urine or it can be internalized by hepatic parenchymal cells, where it binds to excess iron to facilitate its elimination through the bile.

Despite it can be orally absorbed, the pharmacokinetic of oral forms is not optimal. Similarly, it has been resulted to be ineffective after its intramuscular injection. Therefore, to be clinically effective, DFO must be administered as a subcutaneous, or less often an intravenous, infusion for several hours per day.

The treatment has remarkable effects on the reduction of serum Ft level and hepatic iron content and, more broadly, on the reduction of body iron load with the consequent prevention of iron-induced complications and even the reversion of some organ-damage due to iron deposition. The principle disadvantages associated with DFO are: *(i)* a low adherence to the therapy due to its short half-life and parenteral administration; *(ii)* the adverse effects, especially at high doses, such as skin reactions, abdominal pain, diarrhea, nausea, vomiting, hypotension, ocular toxicity and ototoxicity or, rarely, growth retardation, renal impairment and pulmonary fibrosis; *(iii)* the high cost of this drug [41, 45].

3.2.3.2 Deferiprone

Deferiprone was the first oral iron chelator to be used and works by forming stable complexes with plasma iron that can be excreted through urine. Like DFO, deferiprone has a short half-life and requires multiple daily dosing.

3.2.3.3 Deferasirox

Deferasirox is a tridentate chelator available for routine use. Unlike DFO, it can be rapidly absorbed after an oral administration and has a bioavailability of about 70% with a long half-life which allows a unique administration daily [46]. Two molecules of deferasirox are required to bind one of iron (2:1 ratio), and the final bound iron is excreted mainly through the feces [41, 45].

3.3 IRON OVERLOAD AND ENDOCRINOPATHIES

Among the several complications associated with iron overload syndromes, the most common endocrinopathies are the hypogonadotropic hypogonadism and the type 2 diabetes mellitus.

3.3.1 Male reproductive axis

Hypogonadotropic hypogonadism (HH) is a disease associated with a dysfunction at the hypothalamic-pituitary-gonadal (HPG) axis. Regarding this latter, it plays vital roles in reproduction and steroid hormone production. The neuroendocrine HPG axis integrates information from extrinsic and intrinsic cues in order to allocate energy and nutrient resources to reproduction as well as to synchronize reproduction-related life events such as sexual differentiation or time to maturation.

The HPG axis consists of three levels: hypothalamus, pituitary and gonads.

3.3.1.1 Hypothalamus

The hypothalamus regulates fundamental aspects of physiological homeostasis and behavior. In particular, it has integral developmental and functional connections with the pituitary gland, through which it controls endocrine hormone release. Some of the basic body functions regulated by pituitary hormones and their targets in the adrenal glands, thyroid and gonads include fluid balance, stress response, reproduction and growth. In addition, the hypothalamus makes neural connections via the autonomic nervous system and other pathways to regulate sleep, body temperature and feeding. The hypothalamus is anatomically configured to allow neurons and other cells to detect circulating factors, hormones, and metabolites in order to adjust homeostatic function in response to stressors and physiologic perturbations. Therefore, it has been seen as a center for responding to the body's physiological status. Dysfunction of

the hypothalamus can thus have a profound effect on diverse areas of health, including energy imbalance, diabetes insipidus and sleep disorders. The hypothalamus constitutes the ventral part of the diencephalon, it is located between the optic chiasm and the cerebellar peduncles and contains a rich supply of fenestrated capillaries with an attenuated blood-brain barrier (BBB) [47]. In contrast to other regions of the central nervous system (CNS) such as the cortex and spinal cord, which are composed of columnar structures, the hypothalamus comprises various nuclei expressing many different neurotransmitters and peptide hormones. The adult mammalian hypothalamus can be anatomically divided into four rostrocaudal levels and three mediolateral zones. From rostral to caudal, the four regions are preoptic, anterior, tuberal and mammillary hypothalamus, each of which has a lateral, medial and periventricular zone. Each hypothalamic region possesses distinct patches of nuclei and associated functions. The preoptic area is known to control thermoregulation, reproduction and electrolyte balance. The anterior hypothalamus, including the supraoptic nucleus (SON), suprachiasmatic nucleus (SCN), paraventricular nucleus (PVN) and anterior periventricular nucleus (aPV), regulates feeding, circadian rhythms and other homeostatic processes. The tuberal hypothalamus includes the arcuate nucleus (ARC), median eminence (ME), and ventromedial (VMH) and dorsomedial (DMH) hypothalamus, and plays a role in energy balance, stress response and aggression. Finally, the mammillary hypothalamus, which includes the mammillary bodies, is involved in arousal and stress response, as well as spatial and episodic memory [48].

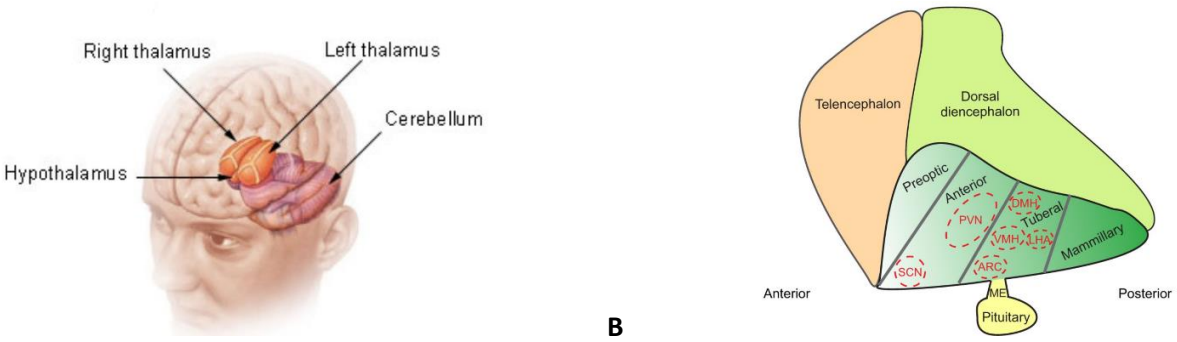

A. SEER Training Modules / U. S. National Institutes of Health, National Cancer Institute

B. Modified by Xie Y. et al. Development. 2017; 144(9):1588-1599 [48].

Fig. 3. ***A*** *Structures of the diencephalon.* ***B*** *Lateral view of the forebrain showing hypothalamic divisions. Four rostrocaudal regions are delineated by solid gray lines, and selected hypothalamic nuclei are outlined by dashed red lines. ARC, arcuate nucleus; DMH, dorsomedial hypothalamus; LHA, lateral hypothalamic area; ME, median eminence; PVN, paraventricular nucleus; SCN, superchiasmatic nucleus; VMH, ventromedial hypothalamus.*

The hypothalamic-pituitary axis is mainly regulated by two types of neuroendocrine neurons: the parvocellular and the magnocellular neurons. The first ones are located in the tuberal nuclei, preoptic nuclei, ARC, aPV and PVN, and project axons to the ME where these neurons secrete releasing or inhibiting hormones into a small portal blood system, the hypothalamic – hypophyseal portal system, connected to the anterior pituitary (adenohypophysis). Instead, the magnocellular neurons are located in the PVN and SCN and they project to the posterior lobe of the pituitary (neurohypophysis) to directly release oxytocin, which regulates a range of physiologic processes, including eating behavior, metabolism as well as smooth muscle contraction, and vasopressin, which has also may physiological actions, such as the control of fluid homeostasis and urine concentration [48].

Among the several hypothalamic functions, the hypothalamus is also involved in the regulation of the sympathetic nervous system activity. In particular, the activation of nuclei located in the hypothalamic frontal part lead to bradycardia, hypotension, increased sweating and salivation, gastric and intestinal hyperactivity, whereas when the posterior hypothalamic nuclei are activated, the result is an increment of sympathetic tone and the consequent effects are opposite to those listed above [49].

3.3.1.2 Pituitary

The pituitary gland is known as the “master gland” of the body, acting as central endocrine regulator of numerous physiologic processes, such as growth, reproduction, metabolism, water balance and response to stress. It is an intermediary organ for physiological signal exchanges between the hypothalamus and the peripheral organs. In particular, this gland can control the adrenals, gonads, and thyroid gland via secretion of specific regulating hormones into the systemic circulation [50, 51].

The pituitary is a bean-shaped gland located at the base of the brain in the midline. Females tend to have larger glands, especially during or after pregnancy. This small organ lies in the bony cavity called *sella turcica,* that surrounds it inferiorly and laterally and it is covered by a dural fold named *diaphragm sellae*, a reflection of the dura mater. Lateral to the sella are the cavernous sinuses; anteroinferior is the sphenoid sinus; anterosuperior is the optic chiasm; superior to it is the hypothalamus [50]. In particular, the pituitary gland is functionally and

anatomically connected to the hypothalamus by the ME via the infundibular stalk through which the hypothalamic factors reach the pituitary gland [52].

The pituitary is composed of two anatomically and functionally distinct parts: an anterior lobe, the adenohypophysis with an epithelial derivation, and a posterior lobe, the neurohypophysis, with a neuronal origin [50].

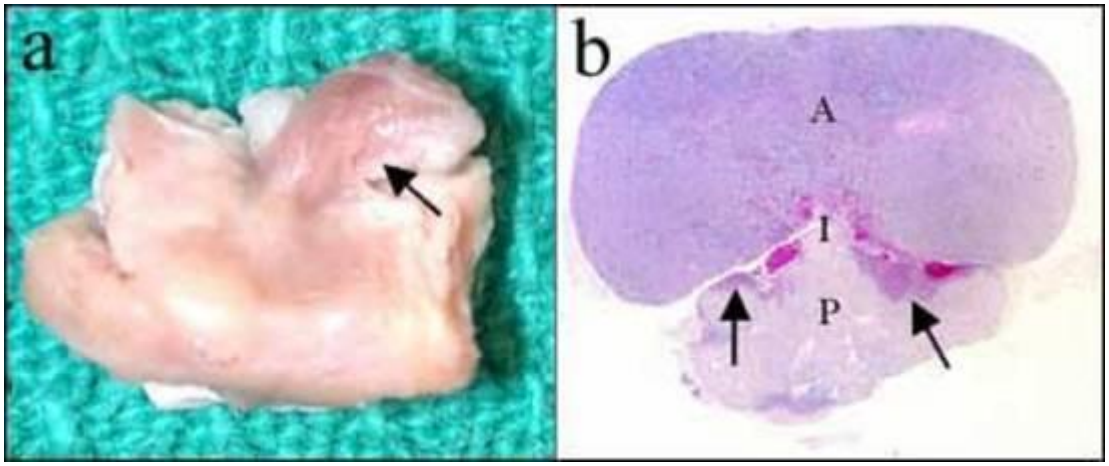

Asa SL. Endotext. 2000 [50].

Fig. 4. ***a)*** *The pituitary gland hangs from the pituitary stalk (arrow), an extension of the hypothalamus that traverses the diaphragm of the sella turcica.* ***(b)*** *A horizontal section of the gland identifies the anterior lobe (A), the posterior lobe (P) and the vestigial intermediate lobe (I), poorly developed in humans. This gland demonstrates "basophil invasion" of the posterior lobe, proliferation of corticotrophs into the neurohypophysis (arrows) that is a normal feature in older patients.*

The neurohypophysis is composed of the infundibulum, which directly connects the pituitary to the hypothalamus, the pituitary stalk, and the *pars nervosa* of the pituitary. The cell types of the neurohypophysis include pituicytes, which are modified glial cells, and the axonal processes of neurons, whose cell bodies are located in the hypothalamus and which end in fenestrated capillaries, where they release hormones. To this regard it is important to highlight that the neurohypophysis is one of the regions of the CNS which lacks the BBB. Hence, at this level, the axons are directly in contact with capillaries, with a fenestrated endothelium [49]. The neurohypophysis is responsible for storing and secreting vasopressin and oxytocin [50, 53].

The adenohypophysis is composed of three regions, the *pars distalis* or anterior lobe, the largest portion of the adenohypophysis, the pars intermedia or intermediate lobe, located in

the marginal area between the anterior pituitary and the posterior pituitary and the *pars tuberalis*, an extension of epithelium that wraps around the infundibulum of the pituitary stalk. The adenohypophysis is composed of acini that contain the specialized cell types, all of which have their own unique hormonal function and characteristics [50, 52]. These cells and their specific hormones are: lactotrophs, which produce prolactin (PRL), somatotrophs, which produce growth hormone (GH), corticotrophs, which produce adrenocorticotropic hormone (ACTH), thyrotrophs, which produce thyroid stimulating hormone (TSH) and gonadotrophs, which produce gonadotropins [51, 53]. These, in particular, produce the two gonadotropins, follicle-stimulating hormone (FSH) and luteinizing hormone (LH) and they account for 10% of adenohypophysial cells. They are scattered throughout the *pars distalis* and *pars tuberalis*. With increasing age, these cells tend to undergo oncocytic and squamous metaplasia [50]. LH, FSH and TSH are called pituitary glycoproteins and consist of two subunits. The alpha-glycoprotein subunit is common to the three hormones and the beta subunit is specific to each one [51, 53]. The pituitary receives its vascular supply from the superior, middle, and inferior hypophyseal arteries, all of which originate from the internal carotid arteries. The superior hypophyseal arteries vascularize the hypothalamus, flow through the infundibulum of the neurohypophysis and form the portal vessels that transport regulatory hormones from the hypothalamus to the pituitary gland. The middle hypophyseal arteries supply blood directly to the adenohypophysis, while the inferior hypophyseal arteries supply the *pars* nervosa [50]. Thanks to this hypothalamic-hypophyseal portal system, hypothalamic stimulatory and inhibitory factors, together with feedback signals derived from target organs (which include hormones and nonhormonal neurotransmitting agents), converge with the auto- and paracrine factors, to induce transcriptional regulation, translation, and secretion of the pituitary hormones [52].

3.3.1.3 Gonads

In male, the term “gonads” is referred to the testes. The testis is an essential organ of the male reproductive system because of its ability to produce sperm and androgens. From an anatomic point of view, the testis lies within the scrotum and is covered on all surfaces, except its posterior border, by a serous membrane, called the *tunica vaginalis*, which represents the remnants of the *processus vaginalis* into which the testis descends during fetal development. Along its posterior border, the testis is linked to the epididymis which at its lower pole gives rise to the *vas deferens*. Below the *tunica vaginalis*, the testis is surrounded by a fibrous

connective tissue capsule called the *tunica albuginea*. This latter is particularly thick at the posterior part of testis where it forms the *mediastinum*. From the internal surface of the *tunica albuginea* several septa originate and run in a posterior direction to join the *mediastinum*, dividing the testis into 200–300 small segments, called lobules. Each of these lobules contains several highly convoluted tubes, called seminiferous tubules. These latter consist of a basement membrane lined by Sertoli cells, interspersed with germ cells at various stages of maturation. The seminiferous tubules form loops ending as straight tubular extensions, the *tubuli recti*, at the *mediastinum* level in a network of tubules called the *rete testis*. From the *rete testis*, a series of six to twelve fine efferent ducts join to form the duct of the epididymis. This duct is extensively coiled and forms the structure of the epididymis that can be divided into the head, body and tail of the epididymis, from which the *vas deferens* originates [49, 54].

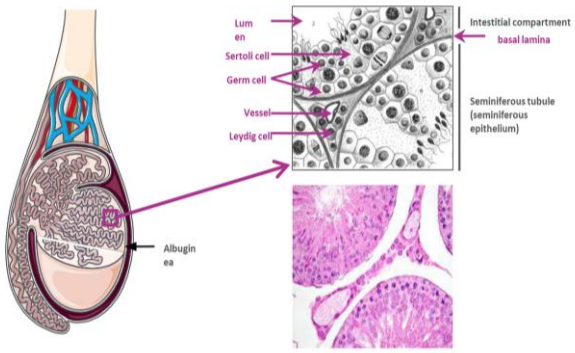

Sèdes L. et al. Mol Aspects Med. 2017; 56:101-109 [55].

Fig. 5. *Schematic representation and histological view of the structure of the testis.*

Relative to the blood circulation at the testicular level, the arterial supply to the testis arises at the level of the second lumbar vertebra from the aorta on the right and the renal artery on the left and these vessels descend retroperitoneally to form, through the inguinal canal, part of the spermatic cord. The testicular artery enters the testis on its posterior surface sending a network of branches that follow the lobular division of seminiferous tubules, so that each lobulus is supplied by one recurrent artery; segmental arteries and capillaries become branched between the Leydig cells and then give rise to the venous system. The venous drainage passes posteriorly and emerges at the upper pole of the testis as a plexus of veins termed the *pampiniform plexus* [54, 56]. At this level, the convoluted testicular artery is surrounded by several veins coiling

around the artery many times. In this way, the arterial blood is cooled down by surrounding venous blood and the testicular temperature is maintained lower than the all body one [56].

Moreover, at the testicular level an important ultrastructure is present, the blood-testis barrier (BTB), essential for spermatogenesis. It is formed by tight junctions between adjacent Sertoli cells, located near the basement membrane in the seminiferous epithelium [57, 58]. The peculiarity of this barrier is that, unlike most other tissue barriers, it is not only comprised of tight junctions, but these coexist and cofunction with ectoplasmic specializations, desmosomes, and gap junctions to create a unique microenvironment for the completion of meiosis and the subsequent development of spermatids into spermatozoa via spermiogenesis [59]. In this way, the BTB creates an immunological barrier that separates advanced germ cells within the testis from the immune system, that would otherwise recognize them as “foreign” [60]. Moreover, the BTB divides the epithelium into two distinct compartments, the basal and apical (adluminal) ones. In this way, it functions also as a physiological barrier that regulates the passage of nutritional substances (*ie.* sugars, acids), vital molecules (*ie.* hormones, electrolytes) and toxic compounds (*ie.* drugs, chemicals) between the basal and the apical compartments (transcellular barrier), and also between adjacent Sertoli cells (paracellular barrier) [55, 58].

From a functional point of view, testes exert both endocrine (steroidogenesis, the production of the steroid hormones that support male reproductive development and function) and exocrine functions (production of spermatozoa).

Regarding the endocrine functions, the main secretory product of the testis is testosterone, which is the major source of circulating androgens. Beside it, estrogen and progesterone are also produced at the testicular level.

The testicular exocrine function, instead, consists in a process called spermatogenesis, through which undifferentiated germ cells multiplie and differentiate to form spermatozoa [56]. As mentioned above, in the seminiferous epithelium, the germ cells are sequentially organized from the base of the tubule to the lumen, according to their stage of development. The BTB regulates the flow of nutrients and growth factors that are required for the development of these germ cells [56, 61]. Once the immature sperm is formed, it is transferred through different ducts into the epididymis, where the spermatozoa mature into a form ready for ejaculation [62].

3.3.2 The hypothalamic-pituitary-gonadal axis

Precise regulation of testicular function is conferred by the HPG axis in an elegant feedback loop in which the secretion of pituitary gonadotropins is *(i)* stimulated by gonadotropin-releasing hormone (GnRH) from the hypothalamus and *(ii)* modulated by testicular hormones, such as testosterone and estradiol.

In detail, the decapeptide GnRH is produced by scattered GnRH neurons located mainly in the preoptic area (POA) of the hypothalamus and it is released from axon terminals in the ME and infundibulum, where they enter the hypophyseal portal system. Thus, GnRH is taken to the anterior pituitary, precisely to the gonadotrophs, where it binds to its receptors leading to the release of FSH and LH into the systemic circulation. These two hormones reach the testis by testicular arteries to promote gametogenesis and steroidogenesis [55, 56, 63, 64]. LH acts on Leydig cells in the testicular *interstitium* to promote the synthesis of testosterone (T), while FSH affects the Sertoli cells thereby stimulating spermatogenesis, acting also as the main stimulator of seminiferous tubule growth during development. Moreover, the HPG axis is characterized by the presence of a negative feedback which further regulates the secretion of testicular hormones. Indeed, they decrease gonadotropin release both by reducing GnRH production and the sensitivity of the pituitary to GnRH stimulation; this process leads to a decreased stimulation of their own secretion [55, 56, 63] [Fig. 6].

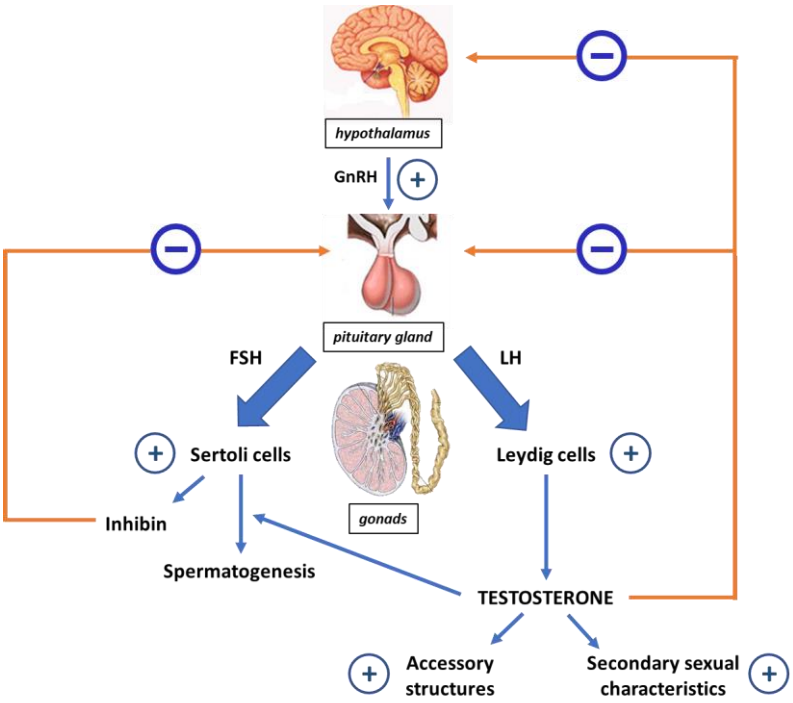

Fig. 6. *Schematic representation of the male hypothalamic–pituitary–gonadal (HPG) axis. The blue arrows represent stimulation and the orange arrows illustrate the negative feedback control of the HPG axis. Gonadotrophin releasing hormone (GnRH) is released from hypothalamus and acts on anterior pituitary gland, causing the release of two gonadotropins, follicle-stimulating hormone (FSH) and luteinizing hormone (LH). These hormones, in turn, act on gonads, precisely, FSH at the Sertoli cells level stimulating spermatogenesis and LH on Leydig cells promoting the synthesis of testosterone. The HPG axis is regulated by a negative feedback exerted by several gonadal hormones, ie testosterone and inhibin, on the secretion of GnRH by the hypothalamus and FSH and LH by the pituitary gland.*

In humans, the HPG axis is active in the mid-gestational fetus, but silenced towards the end of gestation. This restraint is removed at birth, leading to reactivation of the axis with an increase in gonadotropin concentrations. These concentrations then gradually decrease towards 6 months of age. In boys, T concentration rises to a peak at age 1–3 months, but then falls in conjunction with the falling LH concentration. Prenatal and postnatal activation of the HPG axis, in male, is associated with penile and testicular growth and testicular descent, it is therefore important for the development of male genitalia.

At about age 6 months in boys, there is an active inhibition of GnRH secretion, which persists throughout childhood. Puberty is then initiated by a sustained increase in pulsatile release of GnRH from the hypothalamus after this quiescent period [65].

3.3.2.1 Gonadotropin-releasing hormone

Gonadotropin-releasing hormone (GnRH) is a decapeptide produced by GnRH neurons. They derive from the olfactory placode and, after entering the forebrain during early embryonic development, they reach the hypothalamus at the POA level and in more caudal areas in the mediobasal hypothalamus (MBH). At this level, they extend processes to the ME, which is in contact with the pituitary gland by the presence of a network of blood [66-68].

GnRH has a pulsatile secretion and a half-life of approximately 10 minutes, and it is secreted into the hypothalamic-hypophyseal portal blood system, which carries GnRH to the pituitary gland [66]. Once secreted, GnRH acts on the pituitary gonadotrophs by binding G-protein coupled receptors that activate phospholipase-C resulting in inositol trisphosphate and diacylglycerol production. This step triggers a biphasic increase in intracellular calcium, which is closely paralleled by and is required for LH release. FSH, in contrast, is sorted to the constitutive secretory pathway and is therefore released in direct association with its synthesis [67, 69]. The GnRH-receptor complex undergoes intracellular degradation; thus, the cell requires some time to replace the receptors, which is reflected by the 60-90 minutes interval between GnRH pulses [66].

There are several mechanisms governing GnRH release. One of the most important is kisspeptin, a hypothalamic peptide encoded by the *KISS1* gene. This neuropeptide acts as a pivotal regulator in the onset of puberty and in the control of fertility. Kisspeptin has been recognized to act upstream of GnRH, stimulating GnRH neurons to release GnRH after interaction with its receptor. GnRH further stimulates gonadotrophs in the pituitary gland to secrete FSH and LH into the peripheral circulation [56, 70].

The *KISS1* gene is located on human chromosome 1 (1q32) and produces a 145 aminoacid precursor peptide (prepro-kisspeptin), which is cleaved to 54 amino acid protein (kisspeptin-54, Kp-45). Kp-54 may be further cleaved to lower molecular weight forms of kisspeptins, Kp-14, Kp-13, and Kp-10, sharing a common C-terminal sequence of arginine-phenylalanine-NH2 motif which is sufficient to fully activate GPR54, the kisspeptins receptor. This latter, called KISS1R, is expressed by GnRH neurons and it is encoded by the gene *KISS1R*. Kisspeptin-synthesizing neurons, in humans, are mainly located in two regions of the hypothalamus, the rostral periventricular area of the third ventricle and the ARC [68, 70].

Kisspeptin neurons have been suggested to act as a GnRH pulse generator, required to support the reproductive function in both sexes, such as follicular development, sex steroid production,

and spermatogenesis. It has been hypothesized that the pulsatility originates in ARC kisspeptin neurons containing neurokinin B and dynorphin (KNDy neurons) by reciprocal interplay of stimulatory neurokinin B signals and inhibitory dynorphin inputs. Accordingly, the output of the pulse generator may be transmitted from the ARC to the GnRH neuronal network by release of kisspeptin from axonal terminals originating from KNDy neurons [67].

3.3.2.2 Gonadotropins

Gonadotropins FSH and LH are glycoproteins consisting of a common α-subunit and a hormone-specific β -subunit, which are associated through noncovalent interactions. While the β-subunits determine the functional specificity of gonadotropins, their intrinsic bioactivity is largely determined by their degree of glycosylation. Weakly glycosylated forms of the hormones have a short circulatory half-time, and although totally deglycosylated gonadotropins are able to interact with their receptor, they are unable to evoke generation of a second messenger signal. Highly glycosylated isoforms (acidic) display longer half-life and stronger biologic power.

Gonadotropins are essential for spermatogenesis and secretion of testicular androgens. More precisely, FSH, in men, targets Sertoli cells to regulate spermatogenesis, as it maintains normal testicular size, seminiferous tubular diameter, and sperm number and motility. In parallel, LH, acting directly on the Leydig cells, stimulates the production of gonadal hormones, including T. Once synthesized, LH and FSH are stored in granules in the pituitary gland. GnRH induces exocytosis of the granules and the release of these hormones into the circulation. A low GnRH pulse frequency tends to preferentially release FSH, whereas higher frequencies are associated with preferential secretion of LH [66]. Both FSH and LH act through classic protein hormone receptor mechanisms, involving a G-protein associated transmembrane receptor. LH, in particular, leads to the transcriptional activation of target genes such as the steroidogenic acute regulatory (*StAR*). LH, stimulating the synthesis of StAR protein, accelerates the transfer of cholesterol from the outer to the inner mitochondrial membrane, the first step in steroid hormone biosynthesis [55, 63].

Tonic LH secretion is composed of intermittent secretory episodes of the hormone, which reflect a corresponding pattern of pulsatile GnRH release by the hypothalamus [71]. During the development, in male fetus, the expression of LH increases from week 10, reaching a peak before week 20 and decreasing slowly thereafter. After delivery, there is a surge in

gonadotropin levels due to the withdrawal of maternal-derived estrogen. In male infants, LH peaks at 1–3 months of age, declining rapidly thereafter and reaching a nadir at ∼4–9 months of age. In the year or two preceding puberty, the GnRH pulse generator begins to mature and, in response, there is a gradual increase in the frequency and amplitude of nocturnal LH pulsatile secretion. With pubertal progression LH is released with a more regular pulsatility throughout the day. The increase in gonadotropin activity during puberty drives gonadal steroidogenesis [72]. In adult men, secretion of LH is pulsatile with a mean frequency of approximately one event per hour or one every 90–120 min. On the contrary, FSH secretion is predominantly basal, and it seems to be not directly coupled to GnRH pulses [56].

3.3.2.3 Testosterone

Testosterone, in male, is responsible for virilization of the reproductive tract, promoting the formation of the *ductus deferens*, epididymides, seminal vesicles and ejaculatory ducts. It is produced by the Leydig cells, located in the interstitial compartment between seminiferous tubules [55]. The receptor for this hormone is the steroid nuclear hormone receptor, androgen receptor (AR). The T signaling consists in the binding of the hormone to the cellular AR, followed by the translocation of the ligand–receptor complex to the nucleus where it binds to androgen response elements (AREs) in the regulatory regions of genes to modify their translation [73].

The testicular content of T in an adult man is approximately 50 mg/testis and, since the daily production rate, under physiological condition, is 3–10 mg in men [74], it is assumed that this hormone is continuously produced and released into the circulation.

T is transported in plasma bound to circulating proteins. Sex hormone binding globulin (SHBG) is the most important one, with a high-affinity but low-capacity for this hormone. Under physiological conditions, 30–45% of circulating T is bound to SHBG and the remainder is bound to proteins, such as albumin and corticosteroid binding globulin, which, unlike SHBG, are low-affinity, high-capacity binding proteins. Only approximately 2% of total testosterone circulates in blood without being bound to any protein.

The secretion of testosterone follows a circadian rhythm: the highest level of secretion is in the early morning and lower levels are found in the circulation during afternoon [55, 56].

Moreover, T plasma levels are strictly correlated to LH levels, as demonstrated by the fact that individual LH pulses in peripheral blood were found to precede T pulses in the spermatic vein

by 80 min. On the other hand, the increase in testosterone level leads to quite a prompt decrease in LH level due to the feedback interplay within the GnRH–LH–T axis [56]. More broadly, the circulating T levels change during the development with three peculiar peaks which follow the three separate waves of increases and declines of Leydig cell numbers. The first one occurs at week 12–14 of gestation, during the fetal differentiation of Leydig cells and then the hormone levels decline until the early neonatal period. The second peak occurs at 2 months postpartum and it is associated with renewed Leydig cell proliferation and, subsequently, T levels decrease precipitously, falling below the limit of detection by 6 months of age [72]. Leydig cells then atrophy a second time, and, for the next decade, the *interstitium* is populated by steroidogenically inactive precursor cells. The adult generation of Leydig cells differentiates pubertally and is complete by 12–13 years of age. In parallel, during puberty the third peak of T occurs and its secretion continues to maintain virilization and spermatogenesis [62].

3.3.3 Hypogonadotropic hypogonadism

Hypogonadism in men is a clinical syndrome that results from failure of the testis to produce physiological levels of T (androgen deficiency) and a normal number of spermatozoa due to disruption of one or more levels of the hypothalamic-pituitary-testicular axis [75]. This disorder can be congenital or acquired; the latter form is more common than the former and it is usually apparent during adulthood [76]. Hypogonadism is classically divided in primary or secondary hypogonadism. The first (hypergonadotrophic hypogonadism) is the result of testicular failure to produce adequate levels of T with an impaired spermatogenesis and is identified by low T and elevated gonadotropin levels. Secondary hypogonadism (hypogonadotrophic hypogonadism) is the result of gonadotropin or luteinizing hormone-releasing hormone (LHRH) deficiency (*eg,* pituitary or hypothalamic failure), which may be congenital or may arise from various pathological processes. It is characterized by low T levels, impairment of spermatogenesis, and low or low-normal gonadotropin levels [75, 77]. These classical definitions of hypogonadism that are based on specifying a testicular or a pituitary-hypothalamic site of failure may not apply to a large portion of hypogonadal men assessed in population-based studies and seen in clinical practice. Indeed, some individuals can present a failure at both the testicular and hypothalamic-pituitary levels. For this reason, several medical societies have proposed revised terminology to clarify the identification, categorization, diagnosis, and treatment of hypogonadal men. The Endocrine Society adds to the classical

dichotomy, the combined primary and secondary testicular failure, which is characterized by low T levels, impairment of spermatogenesis, and variable gonadotropin levels, depending on whether primary or secondary testicular failure predominates [75, 77].

Interestingly, the clinical phenotype can be identical for primary and secondary hypogonadism, whereas it could vary according to the age of hypogonadism onset. Thus, an alternative classification of male hypogonadism is based on the period of life in which the gonadal function begins to fail. According to this new age-of-onset-based classification, male hypogonadism can be subclassified in very-early-onset hypogonadism (VEOH), early-onset hypogonadism (EOH) and late-onset hypogonadism (LOH). When VEOH is present, hypogonadism occurs during the early fetal life. It could result in an almost complete female phenotype, due to the lack of sufficient levels of testis hormones during the critical window of male sex differentiation or to a complete androgen insensitivity. This phenotype is characterized also by virilization defects, such as micropenis or cryptorchidism, which occur when the secretion or the activity of GnRH are impaired. EOH occurs during the peripubertal age and it is characterized by the absence or the arrest of pubertal development. Due to milder central or peripheral defects, such as androgen insufficiency, body proportions are typically eunuchoidal with a high-pitched voice, scant body hair, small testis, reflecting lack or arrest of spermatogenesis, penis and prostate [78, 79]. Finally, LOH occurs with ageing; the most common features are decreased libido, loss of muscle mass and strength, increased body fat, decreased bone mineral density and osteoporosis, as well as physical activity and performance decline, reduction of some cognitive abilities, decreased vitality, depressed mood and sexual dysfunction [78-80].

3.3.3.1 Iron overload and hypogonadotropic hypogonadism

Chronic iron overload and tissue accumulation are able to contribute to the development of endocrine disorders. Among them, hypogonadism is the second most common endocrine abnormality, after diabetes, associated to iron overload. Its frequency in the literature ranges from 10 to 100% [81].

According to McDermott and Walsh, hypogonadism occurs at a relatively advanced stage of iron overload. Biochemical and histologic evidence suggests that the cause of hypogonadism in this context is the iron-induced cellular damage. Findings of autopsy studies have shown that the anterior pituitary gland and, especially, the gonadotrophs, usually contain stainable iron. In contrast, the testes, even when atrophic, usually contain no excess iron or have iron deposits

confined to the vessel walls, leaving the germinal epithelium and the Leydig cells uninvolved [82]. However, from a functional point of view, most studies have found defects in either testicular or pituitary, with little direct evidence of hypothalamic dysfunction as source of hypogonadism.

Regarding the hypothesis of a gonadic origin of hypogonadism, Lucesoli *et al*. reported *in vivo* experiments on rat testis response to acute iron overload: histopathology showed an iron deposition in the interstitial tissue at the periphery of seminiferous tubules and a rarefication of germ cells at this level. Authors also highlighted an association between a moderate iron increase in the testis and an increase in testicular oxidative stress with oxidative damage to lipids, proteins, and DNA. These observations confirmed the importance of the BTB in the protection of germ cells against iron overload. These results also emphasized the possibility of testicular damage directly related to iron deposition, suggesting the potential involvement of testes in the pathogenesis of hypogonadism associated with iron overload [81].

Conversely, Siminoski *et al.* described a case of a hypogonadal male with hemochromatosis with a probably defect in pituitary function and in hypothalamic gonadotropin regulation. Indeed, the patient was presenting low levels of T and normal LH values. The authors excluded the involvement of a testicular impairment by detecting an increase in serum T after a human chorionic gonadotropin (hCG) administration. LH secretion normally raised in response to GnRH administration, while, on the contrary, the FSH response was only partial, suggesting the pituitary defect. The absence of an increase in LH and FSH following clomiphene stimulation, finally, implied a functional defect at the hypothalamic level [83].

Interestingly, it is important in HH patients determine whether the origin of gonadal insufficiency is hypothalamic or pituitary. To this purpose the study of gonadotropin secretion before and after long-term GnRH administration can be useful. This was demonstrated in patients with idiopathic hemochromatosis which showed a weak or absent pulsatile LH activity before pulsatile GnRH treatment for two or four weeks, together with the absence of a significant increase in LH level during treatment and in T levels following chronic pulsatile GnRH administration. This unresponsiveness to GnRH suggested that a pituitary rather than hypothalamic defect occurred in these hypogonadal subjects [84].

There are also several studies regarding the possible recovery of reproductive function in patients affected by HH caused by iron overload. Siemons *et al.* described a case report about a man with a diagnosis of HH due to idiopathic hemochromatosis, who underwent an

aggressive phlebotomy. This treatment resulted in restoration of normal T, LH and FSH levels and return of potency and libido [85]. In this context, the most important factor determining whether HH can be reversible is the severity of iron overload. Indeed, it is possible that there is a transient, reversible phase affecting GnRH and gonadotropins secretory dynamics early in the natural history of HH, but when iron overload becomes more severe, the HH is likely irreversible. An example of this situation is given by thalassemic patients which depend on repeated blood transfusions for their survival; the transfusional iron overload progressively damages the HPG axis in an irreversible way [86]. The importance of an early treatment of iron overload has been highlighted also in a patient with HH and juvenile hemochromatosis, who responded quickly and successfully to the venesection therapy, probably because the treatment was introduced early and continued intensively [87]. Furthermore, Piperno *et al.*, analyzing patients with genetic hemochromatosis, hypothesized that hypothalamic dependent gonadal dysfunction can develop in the early stage of the disease. Then, with the increasing iron overload, endocrine alterations probably worsen and pituitary hypogonadism, as well as testicular failure develop. Also these results suggest that the reversibility of endocrine dysfunctions in hemochromatosis is possible in the early stages of hypothalamic-pituitary damage [24].

Finally, the best strategy for a rapid improvement in a patient's health status and quality of life appears to be the combination of iron depletion and hormonal replacement therapy. This latter helps to maintain a physiological level of T and its metabolites (including dihydrotestosterone and estradiol) to optimize the maintenance of libido and sexual function. In addition, the correction of iron overload by phlebotomy is not always sufficient to normalize pituitary function [81].

3.3.4 Iron, insulin resistance and type 2 diabetes

It is increasingly recognized that iron influences glucose metabolism, as shown by studies demonstrating a positive association between body iron stores and the development of glucose intolerance, type 2 diabetes mellitus (T2DM) and gestational diabetes [88]. The existence of this link is supported by evidence collected in iron overload patients, which present impaired glucose metabolism, characterized by higher insulin concentration and insulin resistance (IR) [17].

In particular, since elevated serum Ft levels are being associated to increased levels of body iron stores, several authors focus their attention on the possible correlation existing between this marker and an impaired gluco-metabolism. In this context, increased Ft levels are associated with surrogate measures of both impaired β cell function and decreased insulin sensitivity [89] and are positively correlated with serum glucose [88]. Therefore, Ft levels are associated with the risk to develop metabolic syndrome and T2DM. In particular, in patients affected by hereditary hemochromatosis, circulating levels of Ft are inversely correlated with insulin sensitivity. In contrast, lowering the levels of Ft (*i.e.*, using iron chelators such as DFO) protects against T2D [89]. In turn, acquired abnormalities of iron metabolism can lead to the dysmetabolic hyperferritinemia, characterized by normal to mildly elevated Tf saturation without intrahepatic iron deposition, as well as to the dysmetabolic iron overload syndrome (DIOS). This latter is a common cause of hyperferritinemia with mild to moderate hepatic iron concentration, characterized by fatty liver, increased Ft levels and increased body iron stores in the presence of IR. It is a frequent condition predisposing to metabolic, cardiovascular and hepatic damage, characterized by preserved up-regulation of hepcidin. The pathogenesis of iron accumulation in DIOS has been related to altered iron trafficking associated with steatosis, hepatic inflammation, and IR. Also in this context, iron removal, through, for example, phlebotomy or iron chelation therapy, could improve insulin sensitivity [33, 90].

It has long been recognized that iron overload can increase the risk of diabetes, particularly in iron overload syndromes such as hemochromatosis and thalassemia. Diabetes mellitus, in particular, is the most common endocrinopathy associated to iron overload. The association between this condition and diabetes was first proposed in the mid-nineteenth century based on patients with hereditary hemochromatosis, which was also termed “bronze diabetes” due to the pigmentation that occurs with the disease [91]. Functionally, iron overload-mediated diabetes is characterized by both IR and insulin deficiency and may therefore mimic both T2DM and idiopathic type 1 diabetes [89].

The role of iron in the pathogenesis of diabetes is suggested by *1*) an increased incidence of T2DM in diverse iron overload syndromes and *2*) reversal or improvement in diabetes (glycemic control) with a reduction in iron load achieved using either phlebotomy or iron chelation therapy. The mechanisms underlying iron-induced diabetes are not yet fully elucidated, but they may involve impaired insulin secretion from pancreatic β cells, insulin resistance and

hepatic dysfunction, associated to decreased insulin sensitivity at the hepatic, muscle, and adipose tissue level [89, 92].

The liver is the major reservoir of iron in the body. Excess of iron in this organ interferes with glucose metabolism, causing hyperinsulinemia via both decreased insulin extraction and impaired insulin signaling. In fact, the initial and most common abnormality seen in iron overload conditions is hepatic IR [88]. On the other hand, hyperinsulinemia favors the intrahepatic deposition of iron. Indeed, insulin enhances the uptake of extracellular iron, inducing the redistribution of TfRs to the cell surface while down-regulating hepcidin expression [90].

There is some evidence that iron overload also affects skeletal muscle, the main effector of insulin action [90]. Mehdad *et al*., for example, showed that mice fed an iron-restricted diet for 78 days had increased expression of the insulin receptor and glucose transporter 4 (Glut4) in skeletal muscle, compared to mice fed with iron-supplemented diet [93].

The mechanisms by which iron overload impairs insulin action in both muscle and liver are not yet fully understood. One mechanism is believed to be the activation of stress pathways with the formation of ROS, which, via hydroxylation of phenylalanine residues of insulin, results in reduced affinity of the insulin receptor for insulin. ROS can also activate, in one side, forkhead box protein O1 (FOXO1) leading to IR, and, on the other, AMPK, promoting glucose uptake and fatty acid oxidation [89].

With regard to the adipose tissue, adipocytes require iron for normal function and differentiation. Insulin is known to cause a rapid and marked stimulation of iron uptake by fat cells, redistributing TfRs from an intracellular membrane compartment to the cell surface [88]. Moreover, alterations in adipocyte mitochondrial iron content and mitochondrial Fe-S proteins affect adipocyte differentiation and insulin sensitivity. Although the precise mechanism is unknown, it is proposed that iron enhances mitochondrial biogenesis in adipocytes, as iron chelation leads to reduced expression of genes involved in both mitochondrial biogenesis and adipogenesis [89]. Iron overload leads also to an increment of adipocyte ROS formation and induces adipocyte dysfunction.

Besides liver, muscles and adipose tissue, it is interestingly to note that patients with transfusional iron overload have increased iron deposition in β cells [89]. In fact, at the pancreatic level, islets iron deposition is restricted to β cells and, despite the essential role of iron, these latter are highly vulnerable to perturbations in iron homeostasis. There are several

plausible reasons for this vulnerability. First, the expression of antioxidant enzymes is relatively low in pancreatic islets making the β cells particularly sensitive to oxygen radicals [88, 91]. In this context, it has been shown that in a mouse model of hemochromatosis, iron excess led to β cell oxidant stress and decreased insulin secretory capacity due to β cell apoptosis and desensitization of glucose-induced insulin secretion [94]. These effects were probably due to the nearly exclusive reliance on mitochondrial metabolism of glucose for glucose-induced insulin secretion together with the above mentioned low expression of the antioxidant defense system [92]. Moreover, compared to other tissues, pancreatic islets have low FPN expression and high DMT-1 expression, which may render them more susceptible to iron accumulation [91].

3.3.5 Iron and metabolic syndrome

Metabolic syndrome (MetS) is a cluster of metabolic disorders and according to the Harmonization definition, it is characterized by (i) raised blood pressure, (ii) raised triglycerides, (iii) lowered high-density lipoprotein cholesterol, (iv) raised fasting glucose, and (v) central obesity occur. A clinical diagnosis is done when three out of the five risk factors [95].

Hyperferritinemia has been associated with MetS by several authors. Chen L *et al.* demonstrated, in a cross-sectional study, that the number of MetS components was positively correlated with increased levels of serum ferritin and that the prevalence of MetS was increased in case of hyperferritinemia [96]. Likewise, in a group of 66 male volunteers the serum ferritin levels were associated with MetS [97]. Similar results were obtained in a prospective, cross sectional study, in which high serum ferritin levels, though within normal range, were significantly associated with MetS [98].

Recently, adipokines were proposed as novel biomarkers and regulators of MetS, since it is well established that individuals that are obese and/or suffer from this syndrome display a characteristic imbalance of their adipokine profile [99]. In detail, adipokines are molecules produced and secreted by the adipose tissue which act as paracrine or endocrine hormones. They are involved in the regulation of appetite and satiety, fat distribution, inflammation and blood pressure, among the others. Their secretion may play a role in several obesity-related metabolic abnormalities, such as hypertension, T2DM, fatty liver and vascular disease [100]. In the context of their link to the pathogenesis of MetS, Zachariah JP *et al.* demonstrated an association between the adipokine panel and the incident MetS in participants in the

community-based Framingham Third Generation Cohort who attended examination cycle 1 [101].

Among the several existing adipokines, it has been reported that leptin is an important factor linking obesity, MetS, and cardiovascular disorders [102]. Leptin, a 16 kDa protein of 146 amino acids, is a cytokine-like hormone secreted primarily by the white adipose tissue. The first described major action of this hormone was the control of body weight and fat deposition, through the hypothalamus, by the induction of satiety and the increment of energy expenditure [100, 103]. Besides its important role in the regulation of energy metabolism, leptin is also involved in the regulation of puberty onset and gonadal function [104]. This hormone circulates in the blood in two forms: the monomeric one (free leptin) and the higher molecular weight form which is bound to the soluble leptin receptor. Leptin levels exhibit a nocturnal peak and multiple smaller ultradian pulses over 24 h. These circulating levels are affected also by gender and they are higher in women than in men. This is probably due to the higher percentage of body fat and the increased production rate of leptin per unit mass of adipose tissue in female subjects [100, 105, 106]. Leptin exerts its effects through a specific transmembrane receptor (LepR), which is a member of the extended class I cytokine receptor family and has multiple isoforms resulting from alternative splicing. These last have been categorized into short (LepRa, LepRc, LepRd and LepRf) and long (LepRb) isoforms which share a common leptin binding domain but differ in their intracellular domains [100, 103, 106, 107]. The long-form LepRb has a long intracellular domain with putative Janus kinase (JAK)/STAT binding sites, essential for intracellular signal transduction and crucial for leptin's actions. The functions of the short-form LepR (a, c, d, and f) and of the secreted form LepRe are less clear, but it is known that this last isoform serves as a plasma leptin-binding protein [103, 106]. There are several key pathways for LepRb signal transduction including those of (i) the JAKs, (ii) the STATs, (iii) phosphoinositol-3 kinase and (iv) the mitogen-activated protein kinase (MAPK). Of note, negative regulators of leptin signaling have been identified and include suppressor of cytokine-signaling-3 (SOCS3) [100, 103, 107]. In humans, serum leptin levels positively correlate with MetS, independently of the body mass index and, thus, they may represent a sensitive biochemical marker for the identification of the MetS [100, 108, 109]. Interestingly, besides the links between hyperferritinemia and MetS and beteween MetS and leptin, it is important to note that several studies, performed in both mouse models and humans, demonstrate that iron can also play a direct role in determining leptin levels. In particular, Gao Y *et al.* showed that C57Bl6/J male

mice fed iron-enriched diet (2,000 mg/kg) were characterized by lower serum leptin levels compared to those on the low normal–iron diet (35 mg/kg) for 2 months [110]. In turn, Yamamoto K *et al.* demonstrated that leptin could directly affect iron metabolism. Indeed, these authors measured the levels of the central regulator of body iron metabolism, hepcidin, in leptin-deficient (ob/ob) mice and leptin receptor-deficient (db/db) mice. Serum hepcidin levels were significantly lower in ob/ob mice and db/db mice, demonstrating that the activation of leptin receptor plays an important role in hepcidin expression [102]. Regarding clinical studies, a significant negative association between ferritin and leptin as well as between serum iron and leptin was found in individuals with and without diabetes [110]. Moreover, in a cohort of thalassemic patients the mean serum leptin level was found to be significantly lower than in control patients [111]. Differently, Kimura Y *et al.* showed a significant positive association between serum ferritin concentrations and leptin concentrations in male Japanese employees enrolled in a cross-sectional study [112]. In conclusion, these results demonstrate that iron could affect and be affected by leptin levels, suggesting, at least in part, the presence of a link between the iron concentrations and risk of metabolic disorders and related diseases.

Interestingly, Dongiovanni *et al*. demonstrated that in male C57Bl/6 mice an iron-enriched diet led to both a significant reduction of serum leptin levels with a significant increment of circulating resistin, showing that iron can modulate several adipokines besides leptin [113].

Resistin is a 12.5 kDa cysteine-rich peptide hormone, expressed, in humans, predominantly by peripheral blood mononuclear cells and macrophages, while in mice, primarily by adipocytes [114]. To date, the specific receptor for resistin is still unknown. However, recent reports have suggested, as potential receptors for resistin, an isoform of decorin, the mouse receptor tyrosine kinase-like orphan receptor 1, the toll-like receptor 4 or the adenylyl cyclase-associated protein 1 [115]. Similarly, the molecular mechanism of resistin action is still unclear. However, it is well known that resistin activates signalling pathways such as Akt, MAPK, STAT-3 and peroxisome proliferator-activated receptor γ [115]. As for the gender difference of leptin, resistin plasma levels are significantly higher in females than in males [116]. Furthermore, in humans, resistin circulates in different molecular isoforms and the oligomeric one is considered to have a more potent effect on the stimulation of proinflammatory cytokines [117]. Experimental evidence associated plasma resistin levels with metabolic disorders. In particular, in subjects affected by MetS, resistin levels were higher and positively associated with waist circumference and IR, with high resistin level being an independent predictor of the prevalence

of MetS [118]. Moreover, obese individuals who generally have greater infiltration of macrophages in adipose tissue, showed increased expression of resistin in this tissue level and higher circulating levels of the hormone [117]. Unfortunately, few studies regarding the possible link between MetS, resistin and iron are present in the literature. However, it is important to highlight that in the mouse model presented by Dongiovanni *et al.* iron overload led to an increased expression of resistin at the visceral adipose tissue level and this overexpression was associated to the induction of mRNA levels of SOCS3 a target of both resistin and hepcidin and an inhibitor of insulin signaling [113].

4. AIM

Iron is an essential trace element, but due to its ability to generate hydroxyl radicals, when in excess, it may have toxic effects [119]. Among these, encompassing liver diseases (*i.e.* hepatic fibrosis or cirrhosis), cardiac manifestations (*i.e.* cardiomyopathy, arrhythmias, heart failure), arthropathy and skin hyperpigmentation [18], iron overload syndromes are also associated to several endocrinopathies, being diabetes mellitus and hypogonadism the two most common [81]. The mechanisms behind the onset of these diseases and the consequent effects are still not clarified. In this context, this thesis was aimed to investigate the molecular determinants of the reproductive impairment caused by exogenous iron overload. To this purpose, a male murine model fed iron-enriched diet (IED) has been characterized. In this *in vivo* model, the presence of a metabolic impairment (evaluated by measuring body weight, food intake, perigonadal fat pad, basal glycemia and Homeostatic Model Assessment of Insulin Resistance -HOMA-IR- index) caused by iron overload and the expression of genes (neuropeptide Y -NPY- and anorexigenic pro-opiomelanocortin -POMC-) and adipokines (leptin), representing a link between metabolism and reproduction, has been studied. Furthermore, to further clarify which sites could be affected by IED, the hypothalamus-pituitary-gonadal axis has been taken into consideration. Detailed analysis has been performed to evaluate whether iron overload could *(i)* accumulate at the hypothalamic, pituitary and gonadal levels, *(ii)* affect iron homeostasis, *(iii)* determine macro- and microscopic alterations in the HPG axis and *(iv)* modify the gene expression of testosterone, luteinizing and follicle-stimulating hormones, all involved in the regulation of the reproductive function.

To further investigate whether iron overload could impact the reproductive function mediated by the hypothalamus, we used two *in vitro* models of gonadotropin-releasing hormone (GnRH) neurons. Upon iron overload, iron homeostasis, cell migration, oxidative and endoplasmic reticulum stress and related cell signaling pathway have been analyzed.

The data obtained from this thesis' work have been published in Molecular and Cellular Endocrinology [120].

5. MATERIALS AND METHODS

5.1 ANIMALS

All the *in vivo* experiments were conformed to the European Commission Directive 2010/63/EU and were authorized by the Italian Ministry of Health.

Different strategies have been tried to mimic human iron overload and its related complications [121]. Among them, the most commonly applied are the use of *(i)* genetic animal models or wild type animals either *(ii)* with parental or *(iii)* dietary iron overload.

i. An example of a genetic animal model is given by $HFE^{-/-}$ mice, resembling human genetic hemochromatosis, already above described.
ii. Parental iron overload induced in rodents is a model of acquired iron-overload. Bacon *et al*. in 1983 suggested that parenteral administration of iron (ferric nitrilotriacetate) in rats produced homogenous deposition of iron throughout the hepatic lobule in both hepatocytes and Kupffer cells [122]. Among the several iron delivery preparations available, iron-dextran possesses unique properties regarding pH stability, low toxicity [121] and, therefore, it is frequently used in different studies. Das SK *et al.* used iron-dextran to mimic an early and a chronic stage of iron overload. In the first case, they injected male C57BL6 mice with 5 mg of iron-dextran per 25 g body weight on a 5 days/week schedule for a total duration of 4 weeks. In the second one, the authors repeated this treatment, at the end of which, they injected 1.25 mg of iron-dextran per 25 g body weight for 8 weeks [123, 124]. Moreover, Ribeiro Júnior R.F. *et al*., resembled a human condition of chronic iron overload secondary to acquired conditions by injecting rats with 100 mg/kg of iron-dextran for 5 days a week. For short-term iron overload experiments, in adult C57BL/6 male mice, Frýdlová J *et al*. administered a single intraperitoneal injection of iron dextran at the dose of 1,000 mg/kg [125].
iii. In order to resemble a condition of secondary iron overload, administration of iron with the diet is a very common approach. To this purpose, several authors choose carbonyl iron enriched diet; indeed, this approach can lead to a hepatocellular deposition of the metal with a periportal distribution, a condition similar to that seen in patients bearing hereditary hemochromatosis [121]. This model can be used to induce stable changes of

iron status in mice by adding, to the diet, 8.3 g/kg of carbonyl iron [126]. This latter may be used at higher doses as shown by Baum P *et al*. that fed rats with a standard diet complemented with 3% carbonyl iron (29 g/kg) [127].

For the present project, healthy five-week-old male C57BL/6J (C57black6J) mice, with an average weight of 17g, were purchased from Charles River Laboratories (Charles River, Calco, Italy). The animals were housed at Department of Pharmacological and Biomolecular Sciences (Università degli Studi di Milano – La Statale, Milan, Italy) at constant room temperature (22 – 24°C), under 12-h light/dark cycles, with *ad libitum* access to tap water and food, in compliance with the European Union guidelines. Upon arrival, the animals were divided in six cages, with 5 animals per cage and they were fed with regular chow diet for one week, during the acclimatization. Subsequently, the 30 mice were randomly assigned at the two experimental groups. The first one represented the control (CTR) group and consisted of 15 mice fed standard iron concentration diet in pelleted form, containing 180 mg/kg of iron. The second group was the Iron-Enriched Diet (IED) group and consisted of 15 mice fed iron-enriched diet with 3% carbonyl-iron, always in a pelleted form. The treatment lasted 11 weeks [113]. The body weight of each mouse and the food intake of each cage were monitored weekly. The measure of basal glycemia was performed through tail vein blood sampling using the glucometer Accu-Check Aviva (Accu-Check, Roche Diagnostic AVIVA, Mannheim, Germany), after an overnight fast, on week 5 and 8 of treatment. The Homeostatic Model Assessment of Insulin Resistance (HOMA-IR) index was calculated as follows: [glucose (nmol/L) * insulin (µU/mL)/22.5], using fasting values [128]. Alternatively, it was calculated through the following formula: fasting glucose level (mg/dL) × fasting insulin level (ng/mL)/405 [129].

At the end of the treatment, all mice were sacrificed by decapitation under anesthesia, which consisted in a mixture of isoflurane and oxygen. The sacrifice was performed between 10:00 am to 12:00 pm to avoid circadian variations, after an overnight fast. Trunk blood was collected and serum, after being separated by centrifugation (15 minutes at 2,000 rpm), was stored at -80°C until assayed. Hypothalamus, pituitary and testes were carefully dissected, flash frozen in liquid nitrogen and stored at -80°C for RNA extraction. In a subgroup of 3 animals, whole brains were isolated and fixed in 4% paraformaldehyde to allow subsequent immunohistochemistry analysis. The same procedure was performed to collect testes from a subgroup of 5 animals.

Before the fixation, testicular weight and long diameter, as well as perigonadal fat pad weight, were measured.

For the immunohistochemistry analysis brains from $HFE^{-/-}$ mice (Kindly provided by Prof. L. Valenti and Dr P. Dongiovanni) were used as a positive control, since the *HFE* gene knockout model recapitulate both the biochemical abnormalities and the histopathology of human genetic hemochromatosis. In particular, this animal model exhibits abnormally high Tf saturation and excessive iron accumulation in the liver together with a decreased hepatic hepcidin mRNA expression. Histologic examination revealed iron deposition predominantly in hepatocytes, but also in spleen and small intestine [18, 130].

5.2 REPRODUCTIVE HORMONE ASSAYS

LH and T levels were evaluated by radioimmunoassay (RIA). 50 µL of serum were used to determine LH levels through a double-antibody method and RIA kits supplied by the National Institutes of Health (Dr. A. F. Parlow, National Institute of Diabetes and Digestive and Kidney Diseases National Hormone and Peptide Program, Torrance, CA). In IODO-GEN tubes rat LH-I-10 was labelled with ^{125}I, following the instructions of the manufacturer (Pierce Chemical Co., Rockford, IL). The reference preparation LH-RP-3 was used as standard to quantify LH concentrations. Intra- and inter-assay coefficients of variation were less than 8 and 10% and the sensitivity of the assay was 5 pg/tube. All samples were measured in the same assay; accuracy of hormone determinations was confirmed by assessment of rat serum samples of known hormone concentrations [131].

A commercial RIA kit from MP Biomedicals (Costa Mesa, CA) was employed to quantify serum T levels. The sensitivity of the assay was 1ng/mL, and intra-assay coefficient of variation was 4.5%. All medium samples were measured in the same assay.

5.3 ELISA ASSAY

Blood serum was collected and stored at -80°C until assayed. Leptin concentrations were measured by using a Mouse/Rat Quantikine® enzyme-linked immunosorbent assay (ELISA) kit (R&D systems; Space Import – Export Srl, Milan, Italy). In a polyclonal antibody specific for mouse/rat leptin pre-coated microplate, the assay diluent RD1W and 50 µL of standards, prepared starting from a stock solution of 4000 pg/mL, of mouse/rat leptin control and of

diluted samples (20-fold dilution) were pipetted. The microplate was incubated at room temperature for two hours to allow the binding between leptin and the immobilized antibody. After washing away any unbound substances, 100 µL of mouse/rat leptin conjugate was added to each well. The washing step was repeated and 100 µL of substrate solution, prepared mixing a stabilized hydrogen peroxide solution with a stabilized chromogen (tetramethylbenzidine), was pipetted into the microplate, followed by an incubation at room temperature for 30 minutes, protecting the plate form light. The enzyme reaction yielded a blue product that turned yellow when 100 µL of Stop Solution was added. The optical density of each well was determined within 30 minutes using a microplate reader set to 450 nm with a wavelength correction at 570 nm (Wallac Victor 3 1420 Multilabel Counter, PerkinElmer). Data were linearized by plotting the log of the mouse/rat leptin concentrations versus the log of the O.D. on a linear scale, and the best fit line was determined by regression analysis. The assay range was 62.5 – 4,000 pg/mL with a sensitivity of 22 pg/mL.

5.4 HISTOLOGICAL ANALYSIS AND IMMUNOSTAINING

Upon dissection, testes and brains were fixed in a solution of phosphate-buffered saline (PBS) with 4% paraformaldehyde, pH 7.4, overnight at 4°C. Testes were dehydrated and wax-embedded for a routine hematoxylin and eosin staining, whereas brains were cryopreserved in 30% sucrose and OCT (optical cutting temperature) compound-embedded for immunostaining. Formaldehyde-fixed tissue sections were incubated in PBS with 10% normal goat serum and 0.1% Triton X-100 or, with serum-free protein block (DAKO) for primary goat antibodies. Cryostat sections of formaldehyde-fixed samples of median eminence were incubated with hydrogen peroxide to quench endogenous peroxidase activity before incubation with GnRH primary antibody (1:1,000), followed by biotinylated goat anti-rabbit antibody (1:400; Vector Laboratories), and then developed with the ABC kit (Vector Laboratories) and DAB (Sigma-Aldrich) to obtain an immuoperoxidase labelling [132].

5.5 IMAGE PROCESSING AND QUANTITATION

To acquire bright-field images, a Zeiss Axiovert 200 with a Photometrics CoolSNAP ES camera (survival assays) or a Leica DM microscope with a DC500 digital camera (AP assays, HRP-stained sections) were used. Whereas, fluorescence images of mouse tissues were acquired through a Leica TCS SPE1 confocal microscope. Then, all images were processed using Photoshop CS4

(Adobe Inc.). To quantify the abundance of GnRH-positive neurites at the median eminence level of mice fed chow diet or IED and of mice $Hfe^{-/-}$, the pixel intensity of GnRH staining was measured in 20-µm sagittal sections of median eminence. For immunoblotting, 3 independent experiments were performed for each condition, the optical density of signals was measured with ImageJ software (NIH) and the mean pixel intensity was calculated.

5.6 CELL CULTURES

Immortalized murine GN-11 cells (a kind gift of Dr S. Radovick, Children's Hospital, Division of Endocrinology, Boston, MA) are representative of immature GnRH neurons, while the cell line GT1-7 (a kind gift of DR R.I. Weiner, Reproductive Endocrinology Center, University of California, San Francisco, CA) is a model of mature GnRH neurons. These two cell lines were grown in monolayer in a humidified incubator at 37°C with 5% of CO_2. The culture medium for both these two *in vitro* models was the Dulbecco's Minimal Essential Medium (DMEM; Sigma-Aldrich, Milan, Italy) enriched with D-glucose (4.5 g/L) and supplemented with phenol red (0.0159 g/L), L-glutamine (2 mM), sodium pyruvate (1 mM; Biochrom, Berlin, Germany), streptomycin (100 µg/mL; Sigma-Aldrich), penicillin (100 U/mL; Sigma-Aldrich) and 10% fetal bovine serum (FBS; Life Technologies, Monza, Italy). Medium were replaced every 3 days. Once confluent, they were harvested with 0.05% trypsin/0.02% ethylenediaminetetraacetic acid (EDTA; Sigma Aldrich) and seeded in 100 mm Petri dish with 12 mL of medium at the density of 0.1 X 10^6 cells, in case of GN-11 cells and 3.5 X 10^6, in case of GT1-7.

5.7 CHEMICALS

Ferric ammonium citrate (FAC) was purchased from Sigma-Aldrich (Milan, Italy). Desferal® (deferoxamine mesylate, DFO) was obtained from Biofutura Pharma (Milan, Italy). U0126, a specific and non-competitive inhibitor of mitogen-activated protein (MAP) kinase/ extracellular signal-regulated kinase (ERK) 1/2 (MEK 1/2), used *in vitro* at 10 µM, was purchased from Tocris Bioscences (Bristol, UK).

5.8 MEASUREMENT OF TISSUTAL AND CELLULAR IRON CONTENT

Hypothalamic, testicular and cellular iron content was measured by atomic absorption spectrometry (AAS). This is an analytical technique that measures the concentrations of

elements in several kinds of samples. It is based on the principle according to which atoms of different elements absorb characteristic wavelengths of light. Technically, the sample is atomized and targeted by electromagnetic radiation; some of it is absorbed and the greater the number of atoms there is in the sample, the more radiation is absorbed. The amount of light absorbed is used to calculate the concentration of the element in the sample.

The iron deposition at the hypothalamic and testicular levels of CTR and IED mice was determined at the end of the treatment; the samples, before being assayed, were dried for two hours at 100°C.

To determine the iron accumulation in the *in vitro* models, GN-11 and GT1-7 cells were treated with 200 µM FAC. At the end of the treatment, the cells were washed three times with PBS and, in the same buffer, harvested with cell scrapers. Subsequently, lived cells were isolated by using Trypan Blue. Indeed, this dye cannot enter lived cells because of their intact cytoplasmic membrane, while, conversely, can color the cytoplasm of dead cells. Lived cells were counted, centrifuged at 1200 rpm for 5 minutes and the pellet was stored at -20°C.

The intracellular amount of iron in both tissues and cells was then measured by an atomic absorption spectrometer. The total iron concentration has been expressed as µg/100mg of dry tissue for hypothalamus and testes and as µg/10^6 cells for GN-11 and GT1-7.

5.9 CELL VIABILITY ASSAYS

The effect of iron on cell viability was assessed by using two different techniques: *(i)* the ATPlite™ 1step assay kit (PerkinElmer, Monza, Italy) and *(ii)* the Trypan Blue exclusion test performed with the LUNA™ Automated Cell Counter (Logos Biosystems, Inc., Annandale, VA).

5.9.1 ATPlite™ 1step

The ATPlite™ 1step (Luminescence ATP Detection Assay System) is an assay employed for the quantification of viable cells, which uses adenosine triphosphate (ATP) as a marker for cell viability. ATP is ideal because it is present in all metabolically active cells and its concentration decreases when the cells undergo necrosis or apoptosis. The ATPlite™ 1step is a luminescence test based on the production of light during the reaction between ATP, D-Luciferine and oxygen, catalyzed by luciferase.

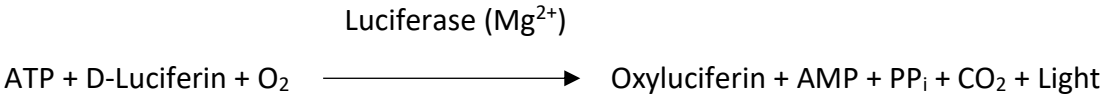

The luminescent signal is correlated to the cell number. To perform this assay, GN-11 cells were seeded in a 96-well microplate at 0.02 X 10^6 cells/well and, the day after, exposed to 200 µM FAC for 3 or 24 hours. Subsequently, the microplate was equilibrated at room temperature (20 -22°C) and the solution containing luciferase and D-Luciferin was added to each well. After shaking the plate, protected from the light, the luminescence, proportional to ATP concentration, was measured and it was expressed as Count per Second (CPS). Comparing the value of CPS of cells treated with FAC *vs* cells CTR (not exposed to FAC), the effect of iron on cell viability was determined.

5.9.2 LUNA™ Automated Cell Counter

The LUNA™ Automated Cell Counter measures the concentration (expressed as number of cells/mL) of total, live and dead cells. This instrument uses a counting algorithm, shows green and red circles to indicate, respectively, live and dead cells and creates a cell size distribution histogram. To obtain viability information, Trypan Blue was used.

For the Trypan Blue exclusion test, GN-11 cells were seeded in 6-well plates at 0.3 X 10^6 cells/well and, after 24 hours, exposed to 200 µM FAC for 3 or 24 hours. Then, the cells were harvested with 200 µL of 0.05% trypsin/0.02% EDTA in PBS without Ca^{++} and Mg^{++}. 10 µL of this cell suspension were mixed with 10 µL of Trypan Blue in the three minutes preceding the count and 10/12 µL of this mixture were loaded into the chamber of a LUNA™ Cell Counting Slide, inserted, then, into the instrument. The image was adjusted focusing on the cell in order to distinguish the live cells, with bright centers and dark edges. Finally, the instrument provided an accurate live/dead cell count.

5.10 TISSUE AND CELLULAR RNA EXTRACTION

5.10.1 Hypothalamus

Total RNA was harvested from the hypothalamus with the NucleoSpin® RNA/Protein kit (Macherey-Nagel, Düren, Germany). The whole hypothalamic samples (6 – 11 mg) were homogenized by using the TissueLyser II (Qiagen) for 3 minutes at 30 Hertz in a mixture

composed of 350 µL Buffer RP1, containing guanidinium thiocyanate, and 3.5 µL β-mercaptoethanol, a reducing agent. Then, the lysate was transferred in a NucleoSpin® Filter and filtrated by centrifugation for 1 minute at 11,000 x g. 350 µL of 70 % ethanol were added to the homogenized lysate before to transfer all the sample in a NucleoSpin® RNA/Protein Column. The subsequent centrifugation for 30 seconds at 11,000 x g was required to permit the binding of RNA and DNA to the column membrane, with the parallel release of proteins in the flow-through. Because of the high degradability of RNA, it was isolated immediately, leaving the protein containing flow-through on ice. 350 µL of Membrane Desalting Buffer (MDB) were added to the column in order to enhance the effectivity of the following DNA digestion, carried out by the rDNase. The membrane was, then, washed with Buffer RA2, inactivating the rDNase, and with Buffer RA3. Finally, the RNA was eluted in 40 µL of RNase-free water.

5.10.2 Pituitary, testes, GN-11 and GT1-7 cells

For the RNA extraction from pituitary, testes and neuronal cells the RNeasy Mini Kit (Qiagen, Milan, Italy) was used. This kit guarantees the purification of all RNA molecules longer than 200 nucleotides. Biological samples are lysed and homogenized in the presence of a highly denaturing guanidine-thiocyanate–containing buffer (RLT), which immediately inactivates RNases to ensure purification of intact RNA. In particular, to process the pituitary, the whole sample was homogenized by using a sonicator (4 cycles, power 60%). Instead, the gonads were weighted and 30 mg were disrupted and homogenized with the TissueLyser II (Qiagen) for 3.30 minutes at 30 Hertz. The pituitary and gonadal lysates were, then, centrifuged for 3 minutes at full speed to separate insoluble material eventually present. Instead, both GN-11 and GT1-7 were seeded in 60 mm Petri dishes, directly lysed in 600 µL of RLT, added with 6 µL of β-mercaptoethanol, and harvested with cell scrapers. The lysate was homogenized by the passage through a blunt 20-gauge needle, fitted to an RNase-free syringe, for at least five times. From this step, all the samples were processed in the same way. One volume of 70% ethanol was added to the homogenized lysate to provide appropriate binding conditions and the mixture was first transferred to an RNeasy Spin Column and then centrifuged for 15 seconds at 10,000 rpm, leading to the binding of total RNA to the membrane while the contaminants were efficiently washed away. Following a washing step with 350 µL of Buffer RW1, an on-column DNase digestion was performed with subsequent washes with Buffer RW1 and RPE. The

samples were then centrifuged to eliminate any possible carryover of ethanol and Buffer RPE. Finally, the RNA was eluted in RNase-free water.

5.10.3 RNA quantification

The amount of RNA was quantified with a biophotometer (Eppendorf, Milan, Italy), measuring the absorbance at 260 nm (wavelength of nucleic acid absorption) and at 280 nm (wavelength of nucleic acid and protein absorption). The nucleic acid concentration was calculated assuming that an absorbance at 260 nm of 1.0 is equivalent to 40 µg/mL single-stranded RNA. The ratio between the two absorbances was used to assess RNA purity: a value of ~2.0 is indicative of highly purified RNA.

5.11 REVERSE TRANSCRIPTION – POLYMERASE CHAIN REACTION (RT-PCR)

The RT-PCR technique was used to evaluate the cellular gene expression of TfR and FtH and to determine the X-box binding protein-1 (XBP-1) mRNA splicing at the hypothalamic level and in GN-11 cells.

One µg of total RNA was retro-transcribed into first-strand complementary DNA (cDNA) by using the iScript™ Reverse Transcription Supermix for RT-qPCR (Bio-Rad Laboratories, Segrate, Milan, Italy). The reaction was performed in 20 µL final volume, which contained the RNA template and the 5X iScript™ RT supermix. This latter was composed of *(i)* iScript RNase H+ MMLV reverse transcriptase; *(ii)* RNase inhibitor, to avoid the RNA degradation, *(iii)* deoxynucleotide triphosphates (dNTPs), *(iv)* oligo(dT) and random primers to initiate the reverse transcription: oligo(dT) primers anneal to poly(A) tails of mRNA while the random primers are often six nucleotides long with random base sequences; *(v)* buffer, to optimize the reaction; *(vi)* $MgCl_2$, a cofactor for the reaction; *(vii)* stabilizers. In parallel to this reaction, a no-RT control reaction, with iScript™ No-RT Control Supermix and the same amount of total RNA, was set up to detect genomic DNA amplicons. Moreover, in all the RTs, a reaction was performed replacing the RNA template with water as an internal negative control. The complete reaction, mixes were incubated in a thermal cycler (GeneAmp PCR System 2700 and 2900; Applied Biosystem, Monza, Italy) using the following protocol:

STEP	TEMPERATURE	TIME
Priming	25°C	5 minutes
Reverse transcription	42°C	30 minutes
RT inactivation	85°C	5 minutes

Table 3. *Conditions for RT reaction.*

The ribosomal protein 18S was used as internal control.

At the end of the RT, a final-time PCR was performed with 1 µL of the synthetized cDNA using GoTaq® Green Master Mix (Promega, Milan, Italy). The final volume of 25 µL contained:

COMPONENT	FINAL CONCENTRATION
GoTaq® Green Master Mix, 2X	1X
upstream primer	1 µM
downstream primer	1 µM
DNA template	50 ng
Nuclease-Free Water	

Table 4. *Components for a PCR reaction.*

The GoTaq® Green Master Mix, 2X, in turn, contained bacterially derived Taq DNA polymerase, dNTPs, $MgCl_2$, reaction buffers at optimal concentrations for efficient amplification of DNA templates by PCR and two dyes (blue and yellow) that allow monitoring of progress during electrophoresis. The conditions used for the amplification by PCR were the follows:

STEP	TEMPERATURE	TIME	CYCLES
Initial denaturation	95°C	5 minutes	1
Denaturation	94°	1 minute	40 (exception: 13 for 18S)
Annealing	see Table 8	1 minute	
Extension	72°C	1 minute	
Final extension	72°C	10 minutes	1

Table 5. *Conditions for PCR reaction.*

The sequences of primers and the relative annealing temperature used are listed in table 8.

Subsequently, amplification products were separated by 2% (4% in case of XBP-1) agarose gel electrophoresis and detected by ethidium bromide fluorescence on a UV trans-illuminator (Bio-Rad Laboratories). A Step Ladder (Sigma Aldrich) was used as electrophoresis marker for DNA. It contained 17 bands ranging from 50 bp to 3000 bp and it was chosen based on the size of amplification products obtained.

5.12 REAL-TIME QUANTITATIVE PCR (qRT-PCR)

qPCR, using 1 µL of cDNA, was carried out by using either a dye-based method (SYBR Green) or a probe-based one (TaqMan). Both these two techniques utilize a fluorescent signal to measure the amount of DNA in a sample. The real-time PCR detection system used was CFX96 C1000 Touch^{TM} Real-Time (Bio-Rad Laboratories) and all the reactions were performed in triplicate in 96-well PCR plates. For each primer set or probe, no-template controls, obtained replacing the cDNA with water, and -RT controls were included to detect possible contaminations. The ribosomal protein 18S was used as internal control. Relative differences in target mRNA levels between control and treated conditions were calculated with the ΔΔCt method.

5.12.1 SYBR Green

The reactions were carried out in 10 µL final volume containing:

COMPONENT	FINAL CONCENTRATION
iTaqTM Universal SYBR® Green Supermix (2X) (Bio-Rad Laboratories)	1X
sense primer (Sigma-Aldrich)	500 nM (exception: 300 nM for 18S)
antisense primer (Sigma-Aldrich)	500 nM (exception: 300 nM for 18S)
DNA template	50 ng
Nuclease-Free Water	

Table 6. *Components for a SYBR Green qRT-PCR.*

The iTaqTM Universal SYBR® Green Supermix (2X) was composed of: antibody-mediated hot-start iTaq™ DNA Polymerase, dNTPs, $MgCl_2$, SYBR® Green I Dye, enhancers, stabilizers and a blend of passive reference dyes (including ROX and fluorescein).
Table 8 reports the sequences of primers and the relative annealing temperature used whereas those of probes are listed in table 9.

5.12.2 TaqMan

The reactions were carried out in 20 µL final volume containing:

- cDNA template (50ng)
- 10 µL of SsoFast™ Probes Supermix (2x) (Bio-Rad Laboratories) containing antibody-mediated hot-start Sso7d-fusion polymerase, dNTPs, $MgCl_2$, enhancers and stabilizers.
- 1 µL of the specific probe (20X) consisting in a reporter dye (6-Carboxyfluorescein, FAM) on the 5' end and in a minor groove binder (MGB), nonfluorescent quencher on the 3' end (Custom Applied Biosystems™ TaqMan® MGB probes; Life Technologies, Inc., Milan, Italy). The probes are listed in Table 9.
- 8 µL of nuclease-free water

The thermal cycling protocol was:

STEP	TEMPERATURE	TIME	CYCLES
Polymerase Activation, DNA Denaturation	95°C	2 minutes	1
Denaturation	95°	10 seconds	40
Annealing and extension	60°C	30 seconds	

Table 7. *Conditions for TaqMan qPCR detection method.*

Table 8

Gene	T°	Forward Primer (5' – 3')	Reverse Primer (5' – 3')
CHOP	57°C	GTCCCTAGCTTGGCTGACAGA	TGGAGAGCGAGGGCTTTG
FSHβ	59°C	ATGGATTGTTCCAGGCAGAC	TCACTGCATGTGAGGGAAAG
FtH	57°C	CGAGATGATGTGGCTCTGAA	GTGCACACTCCATTGCATTC

GnRH	57°C	GGCCGGCATTCTACTGCTG	CTGCCTGGCTTCCTCTTCA
Gpr54	55°C	CAGTCCCAGGACACAATCCT	ACCAATGAGTTTCCGACCAG
KISS1	54°C	AGCTGCTGCTTCTCCTCTGT	GCATACCGCGATTCCTTTT
LHβ	59°C	TGGCCGCAGAGAATGAGTTC	CTCGGACCATGCTAGGACAGTAG
SOD2	57°C	TCTGGCCAAGGGAGATGTTA	CCTCCAGCAACTCTCCTTTG
TfR	57°C	TCGCTTATATTGGGCAGACC	CCATGTTTTGACCAATGCTG
XBP-1	64°C	TGAGAACCAGGAGTTAAGAACACGC	TTCTGGGTAGACCTCTGGGAGTTCC
18S	57°C	CTCGCTCCTCTCCTACTTGG	CCATCGAAAGTTGATAGGGC

Table 8. *Primer sequences.*

Table 9

Gene	**Applied Biosystems™ Custom TaqMan® 5' FAM - 3' MGB Probes** Assay ID
GnRH1	Mm01315605_m1
IL-6	Mm00446190_m1
KISS1	Mm03058560_m1
NPY	Mm03048253_m1
POMC	Mm00435874_m1
TNFα	Mm00443258_m1
18S	Hs99999901_s1

Table 9. *Probes.*

FAM: 6-carboxy-fluorescein (reporter fluorescent dye).

MGB: minor-groove-binder moiety.

5.13 GN-11 CELL MIGRATION STUDY

Cell migration studies were performed with a 48-well Boyden's chamber (Neuro Probe Inc, Gaithersburg, MD) on GN-11 cells, since this cell line is representative of immature GnRH neurons and is characterized by migratory properties. This study was specifically focused on the analysis of GN-11 microchemotaxis, which consists in cell migration along a chemical concentration gradient toward the highest concentration of chemoattractant.

The Boyden's chamber is composed by:

- an acrylic bottom plate with 48 wells of 25µL volume and a diameter of 3.2mm

- a single 25 x 80 mm piece of filter membrane between the top and bottom plates with a gasket positioned over the filter to create a seal
- a top plate with 48 holes which forms the upper wells when the chamber is assembled

To perform this assay, 28µL of 1% FBS were placed into the lower compartment of the chamber as chemoattractant. In this way, a slight positive meniscus was formed to prevent air bubbles from being trapped when the filter was applied. To this regard, a polyvinyl-pyrrolidone-free polycarbonate porous membrane (8 µm pores; Neuro Probe) was applied above the bottom plate. Previously, this membrane was washed once in acetic acid 0.5 M and twice in PBS without Ca^{++} and Mg^{++}. To improve the cell-adhesion during the migratory process, the membrane was pre-coated with gelatin (0.2mg/mL in PBS without Ca^{++} and Mg^{++}; Sigma-Aldrich) for 72 hours at 4°C. Subsequently, the silicone gasket and the top plate were applied and cell suspension was placed in the open-bottom wells of the upper compartment of the chamber.
In particular, to evaluate the effects of FAC at different doses and different time-points, on cell migration, GN-11 cells were treated for 24 h with 200 µM FAC, 200 µM DFO or both. Afterwards, cells were harvested in 0.05% trypsin/0.02% EDTA in PBS without Ca^{++} and Mg^{++} and washed in DMEM with 0.1% bovine serum albumin (BSA; Sigma-Aldrich). 0.10 x 10^6 cells in 50µL of DMEM/0.1% BSA were then pipetted into upper wells.
To investigate whether the MAPK/ERK1/2 signaling pathway was involved in the inhibition of iron-driven migration stimulated by FBS 1%, the cell suspension (0.10 x 10^6 /50µL of DMEM/0.1% BSA) was incubated for 30 minutes with 10 µM U0126, treated with FAC for 1 hour and then loaded in the open-bottom wells of the upper compartment of the chamber.
The filled chamber was placed in the cell incubator for 1.5 hours. After this step, the chamber was opened, the membrane recovered and the cells migrated trough the pores, thus attached to the side of the membrane directly in contact with the chemoattractant agent, were fixed in cold methanol for 1 minute. Cells remained on the membrane's portion close to the top plate represented the non-migrated cells and, after being washed with PBS without Ca^{++} and Mg^{++}, they were removed by using a scraper. Whereas, the fixed cells were stained using the Diff-Quick kit (Biomap, Milan, Italy), the dye excess was eliminated with Milli-Q water and the membrane was placed on a microscope slide. For quantitative analysis, stained cells were observed using a 20X objective on a light microscope and six random objective fields per well

were counted. The mean number of migrated cells/mm^2 was expressed as percentage of positive control (1% FBS was taken as 100%).

5.14 PROTEIN EXTRACTION

5.14.1 Hypothalamus

In order to isolate proteins from hypothalamic samples, the flow-through, consisting in the ethanolic lysate passed through the RNA binding column and, as such, deprived of nucleic acids, obtained with the NucleoSpin® RNA/Protein kit (Macherey-Nagel) was used. In detail, 150 µL of this solution were mixed with an equal volume of buffer PP (Protein Precipitator) and incubated at room temperature for 10 minutes. Subsequently, this mixture was centrifuged and the obtained pellet was washed with 50% ethanol, centrifuged 1 minute at 11,000 x g and the precipitate was dried 30 minutes. Subsequently, it was resuspended with 100 µL of PSB-TCEP (Protein Solving Buffer - Tris(2-carboxyethyl) phosphine hydrochloride, a reducing agent), incubated for 3 minutes at 95 – 98°C for a complete protein denaturation.

The protein quantification was performed by using the Protein Quantification Assay kit (Macherey-Nagel). The standard curve was created preparing dilution-series of BSA standards starting from a BSA reference protein stock solution (1 mg/mL in Protein Solving Buffer, PSB). A Quantification Reagent (QR) was added to standards and protein samples and the relative optical densities were measured through a spectrophotometer at 560 nm (Wallac Victor 3 1420 Multilabel Counter, PerkinElmer).

5.14.2 GN-11

To evaluate the possible effect of FAC on ERK1/2 signaling pathway, GN-11 cells were seeded in 60 mm Petri dish. Once confluent, they were starved (DMEM without FBS) overnight and treated with 200 µM FAC for 5 – 180 minutes and 24 hours. To harvest the cells, they were washed twice with warm (37°C) PBS containing Ca^{++} and Mg^{++} and lysed with 200 µL of Mammalian Protein Extraction Reagent (M-PER; Thermo Scientific, Rockford, Il) to which was added 1% protease (Complete Mini EDTA-free, Protease Inhibitor Cocktail Tablets; Roche Diagnostic, Mannheim, Germany) and phosphatase (PhosSTOP, Phosphatase Inhibitor Cocktail Tablets; Roche Diagnostic) inhibitors. The lysis procedure with M-PER was conducted on a shaker for 10 minutes at room temperature. Then, the lysate was collected and centrifuged 10

minutes at 14,000 rcf at 4°C and the supernatant, containing cytoplasmic and nuclear protein extract, was transfer to a new tube for analysis. The Thermo Scientific™ Pierce™ BCA Protein Assay based on bicinchoninic acid (BCA) was employed for the colorimetric detection and quantitation of total proteins. 2mg/mL of albumin standard was used to prepare a set of diluted standards in M-PER, used for the creation of the standard curve. The absorbance of standards and samples was measured at 550 nm on a plate reader (ELX 800 BioTek, Winooski, VT). Sample concentrations were interpolated according to a quadratic polynomial equation ($y = a + bx + cx^2$).

5.15 WESTERN BLOT ANALYSIS

Sample preparation, protein electrophoresis and transfer to a nitrocellulose membrane were performed through the Protein Electrophoresis workflow NuPAGE® (Life Technologies™). To 20 µg protein sample, deionized water, NuPAGE® Sample Reducing Agent (10X) (Novex®, Life Technologies™), containing 500 mM dithiothreitol (DTT), NuPAGE® LDS (lithium dodecyl sulfate) Sample Buffer (4X) (Novex®, Life Technologies™) were added and then samples were heated at 70°C for 10 minutes. In this way, the electrophoresis was conducted in denaturing and reducing conditions allowing the separation of proteins by their molecular mass. Samples and 7 µL of a Protein Standard (Novex™ Sharp Pre-Stained Protein Standard; Invitrogen™, Life Technologies™) were loaded in a precast polyacrylamide gel (NuPAGE™ 4-12% Bis-Tris Protein Gels, 1.5 mm, 10-well; Invitrogen™, Life Technologies™). The gel run using a specific running buffer to better resolve small/medium-sized proteins (NuPAGE™ MES SDS Running Buffer (20X); Invitrogen™, Life Technologies™), with the addition of an antioxidant (NuPAGE™ Antioxidant; Invitrogen™, Life Technologies™) in the upper (cathode) buffer chamber to maintain proteins in a reduced state during protein gel electrophoresis. This latter was performed with a constant voltage (200 V) and a run time of 35 minutes.

After performing electrophoresis, proteins were transferred to a nitrocellulose membrane (0.2 µm pore size) (iBlot™ Transfer Stacks, Invitrogen™, Life Technologies™) using a dry transfer device (iBlot™ Gel Transfer Device; Invitrogen™, Life Technologies™), selecting the P3 method, which allows a run of 7 minutes and 40 seconds at 20 V. Subsequently the membrane was washed in TBST (Tris-buffered saline, 0.1% Tween 20) and blocked in a solution of 5% BSA in TBST for 1 hour and 30 minutes. The primary antibody was diluted in either 5% BSA or 5% milk

solution and the membrane incubated overnight at 4°C. The day after, the membrane was washed in TBST and incubated for 1 hour and 30 minutes at room temperature with the horseradish peroxidase (HRP)-conjugated secondary antibody diluted in a 5% milk solution. After further washing steps, the membrane was exposed to chemiluminescence substrates (Clarity™ Western ECL Substrates; Bio-Rad) for 5 minutes. The images were acquired through the ChemiDoc™ XRS System (Bio-Rad) and analyzed by using the Image Lab™ 3.0 Software (Bio-Rad).

To evaluate the expression of several proteins on a same membrane, this latter was incubated 10 minutes at room temperature with the NewBlot™ Nitrocellulose 5X Stripping Buffer (LI-COR, Carlo Erba Reagents, Milan, Italy) before re-probing it with a different primary and subsequent secondary antibody.

The antibodies used in this project are listed in Table 10.

Table 10

NAME	kDa	PRIMARY ANTIBODY	SECONDARY ANTIBODY
Anti-pERK1/2	42 – 44	1:150	1:6,000 (anti-mouse)
Anti-ERK1/2	42 – 44	1:1,000	1:9,000 (anti-rabbit)
Anti-Tubulin	55	1:2,000	1:8,000 (anti-mouse)

Table 10. *Dilutions of used antibodies.*

pERK1/2 and ERK from Santa Cruz Biotechnology, Inc., Dallas. Texas, USA

Tubulin from Sigma-Aldrich

5.16 ANALYSIS OF THE DATA

Statistical analysis was performed using the Prism statistical analysis package (GraphPad Software, San Diego, CA). Data are expressed as mean of obtained values ± standard error of the mean (SEM). With regard to tables 11 and 12 showing the effects of iron-enriched diet (IED) on body weight and food intake, respectively, data are expressed as mean of obtained values ± standard deviation (SD). Differences between treatment groups were evaluated by Student's t-test when the comparison was made between two groups, or by ANOVA, followed by post-hoc Dunnet's or Tukey's test, for multiple comparisons; differences were considered significant at $p < 0.05$. Results are representative of three independent experiments.

6. RESULTS

6.1 ANIMAL STUDIES

6.1.1 Effect of IED on metabolic phenotype

Increased body iron stores and dietary iron intake have been associated with insulin resistance and type 2 diabetes mellitus and, as previously demonstrated by our research group [113], C57Bl/6 mice fed IED for 16 weeks developed a 40% increase in glucose levels. To confirm that in the animal model used in the present project, 11 weeks of IED could induce a dysmetabolic phenotype, mice were fasted overnight and, then, the basal glycemia was measured. IED led to a +57% increment of basal glycemia compared to control (CTR) mice, specifically 77.50 ± 4.16 mg/dL in CTR *vs* 122.0 ± 11.31 mg/dL in IED mice; p = 0.0042 [Fig. 7 A]. Moreover, IED was also associated to an increased Homeostatic Model Assessment of Insulin Resistance (HOMA-IR) index (+67%, p = 0.0038) [Fig. 7 B].

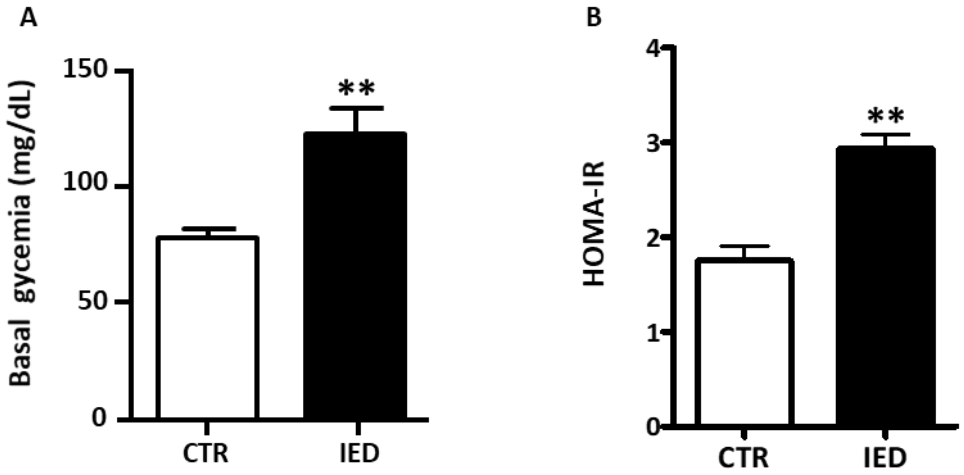

Fig. 7. *Effect of iron enriched diet (IED) on metabolic phenotype. Basal glycemia was measured after an overnight fasting in mice fed IED compared to mice fed chow diet at week 11 of treatment. White bar is CTR mice and the black one represents IED mice. Data are representative of 15 mice and are expressed as mean ± SEM. Differences between treatments were assessed by Student's t-test, **p<0.01.*

6.1.2 Phenotypic effects of IED

The carbonyl-iron supplementation was well tolerated, although a significant reduction of body weight was found in IED mice compared to the CTR group. Specifically, body weight differences between the two groups were already significant after 1 week of IED (-2.5 g *vs* CTR, $p<0.05$) and progressively increased throughout the 11-week time frame until reaching 5.41 g of difference at the end of the treatment [Table 11; Fig 8]. This result is in line with previous studies using the same supplemented diet [113, 133].

	Body weight (g)			
Weeks of diet	**CTR** (Mean ± SD)	**IED** (Mean ± SD)	**Δ** (mean CTR - mean IED) (g)	**p value**
1	18.79 ± 1.406	16.29 ± 1.891	2.50	0.04493
2	20.40 ± 1.324	17.18 ± 1.697	3.22	0.01009
3	21.79 ± 1.300	17.59 ± 1.637	4.19	0.00204
4	22.32 ± 1.378	17.63 ± 1.612	4.69	0.00113
5	22.69 ± 1.148	18.49 ± 1.530	4.20	0.00117
6	23.22 ± 1.352	18.48 ± 1.745	4.74	0.00135
7	23.85 ± 1.247	19.13 ± 1.787	4.72	0.00129
8	24.66 ± 1.244	19.21 ± 1.660	5.45	0.00037
9	24.46 ± 1.168	19.38 ± 1.795	5.09	0.00072
10	24.64 ± 1.080	19.48 ± 1.706	5.16	0.00045
11	25.29 ± 1.256	19.88 ± 1.519	5.41	0.00028

Table 11. *Effect of iron-enriched diet (IED) on body weight. Mice were fed chow-diet (control - CTR - group) or IED (3% carbonyl-iron), respectively, for 11 weeks. Body weight difference between CTR and IED is reported for each week. Fifteen mice per group were analyzed. Differences between the two groups were assessed by Student's t-test and the p values are reported. Data are expressed as mean ± SD.*

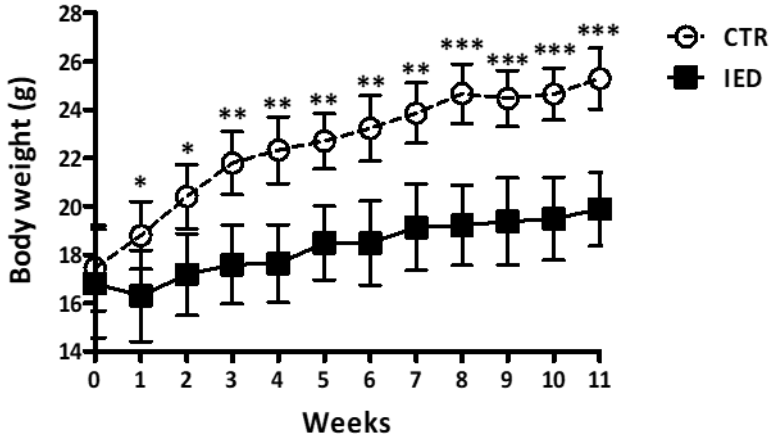

Fig. 8. *Effect of iron-enriched diet (IED) on body weight. Mice were fed chow-diet (control group - CTR) or IED group (3% carbonyl-iron) for 11 weeks, respectively. White circles are controls; black squares are IED mice. Fifteen mice per group were analyzed. Data are expressed as mean ± SEM. Differences between treatments were assessed by Student's t-test, *p < 0.05, **p < 0.01 and ***p < 0.001.*

In parallel with the lower body weight gain, IED mice showed a significant decreased weekly food intake (17.9 ± 0.98 g per mouse) if compared to the CTR group (23.8 ± 0.97 g, p< 0.0001) [Table 12]. This latter finding could explain the reduced body weight associated to IED-feeding.

	CTR		IED		
Weeks of diet	**Food intake per mouse (g)**	**Mean ± SD (g)**	**Food intake per mouse (g)**	**Mean ± SD (g)**	**p value**
1	22.46	23.84 ± 0.972	17.43	17.99 ± 0.976	p < 0.0001
2	23.17		19.03		
3	23.56		19.08		
4	24.13		19.73		
5	23.69		18.08		
6	22.55		17.93		
7	23.74		17.45		
8	23.62		17.18		
9	24.58		16.42		
10	25.23		17.35		
11	25.48		18.23		

Table 12. *Effect of iron-enriched diet (IED) on food intake. Mice were fed chow-diet (control group - CTR) or IED (3% carbonyl-iron) for 11 weeks, respectively. Data are expressed as weekly food intake per mouse and mean food intake per group. Fifteen mice per group were analyzed. Differences between the two groups were assessed by Student's t-test and the p value is reported. Data are expressed as mean ± SD.*

The effect of IED on perigonadal fat pad weight was in line with reduced body weight and food intake. Indeed, IED mice showed a significant decrement of perigonadal fat pad weight (CTR: 0.80 ± 0.1 g; IED: 0.46 ± 0.04 g) [Fig 9].

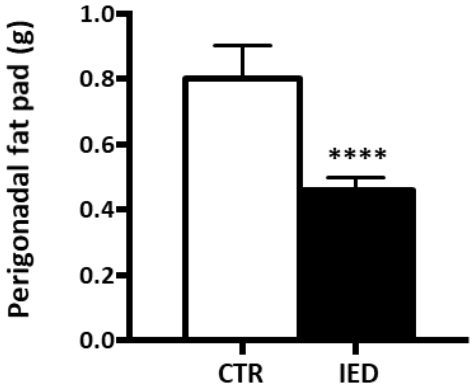

Fig. 9. *Effect of iron-enriched diet (IED) on perigonadal fat pad. Mice were fed chow-diet (control group - CTR) or IED (3% carbonyl-iron) for 11 weeks, respectively. White bar is CTR; black bar is IED group. Fifteen mice per group were analyzed. Data are expressed as mean ± SEM. Differences between treatments were assessed by Student's t-test, ****p < 0.0001.*

Serum leptin levels were reduced in mice fed with IED (-56% *vs* CTR, $p < 0.05$) [Fig 10].

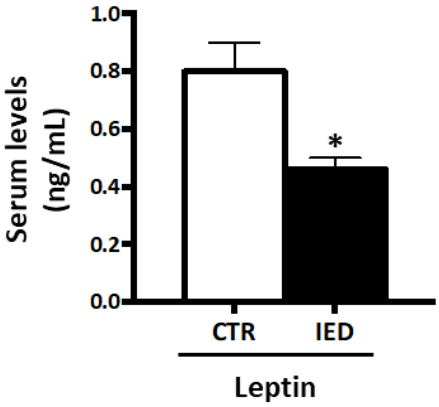

Fig. 10. *Effect of iron-enriched diet (IED) on serum leptin levels. Mice were fed chow-diet (control group - CTR) or IED (3% carbonyl-iron) for 11 weeks, respectively. White bar is CTR; black bar is IED group. Fifteen mice per group*

*were analyzed. Data are expressed as mean ± SEM. Differences between treatments were assessed by Student's t-test, *p < 0.05.*

Upon the collection of these data, which confirmed an IED-induced dysmetabolic phenotype, the hypothalamic gene expression of the orexigenic signal neuropeptide Y (NPY) and of the anorexigenic pro-opiomelanocortin (POMC), both involved in the regulation of energy balance, appetite and reproductive function, were evaluated. IED led to a significant increment of NPY mRNA levels (+ 158% *vs* CTR, p < 0.05) [Fig 11 A] as well as to a reduction of POMC gene expression, though not reaching a statistical significance (-52% *vs* CTR, p = 0.247) [Fig 11 B].

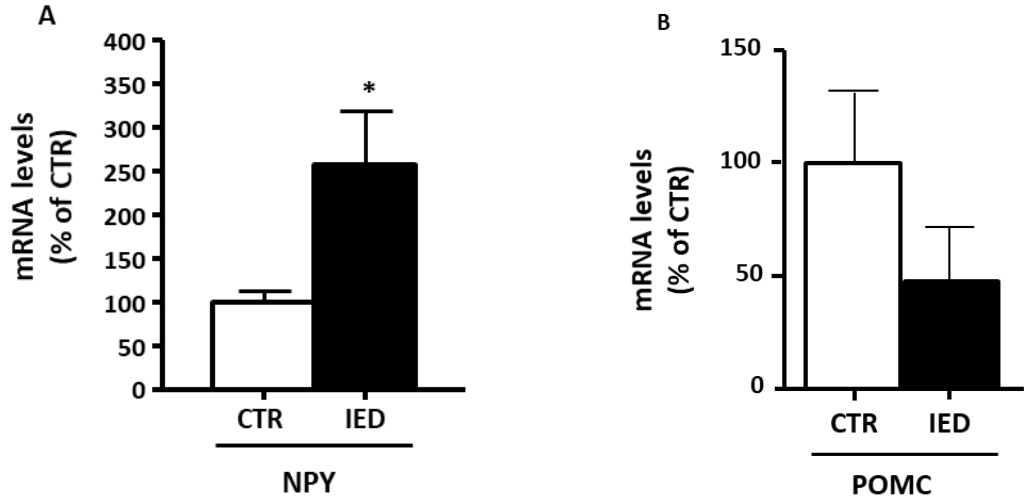

Fig. 11. *Effect of iron-enriched diet (IED) on hypothalamic gene expression of neuropeptide Y (NPY) and pro-opiomelanocortin (POMC). Mice were fed chow-diet (control group - CTR) or IED (3% carbonyl-iron) for 11 weeks, respectively. White bars are CTR and black bars are IED mice. Fifteen mice per group were analyzed. Data are expressed as percentage of control (mean ± SEM). Differences between treatments were assessed by Student's t-test, *p < 0.05.*

6.1.3 Effect of IED on iron homeostasis on the hypothalamus-pituitary-gonadal axis

To evaluate the effect of iron overload on the reproductive axis, a detailed analysis of testes, pituitary and hypothalamus was performed.

First of all, to investigate whether IED had an impairment at the testicular level, at sacrifice testes were isolated and their weight and length evaluated. IED led to a significant reduction (-22%) in testicular weight (CTR: 0.21 ± 0.018 g; IED: 0.16 ± 0.022 g; p < 0.01; [Fig. 12 A]) and in longer diameter (-21%; CTR: 7.73 ± 0.45 mm; IED: 6.1 ± 0.42 mm; p < 0.01; [Fig. 12 B]). Since

the IED-fed mice showed a reduction of their body weight, probably due to a decreased food intake (as shown in table 12), the data collected from this testicular analysis were adjusted for body weight, which was, in turn, normalized for the food intake. Interestingly, the differences were maintained for both the testicular weight and long diameter. When compared to CTR mice in the first case, iron overload led to a reduction of 30% (CTR: 0.21 ± 0.011 g; IED: 0.14 ± 0.018 g; $p < 0.001$; [Fig. 12 C]). With regard to the testicular long diameter, IED was associated to a decrement of 29% (CTR: 7.45 ± 0.28 mm; IED: 5.27 ± 0.32 mm; $p < 0.001$; [Fig. 12 D]).

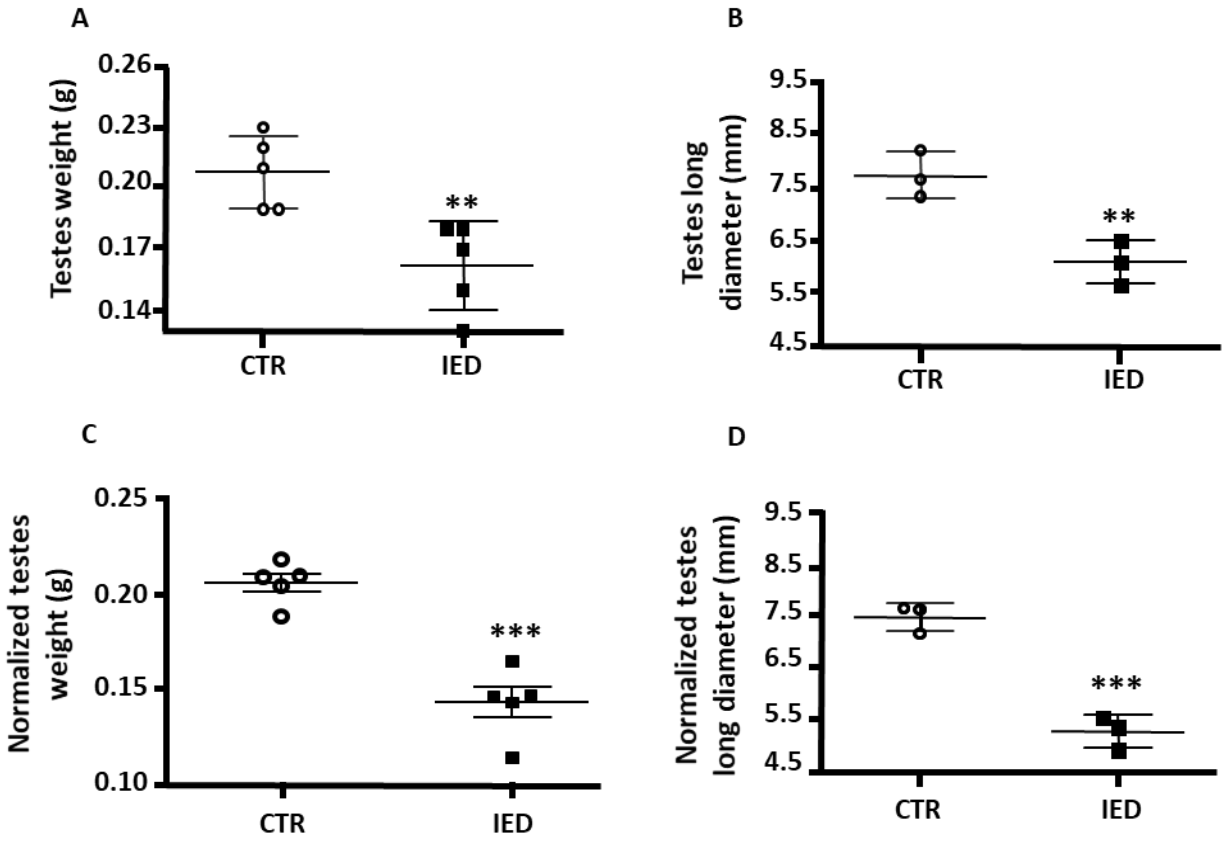

Fig. 12. *Effect of iron-enriched diet (IED) on testes. Panels A and B show absolute values of testes weight (g) and long diameter (mm), respectively. Panels C and D show normalized testes weight (g) and long diameter (mm), respectively. White circles are CTR mice and black squares are IED mice. Panels A and C are representative of 5 mice whereas that of panels B and D were 3. Data are expressed as mean ± SEM. Differences between treatments were assessed by Student's t-test, **p < 0.01 and ***p < 0.001.*

To further investigate a possible gonadal defect mediated by iron overload the testicular morphology of both groups was analyzed. To this purpose, in a subgroup of 5 animals, eosin and hematoxylin were used to stain the seminiferous tubules and this technique revealed that IED led to a reduction of the seminiferous tubules' number. As shown in figure 13B, that were

significantly reduced (-20%, $p < 0.01$) in mice fed IED compared with CTR. A representative stained section is reported in figure 13A.

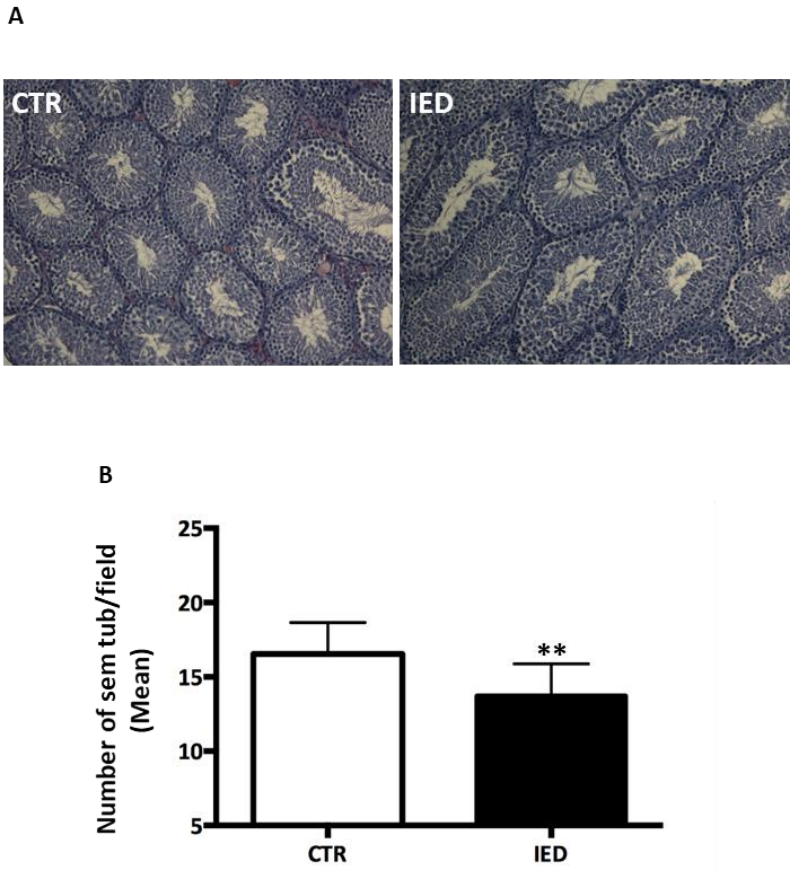

Fig. 13. *Effect of iron-enriched diet (IED) on seminiferous tubules' number. White bar is control (CTR) mice and the black one is IED mice. Data are representative of 5 mice. Data are expressed as mean ± SEM. Differences between treatments were assessed by Student's t-test, **p < 0.01. sem, seminiferous; tub, tubules.*

The project continued analyzing possible impairments in hormones involved in the reproductive function. In particular, circulating level of testosterone (T) and luteinizing hormone (LH) were evaluated. As shown in figure 14, 11 weeks of IED were associated to a pronounced reduction of serum levels of both T (IED: 0.24 ± 0.10; CTR: 1.39 ± 0.55 ng/mL; $p = 0.058$; [Fig. 14 A]) and LH (IED: 0.25 ± 0.15; CTR: 1.82 ± 0.43 ng/mL; $p < 0.01$; [Fig. 14 B]).

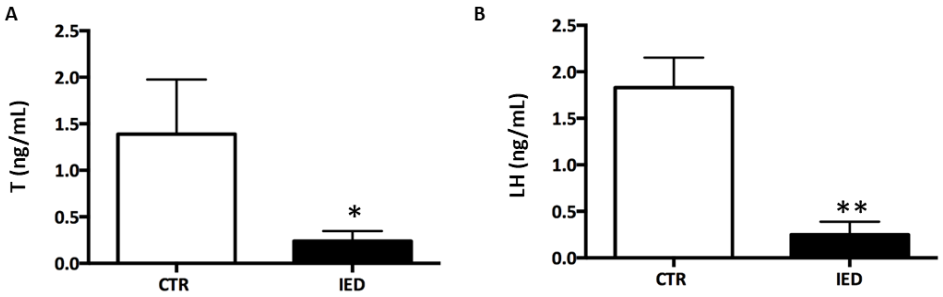

Fig. 14. *Effect of iron-enriched diet (IED) on reproductive function. White bars are control (CTR) mice and the black ones are IED mice. Data are representative of 15 mice. Data are expressed as mean ± SEM. Differences between treatments were assessed by Student's t-test, *p < 0.05 and **p < 0.01.*

Pituitary levels of LH, together with those of follicle-stimulating hormone (FSH), were also specifically measured. Since these two gonadotropins consist of a common α-subunit and a hormone-specific β-subunit, which confers the specific actions of the glycoproteins, LHβ and FSHβ were taking into account for the analysis. Dietary iron overload did not affect pituitary mRNA levels of FSHβ (p = 0.745 [Fig. 15 A]), whereas those of LHβ showed a trend toward reduction without reaching a statistical significance (-25% *vs* CTR, p = 0.156; [Fig. 15 B]).

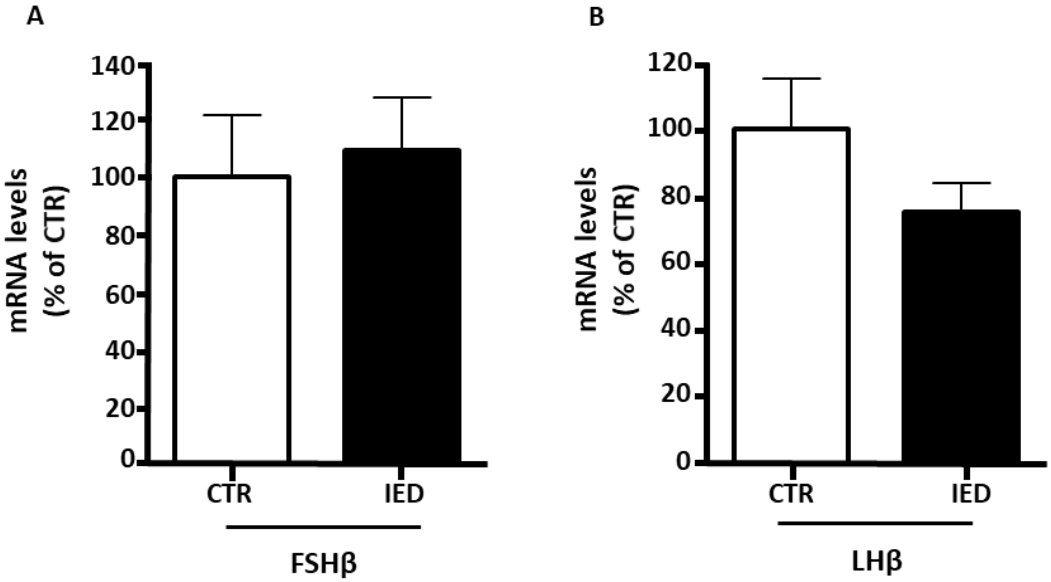

Fig. 15. *Effect of iron-enriched diet (IED) on reproductive function. White bars are control (CTR) mice and the black ones are IED mice. Data are representative of 15 mice. Data are expressed as percentage of control (mean ± SEM).*

6.1.4 Iron accumulation at the hypothalamus-pituitary-gonadal axis

6.1.4.1 Testes

To elucidate the effect of iron overload on the hypothalamic-pituitary-gonadal (HPG) axis, these three different compartments were analyzed in both the CTR and the IED group.

Starting from testes, the atomic absorption spectrometry (AAS) showed that 11 weeks of IED led to a significant accumulation (+47%) of the metal at this level with respect to mice fed with standard diet (IED: 9.80 ± 0.82; CTR: 6.57 ± 0.83 µg/100 mg dry tissue [Fig. 16 A]).

Physiologically, iron balance is controlled by mechanisms involving the Iron Regulatory Proteins (IRPs) and the Iron Responsive Elements (IREs). When an excess of this metal is present, the IRP/IRE system leads, on one side, to a decrease in transferrin receptor (TfR) mRNA expression and, on the other side, to an increment of the translation of ferritin (Ft) mRNA. This results in a reduction of iron internalization together with the storage of excessive intracellular iron into Ft.

Eleven weeks of IED did not impair the testicular gene expression of TfR ($p = 0.131$; [Fig. 16 B]) and of Ft, specifically FtH ($p = 0.517$; [Fig. 16 C]).

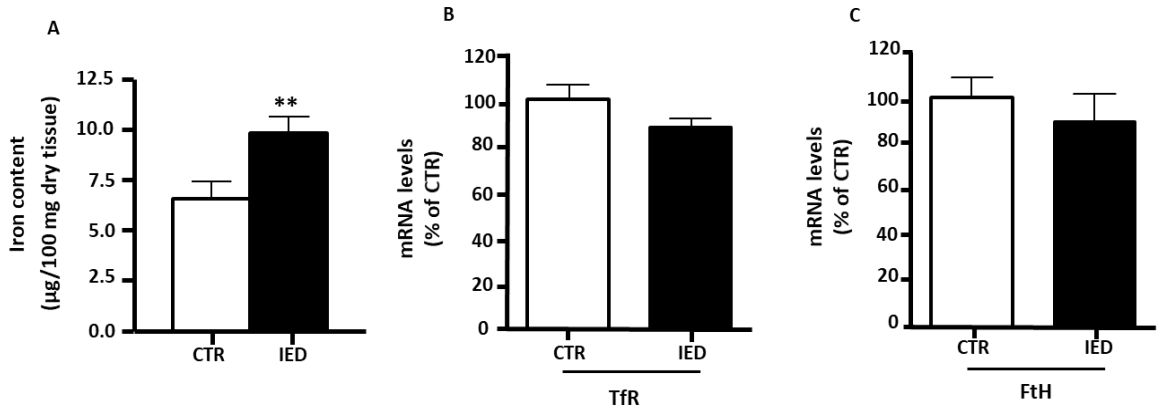

Fig. 16. *Evaluation of iron content and homeostasis in testes. Panel A shows testes iron content evaluated by atomic absorption spectrometry. Panel B and C report testicular gene expression of transferrin receptor (TfR) and ferritin H (FtH), respectively. White bars are control (CTR) mice and the black ones are iron-enriched diet (IED) mice. Data are representative of 15 mice. In panels A data are expressed as mean ± SEM. In panels B and C, data are expressed as percentage of control (mean ± SEM). Differences between treatments were assessed by Student's t-test, **p < 0.01.*

6.1.4.2 Pituitary

At the pituitary level, iron content was not quantified by AAS because of its size and methodological limitations. Therefore, since Ft is widely considered as a surrogate biomarker of iron content [134], mRNA levels of FtH were used to this purpose. RT-qPCR showed that 11 weeks of dietary iron overload resulted in a significant increment of pituitary gene expression compared to CTR mice (+48%, $p < 0.05$; [Fig. 17]), suggesting iron accumulation at this site.

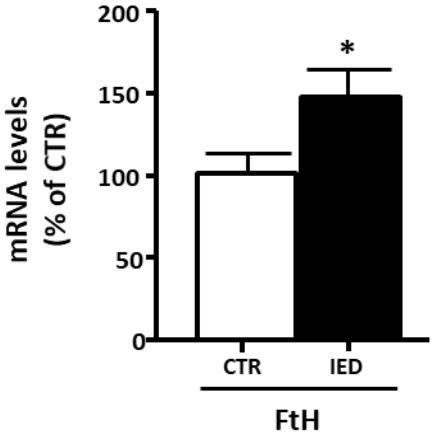

Fig. 17. *Evaluation of iron content in pituitary. White bar represents control (CTR) mice and the black one the iron-enriched diet (IED) mice. Data are representative of 15 mice. Data are expressed as percentage of control (mean ± SEM). Differences between treatments were assessed by Student's t-test, *p < 0.05.*

6.1.4.3 Hypothalamus

Following the evaluation of iron accumulation at the testicular and pituitary levels, AAS was performed on whole hypothalamus. No differences in iron content were found between IED and CTR mice (IED: 6.37 ± 1.91; CTR: 6.37 ± 2.28 µg/100 mg dry tissue; [Fig 18 A]).

Furthermore, to exclude the possibility that 11 weeks of dietary iron overload could determine a hypothalamic iron accumulation, the gene expression of TfR and FtH was evaluated. RT-qPCR did not show any change in TfR ($p = 0.261$ [Fig 18 B]) and FtH ($p = 0.245$ [Fig 18 C]) mRNA levels between IED and CTR mice.

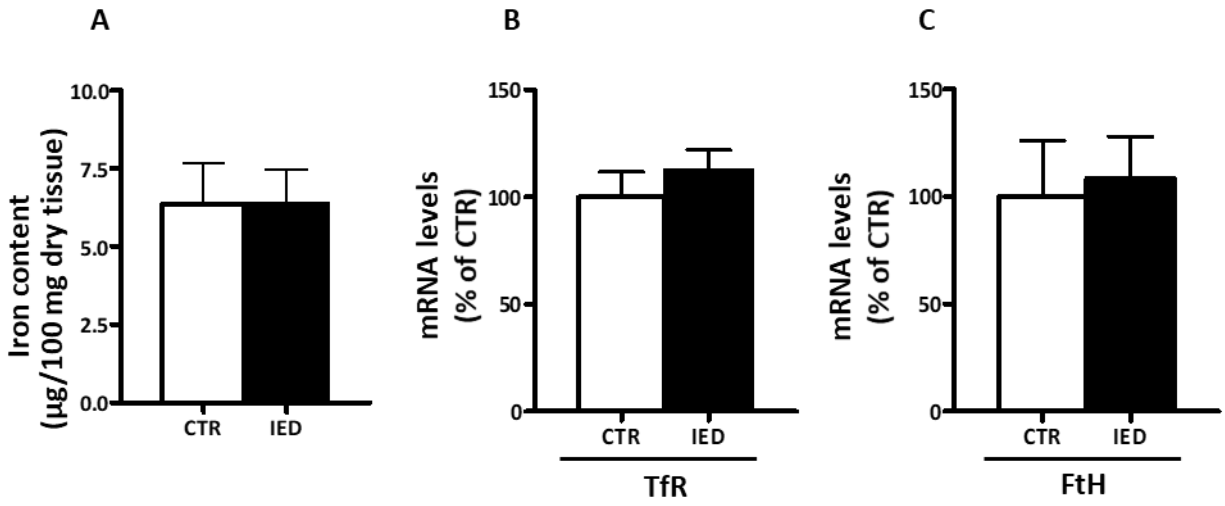

Fig. 18. *Evaluation of iron content and homeostasis in hypothalamus. Panel A shows hypothalamic iron content evaluated by atomic absorption spectrometry. Panels B and C show hypothalamic transferrin receptor (TfR) and ferritin H (FtH) mRNA levels, respectively. White bars are control (CTR) mice and the black ones are iron-enriched diet (IED) mice. Data are representative of 15 mice. In panel A data are expressed as mean ± SEM. In panels B and C data are expressed as percentage of control (mean ± SEM).*

6.1.5 Effect of IED on hypothalamic and pituitary factors controlling reproduction

Since IED led to an accumulation of iron in the pituitary, the following step was to evaluate whether iron overload had an impact on central factors governing the reproductive system, even in the absence of a significant deposition of this metal at the hypothalamic level. To this purpose the hypothalamic gonadotropin-releasing hormone (GnRH) gene expression was evaluated together with the mRNA levels of kisspeptin (KISS1) and the related G protein-coupled receptor 54 (GPR54), which are two master key regulators of reproduction and, acting upstream of GnRH, they control the GnRH release.

Mice fed with IED showed a significant increment in hypothalamic GnRH gene expression (+34%, $p < 0.01$; [Fig. 19]) compared to mice fed with a standard diet. Conversely, the RT-qPCR performed on hypothalamic samples showed that the levels of Kiss1 and GPR54 were not different between the IED and the CTR group [Fig. 19].

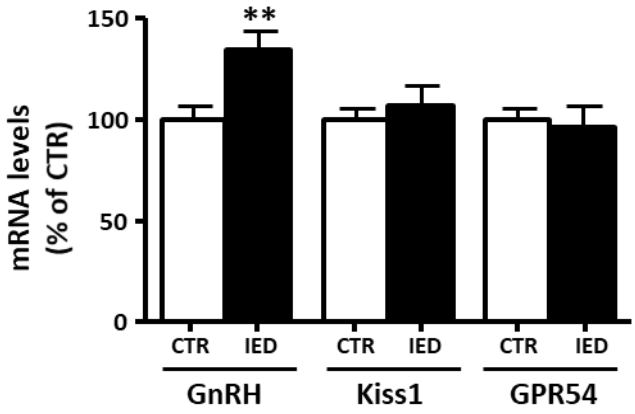

Fig. 19. *Effect of iron on reproductive system. White bars are control (CTR) mice and the black ones are iron-enriched diet (IED) mice. Data are representative of 15 mice. Data are expressed as percentage of control (mean ± SEM). Differences between treatments were assessed by Student's t-test, **p < 0.01.*

In adults, GnRH neurons project to the median eminence (ME), where they release GnRH into the portal blood vessels of the pituitary gland. Therefore, since the gene expression of GnRH was increased in mice fed with IED, the presence of GnRH neurons projections at the ME was assessed by measuring the GnRH pixel intensity in ME neurites of IED and CTR mice. The ME of mice fed with IED was much more innervated (1.5 fold) by GnRH-positive neurites with respect to mice fed a standard diet [Fig. 20]. A possible explanation for this increment is the lack of a negative feedback driven by circulating T. Moreover, as a positive control, the GnRH pixel intensity was evaluated also in ME of $HFE^{-/-}$ mice, a model of human genetic hemochromatosis. As expected, it was more intense with respect to CTR mice (1.4 fold) [Fig. 20].

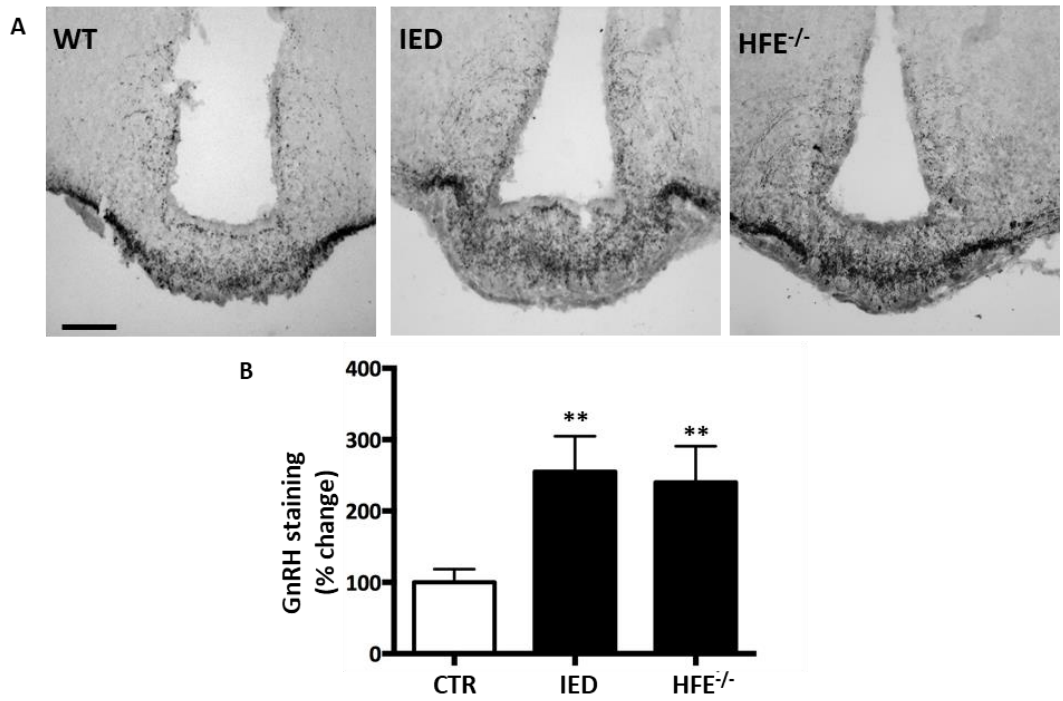

Fig. 20. *Effect of iron on reproductive system. Panel A shows GnRH neurites staining in the median eminence of mice fed standard diet or IED and HFE$^{-/-}$ mice. Pictures are referred to sagittal sections of 20 mm. Panel B reports the GnRH quantification expressed as pixel intensity. White bar is control (CTR) mice and the black ones are iron-enriched diet (IED) mice. Data are representative of 3 mice. Data are expressed as percentage of control (mean ± SEM). Differences between treatments were assessed by one-way ANOVA, **p < 0.01. In panel A, scale bar was 50 mm.*

6.1.6 Effect of IED on hypothalamic oxidative and endoplasmic reticulum stress

Despite the essential roles of iron, this transition metal can lead to the generation of hydroxyl radicals, triggering oxidative stress, lipid peroxidation, and DNA damage. Therefore, it was evaluated whether 11 weeks of dietary iron overload could cause oxidative and endoplasmic reticulum stress.

Superoxide dismutase (SOD) is a major antioxidant enzyme which neutralizes superoxide anions forming hydrogen peroxide and molecular oxygen. Among the different existing isoforms of SOD, SOD2 is one of the most important. It is localized within mitochondria and acts as primary mitochondrial antioxidative enzyme, eliminating the superoxide generated from molecular oxygen in the respiratory chain [135]. For these proprieties, SOD2 was analyzed as an indicator of oxidative stress. Relative to the endoplasmic reticulum (ER) stress, briefly, it consists in an imbalance between the protein folding capacity of the organelle and the functional demand that is placed on it. This imbalance leads to accumulation of unfolded or

misfolded proteins in the ER lumen. In order to restore ER homeostasis, cells trigger the ER stress response, also known as the unfolded protein response (UPR) [136]. Since a prolonged or excessive ER stress induces the expression of CAAT/enhancer binding protein (C/EBP) homologous protein (CHOP), which, in turn, promotes apoptotic cell death, the expression of this gene was studied to analyze the possible ER stress induced by iron overload. Moreover, UPR can activate several pathways, among which the Inositol Requiring Enzyme 1 alpha (IRE1α). Once activated, this latter induces an unconventional splicing of the mRNA encoding the X-box Binding Protein-1 (XBP-1) transcription factor, which subsequently regulates the transcription of genes involved in ER homeostasis [137]. Therefore, XBP-1 was studied as an index of early stage endoplasmic reticulum stress response.

In the current project IED did not change the hypothalamic gene expression of SOD2 (-18% *vs* CTR, p = 0.095; [Fig. 21 A]). Similarly, no differences between IED and CTR mice were detected when mRNA levels of CHOP (p = 0.342; [Fig. 21 A]) and the XBP-1 spliced form (corresponding to a 300-bp band; [Fig. 21 B]) were analyzed. These results suggest that iron overload did not cause oxidative and ER stress at central level.

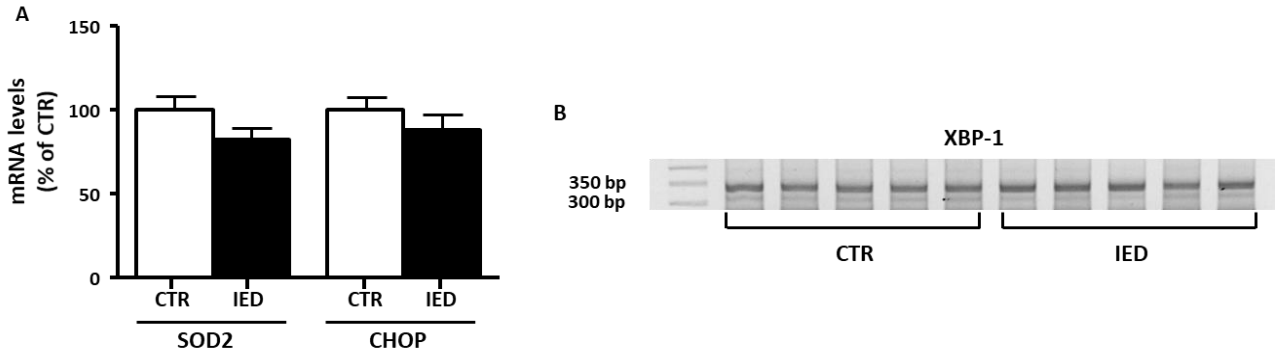

Fig. 21. *Effect of iron on hypothalamic oxidative and endoplasmic reticulum stress. White bars are control (CTR) mice and the black ones are iron-enriched diet (IED) mice. Data were obtained by 5 different mice belonging to each group and data in panel A are expressed as percentage of control (mean ± SEM).*

6.1.7 Effect of IED on the inflammatory pathway

Dietary iron overload did not impact the hypothalamic gene expression of the pro-inflammatory cytokine interleukin-6 (IL-6) (p = 0.752; [Fig. 22 A]) when compared to control mice. Conversely, the mRNA levels of TNFα were significantly increased in IED mice (+102%, p < 0.05; [Fig. 22 B]).

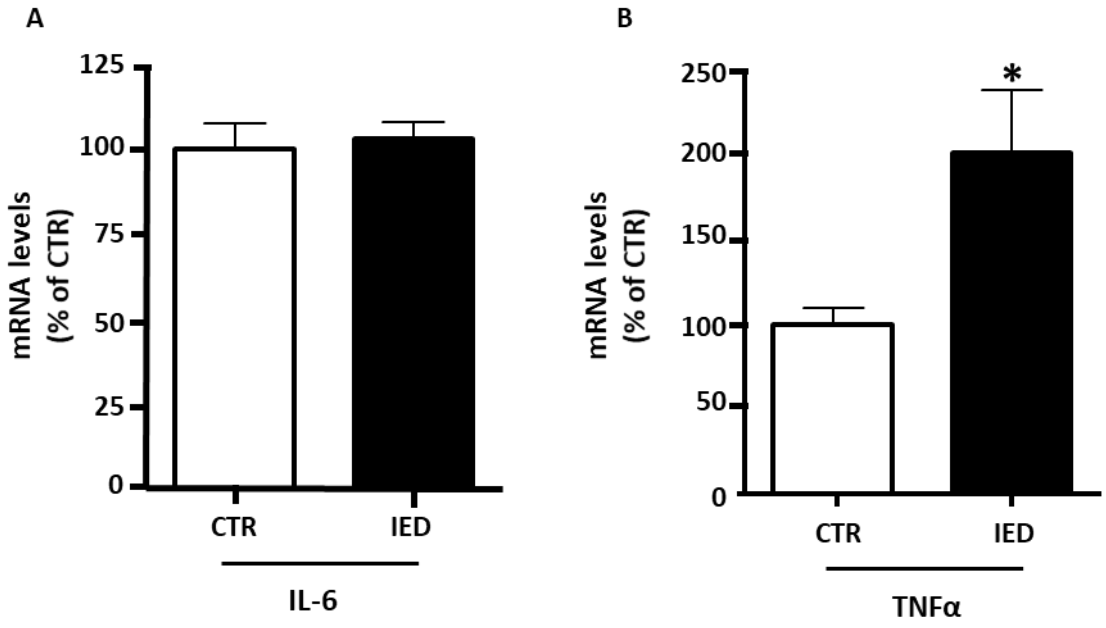

Fig. 22. *Effect of iron on inflammation. White bar is control (CTR) mice and the black one represents iron-enriched diet (IED) mice. Data are representative of 15 mice. Data are expressed as percentage of control (mean ± SEM). Differences between treatments were assessed by Student's t-test, *p < 0.05.*

6.2 *IN VITRO* STUDIES

GnRH neurons can be analyzed *in vitro* using immortalized GN and GT1 cell lines. These *in vitro* models, obviously lacking blood-brain barrier (BBB), have been used as a tool to further investigate the iron overload effects. These cells were isolated from brain tumors induced in transgenic mice by genetically targeting the expression of the simian virus-40 (SV40) large T antigen oncogene fused with a portion of the promoter region of rat (GT1 cells) and human (GN cells) LHRH gene. Of note, GT1 cells have been derived from a tumor developed in the hypothalamus, the site reached by LHRH neurons at the end of their migration and, for this reason, they are representative of post-migratory neurons. Conversely, GN cells were obtained from the olfactory bulb, where the LHRH neurons still possess their migratory ability. Therefore, this cell line retains the phenotypic characteristics of immature LHRH neurons and show high migratory activity *in vitro*, responding to fetal bovine serum (FBS) as a chemotactic stimulus [138, 139]. In the current project, the subclones GT1-7 [Fig. 23 A], polygonal and branched cells, which grow in colonies interconnected by neurite processes, and GN-11 [Fig. 23 B], with a bipolar shape, which grow homogeneously without forming clusters, were employed.

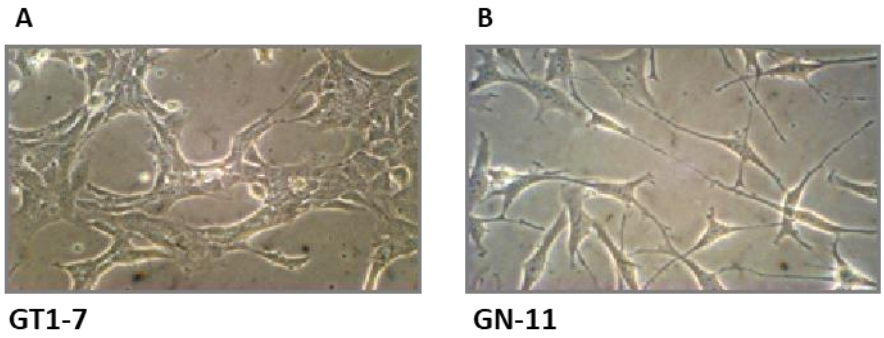

Fig. 23. *In vitro cell-based models. Panel A shows GT1-7 cells; Panel B shows GN-11 cells.*

Because of their characteristics, in the current project, GT1-7 cells were employed to measure the secretion of the hormone GnRH, while GN-11 cell line was used as a tool to study neuronal migration.

To generate a hypothalamic model of *in vitro* iron overload, cells were treated with Ferric Ammonium Citrate (FAC). This compound is a soluble form of low-molecular weight iron and it is a relatively stable formulation of ferric citrate, a species of free iron that increases in hereditary hemochromatosis and other conditions of iron overload [140]. Moreover, FAC is the main form of non-transferrin bound iron (NTBI), which can promote oxidative injury [141]. For all these properties, FAC is often used in *in vitro* experiments to mimic an iron overload environment.

6.2.1 Iron accumulation in GT1-7 and GN-11 cells

Initially, the basal intracellular iron concentration was measured in both GT1-7 and GN-11 cell lines. After 24 hours in their culture medium (DMEM + 10% fetal bovine serum – FBS –), the iron content of GN-11 cells (0.013 ± 0.018 µg/10^6 cells, *ie* 203.7 µg/L) was almost the double compared to that determined in GT1-7 cell line (0.0077 ± 0.46 µg/10^6 cells, *ie* 103.5 µg/L) [Fig. 24].

Moreover, to evaluate whether FAC could lead to iron accumulation in these two *in vitro* models, GT1-7 and GN-11 cells were treated for 24 hours with 200 µM of FAC and, subsequently, AAS was used to quantify the intracellular iron concentration. As shown in figure 24, iron content was significantly increased by 5-fold in FAC-treated GT1-7 cells (0.042 ± 0.46 µg/10^6 cells, *ie* 382.7 µg/L; $p < 0.0001$) and by 10-fold in GN-11 cells treated with FAC (0.13 ±

0.52 µg/10^6 cells, *ie* 3043.2 µg/L; $p < 0.0001$) compared to their respective controls (no FAC) [Fig. 24].

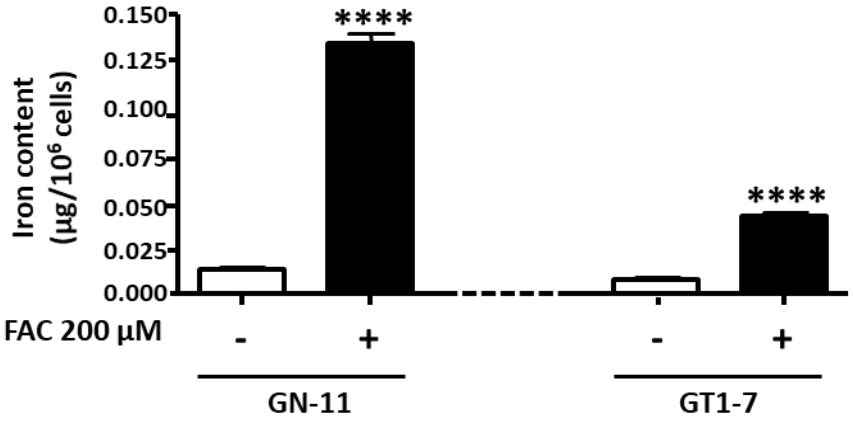

Fig. 24. *Effect of 24-h treatment with ferric ammonium citrate (FAC; 200 mM) on neuronal immature (GN-11) and mature (GT1-7) murine cells iron accumulation. White bars are controls and the black ones are FAC treated. n = 6 per group. Data are expressed as mean ± SEM. Differences between treatments were assessed by Student's t-test, ****p < 0.0001.*

After assessing iron accumulation in the two *in vitro* cell-based models, the possible cellular toxicity of FAC was evaluated. Since iron levels were higher in GN-11 cell line compared to GT1-7 cells, both in basal condition and after FAC treatment, the effect of FAC on cell viability and morphology was analyzed specifically in GN-11 cell line. These cells were treated with FAC 200 and 500 µM for 3 and 24 hours and viability was assessed through two methods: the ATPlite™ 1step assay and the Trypan Blue exclusion test. As a result, FAC at any dose and time did not affect GN-11 viability, as shown in figure 25 panels A and B (no differences in ATP content) and in figure 25 C and D (no differences in cell number). Similarly, 200 and 500 µM FAC for 24 hours did not change the cell morphology [Fig. 25 E, F, G].

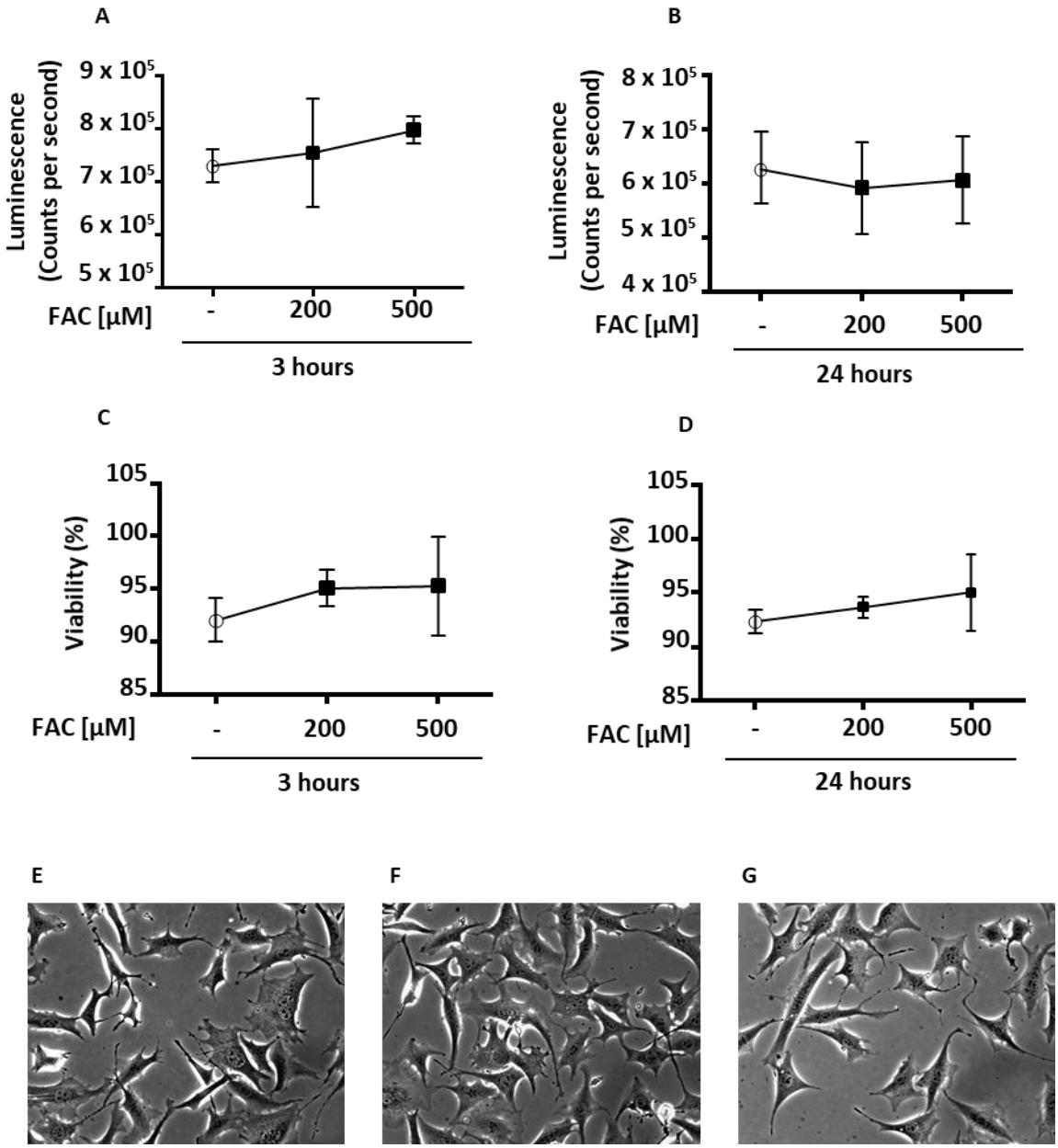

Fig. 25. *Effect of ferric ammonium citrate (FAC) on GN-11 viability and morphology. ATPliteTM 1step assay was used to evaluate the effect of 200 and 500 µM FAC for 3 and 24 hours on GN-11 viability, respectively (Panels A and B). Trypan Blue exclusion test was used to test the effect of 200 and 500 µM FAC for 3 and 24 hours on GN-11 viability, respectively (Panels C and D). Panels E, F and G show the morphology of GN-11 cells in basal condition (panel E), after 24 hours of treatment with 200 µM FAC (panel F) and with 500 µM FAC (panel G). White circles are controls (no FAC), black squares are FAC treated. n = 6 per group. Data are expressed as mean ± SEM.*

6.2.2 Effect of FAC on iron homeostasis in GN-11 and GT1-7 cells

To further evaluate whether GN-11 and GT1-7 cells could be suitable models to study iron overload, the expression of genes involved in iron homeostasis was assessed in the two cell

lines cultured in basal conditions (DMEM +10% FBS). In detail, a final-time PCR was performed to analyze the gene expression of TfR and FtH; the ribosomal protein 18S was used as internal control and water as an internal negative control. As a result, both the cell lines express essential genes for iron internalization (TfR) and storage (FtH) [Fig. 26], confirming the validity of these models for the study of iron overload effects.

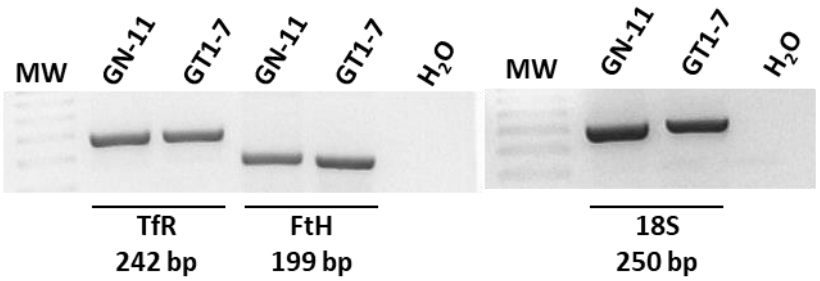

Fig. 26. *Expression of TfR and FtH in GN-11 and GT17 cells. MW, molecular weight; bp, base pairs.*

The ability of the two cell lines to adapt to exogenous iron overload was investigated by analyzing possible variations of TfR and FtH mRNA levels. In particular, in GN-11 cells, treatment with 200 and 500 µM FAC for 24 hours led to a significant reduction of TfR gene expression (FAC 200 µM: -58% vs CTR, $p < 0.0001$; FAC 500 µM: -47% vs CTR, $p < 0.0001$; [Fig. 27 A]) and, conversely, to an increment of FtH mRNA levels (FAC 200 µM: +83% vs CTR, $p < 0.05$; FAC 500 µM: +151% vs CTR, $p < 0.01$; [Fig. 27 B]).

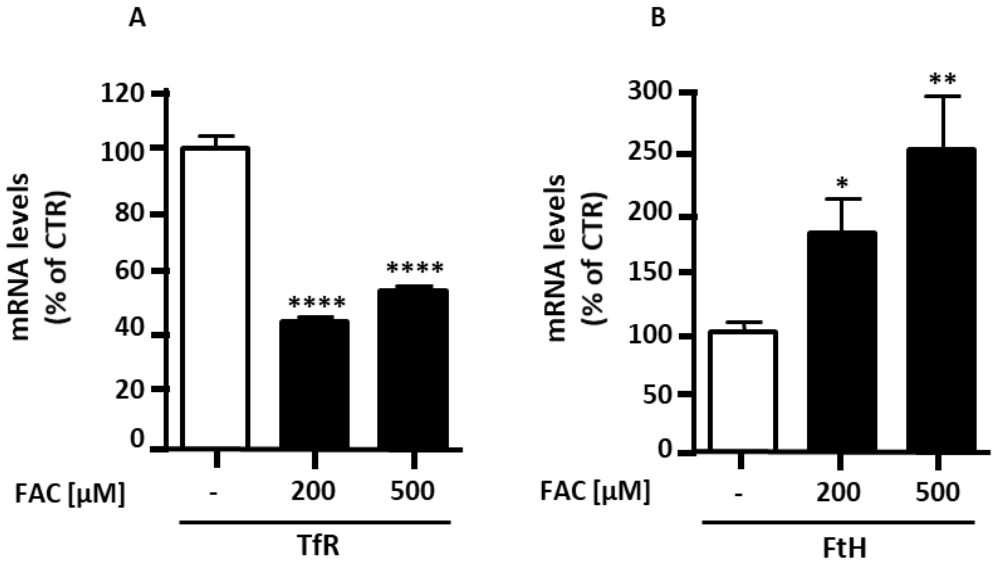

Fig. 27. *Effect of 24 hours treatment with ferric ammonium citrate (FAC) on GN-11 cells. White bars are controls (no FAC) and the black ones are FAC treated. n = 6 per group. Data are expressed as percentage of control (mean*

*± SEM). Differences between treatments were assessed by one-way ANOVA, *p < 0.05, **p < 0.01 and ****p < 0.0001.*

Similarly, in GT1-7 cells, 200 µM FAC for 24 hours caused the reduction of TfR gene expression (-75% vs CTR, p < 0.001) and the increment of FtH mRNA levels (+92% vs CTR, p < 0.05 [Fig. 28]) when compared to cells without FAC treatment (controls).

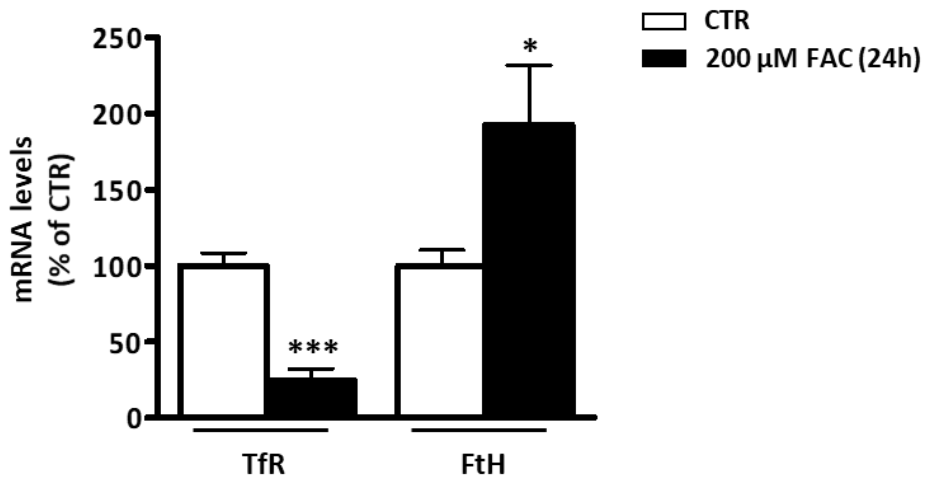

Fig. 28. *Effect of 24 hours treatment with 200 µM ferric ammonium citrate (FAC) on GT1-7 cells. White bars are controls (no FAC) and the black ones are FAC treated. n = 6 per group. Data are expressed as percentage of control (mean ± SEM). Differences between treatments were assessed by Student's t-test, *p < 0.05 and ***p < 0.001.*

6.2.3 Effect of FAC on GnRH expression

To study whether the results obtained in the *in vivo* model were, at least in part, reproducible in the *in vitro* one, the gene expression of GnRH was evaluated in both the cell lines. 24-hour FAC treatment did not affect GnRH mRNA levels in GN-11 cells, either at 200 µM or at 500 µM [Fig. 29 A]. Similarly, exogenous iron (FAC 200 µM, 24 hours) did not change GnRH gene expression in GT1-7 cells [Fig. 29 B].

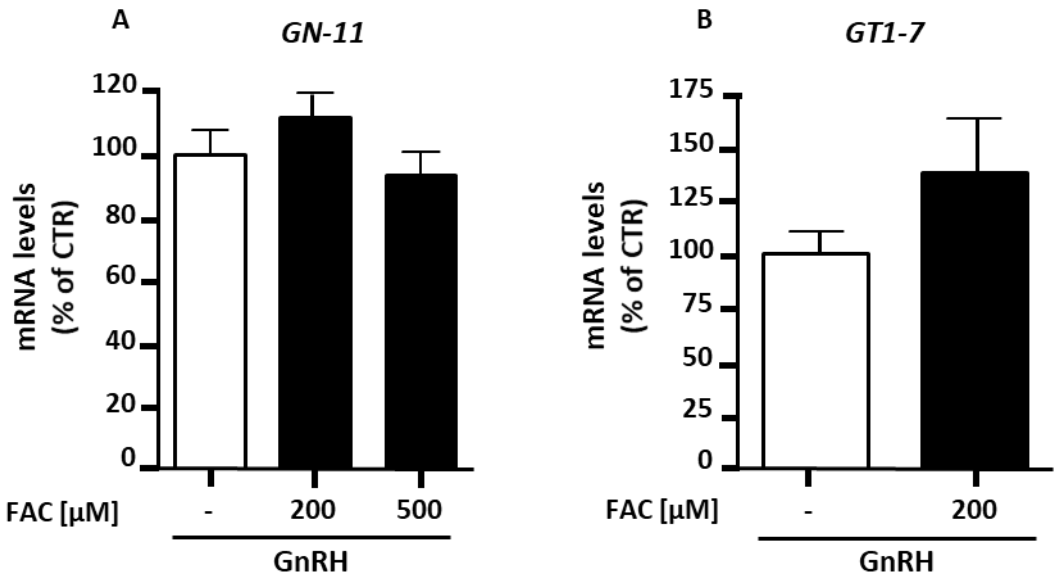

Fig. 29. *Effect of 24 hours treatment with ferric ammonium citrate (FAC) on GnRH gene expression. White bars are controls (no FAC) and the black ones are FAC treated. n = 6 per group. Data are expressed as percentage of control (mean ± SEM).*

6.2.4 Effect of FAC on pro-inflammatory cytokines

The RT-qPCR analysis revealed that IL-6 gene expression was up-regulated in GN-11 cells treated with 24-hours FAC, both at 200 µM (+46% *vs* CTR, p< 0.05) and 500 µM (+175% *vs* CTR, p < 0.01) [Fig. 30 A]. Conversely, the same result was not obtained when mRNA levels of TNFα were analyzed. The gene expression was not affected by a 24-hours FAC treatment (200 µM) (p = 0.497; [Fig. 30 B]).

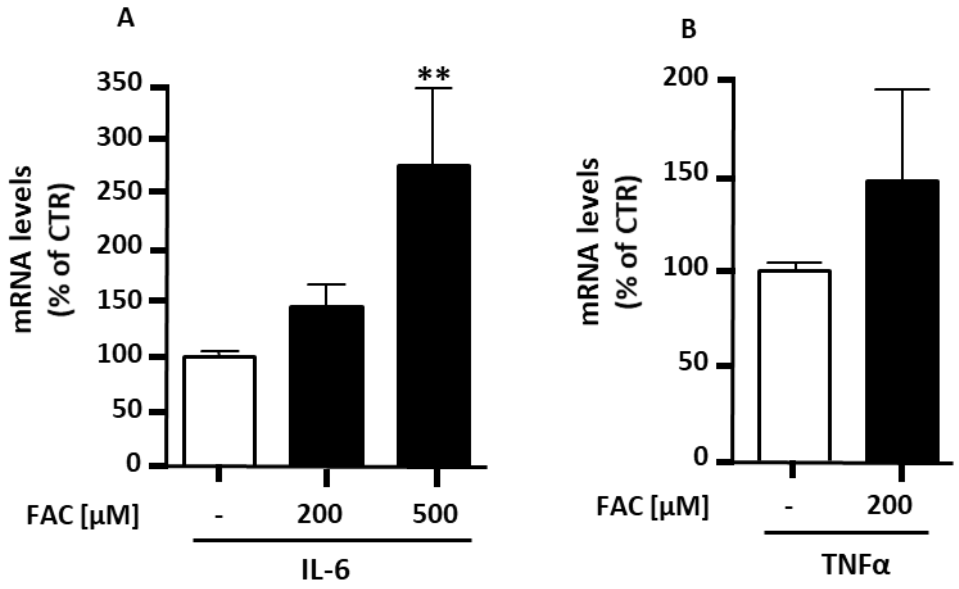

Fig. 30. *Effect of 24 hours treatment with ferric ammonium citrate (FAC) on pro-inflammatory cytokines gene expression. Panel A shows the analysis of IL-6 and Panel B shows the analysis of TNFα. White bars are controls (no FAC) and the black ones are FAC treated. n = 6 per group. Data are expressed as percentage of control (mean ± SEM). Differences between treatments were assessed by ANOVA, **p < 0.01.*

6.2.5 Effect of FAC on oxidative stress

In GN-11 cells, exogenous iron caused a significant increment of SOD2 mRNA levels in a dose-dependent manner. Indeed, 24-hours FAC treatment 200 µM, when compared to untreated cells, led to increased mRNA levels of SOD2 (+51%, $p < 0.05$) and increasing the FAC dose at 500 µM determine a higher SOD2 gene expression (+89% vs CTR, $p < 0.01$) [Fig. 31 A]. Conversely, the same treatment did not affect mRNA levels of CHOP and of alternative splicing of XBP-1 [Fig. 31 B and C].

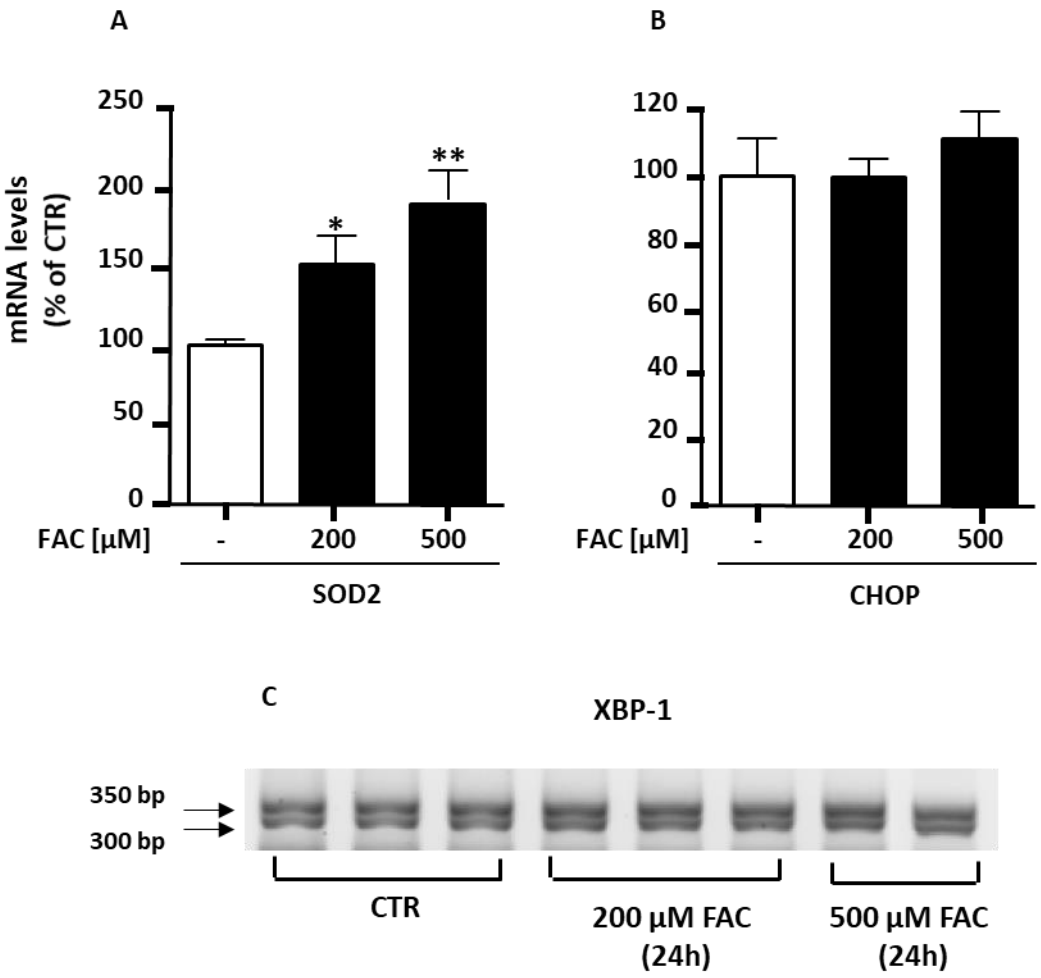

Fig. 31. *Effect of iron treatment on GN-11 cells oxidative stress. Panels A and B show the effect of 24-hours treatment with ferric ammonium citrate (FAC; 200 and 500 µM) on gene expression of oxidative and endoplasmic reticulum stress (superoxide dismutase 2 - SOD2 and CAAT/enhancer binding protein (C/EBP) homologous protein*

*- CHOP, respectively) as well as that of X-box binding protein-1 (XBP-1), an index of early stage endoplasmic reticulum stress response. White bars are controls (CTR) and the black ones are FAC treated. In panels A and B, n = 6 per group. In panels A and B data are expressed as percentage of control (mean ± SEM). Differences between treatments were assessed by one-way ANOVA, *p < 0.05 and **p < 0.01.*

6.2.6 Effect of FAC on GN-11 chemomigration

GnRH neurons derive from the olfactory placode and, during the embryonic development, they migrate to the hypothalamus at the preoptic area level and in more caudal areas in the mediobasal hypothalamus. Among the cell lines used in the current project, GN-11 are representative of immature neurons and possess migratory properties. For this reason, all the studies focused on the evaluation of the effect of FAC on chemotaxis were conducted in these cells. Through the Boyden chamber-based microchemotaxis assay, to obtain a migratory response GN-11 cells were exposed to 1% FBS, an effective chemoattractant [142]. This condition was assumed as internal positive control, in terms of percentage of migrated cells.

GN-11 cells were pretreated for 24 hours with FAC at different concentrations (100, 200, 500, 1000 µM) and then exposed for 1.5 hours to 1% FBS in Boyden's chamber. As a result, FBS-induced chemotaxis was not affected by 100 µM FAC, but it was significantly reduced by 200 µM FAC (-17%, $p<0.01$), 500 µM FAC (-24%, $p<0.01$) and 1000 µM FAC (-22%, $p<0.01$) [Fig. 32 A].

A shorter pre-treatment with FAC was also tested. In detail, GN-11 cells were pre-treated for 1 hour with 200, 500 and 1000 µM FAC before exposure to 1% FBS. The results were similar to those obtained with a 24 hours pre-treatment, as demonstrated by the significant reduction of chemotaxis in response to 200 µM FAC (-34%, $p<0.001$), 500 µM FAC (-38%, $p<0.001$) and 1000 µM FAC (-14%, $p<0.01$) compared to control [Fig. 32 B].

Subsequently, longer pretreatments (24, 48 and 72 hours) with 200 µM FAC were performed, before exposing GN-11 cells to 1% FBS for 1.5 hours in Boyden's chamber. FAC significantly inhibited the 1% FBS-induced chemotaxis in a time-dependent manner, starting from a decrease of 23% ($p < 0.01$) in response to a 24-hours pretreatment, to reach -36% ($p < 0.001$) after a 72-hours pretreatment [Fig. 32 C].

The negative contribution of FAC on neuronal migration was confirmed by a 24-hours cotreatment of GN-11 cells with FAC and deferoxamine mesylate (DFO; 200 µM), an hexadentate chelator, at a 1:1 ratio, before Boyden's chamber assay. The association completely counteracted the inhibition mediated by FAC on 1% FBS-induced GN-11 migration.

As expected, the incubation with 200 µM DFO for 24 hours significantly inhibited the 1% FBS-induced chemotaxis (-49 %, $p < 0.001$) [Fig. 32 D].

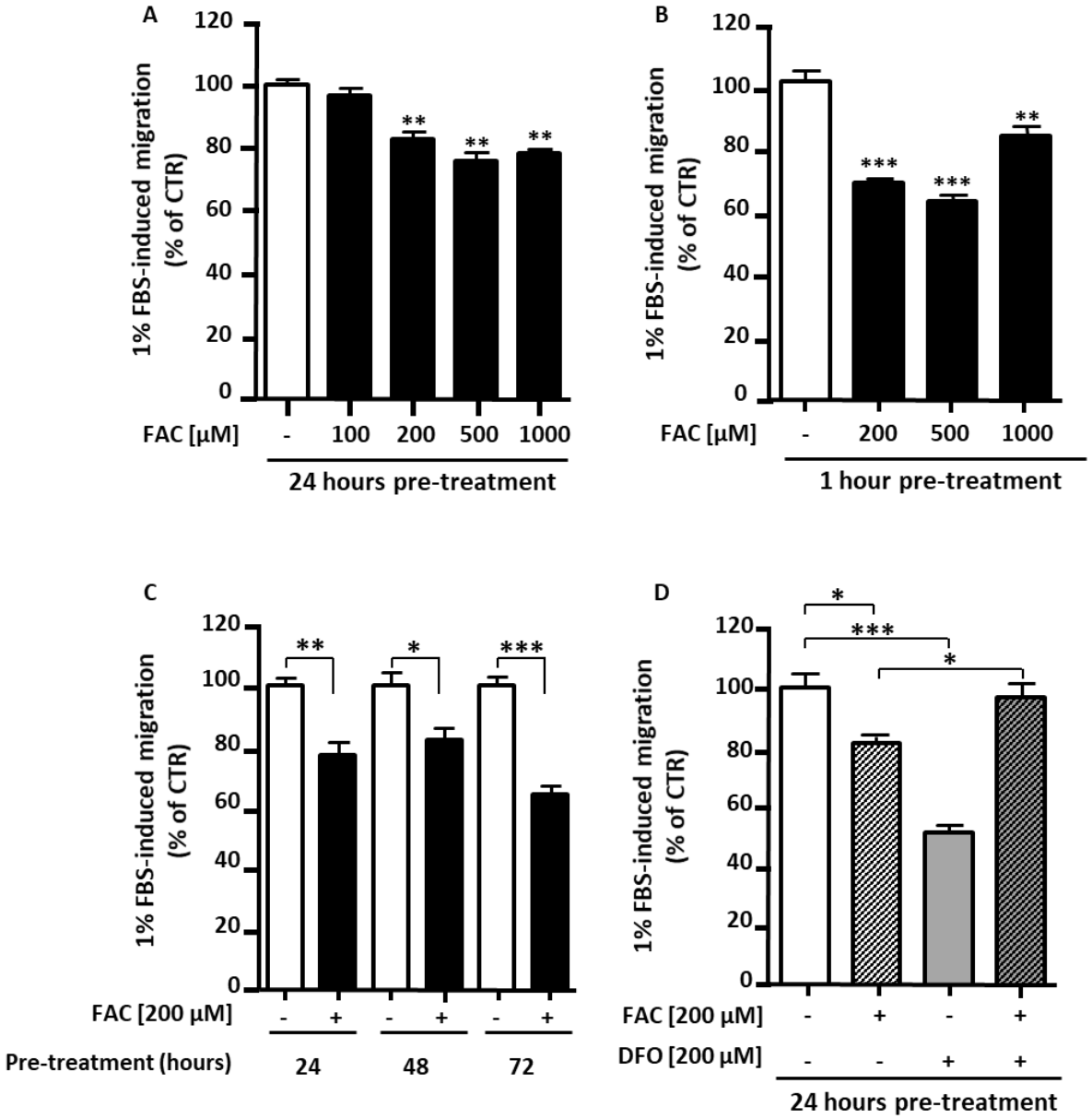

Fig. 32. *Effect of iron treatment on GN-11 cells migratory capacity. n = 6 per group. Data are expressed as percentage of control (mean ± SEM). Differences between treatments were assessed by one-way ANOVA (panels A, B and D) and by Student's t-test (panel C), *p < 0.05, **p < 0.01 and ***p < 0.001.*

6.2.7 The possible involvement of ERK1/2 cell signalling pathway

After assessing the negative effect of iron overload on cell migration, the possible concomitant activation of cell signaling pathways was investigated. Since the extracellular signal-regulated kinase (ERK) 1/2 cell signaling could be involved in cell migration [142], the impact of FAC treatment on this pathway was investigated.

Initially, GN-11 cells were starved overnight (15 hours in DMEM without FBS) and then treated with 200 µM FAC for 5, 10, 20, 30, 60 minutes, 3 and 24 hours. Subsequently the levels of ERK 1/2 phosphorylation were evaluated and normalized for basal ERK 1/2, constitutively present in this cell line. As shown in figure 33, the protein phosphorylation was significantly increased after 5 minutes of FAC treatment and this increment was more significant after 10 and 20 minutes of treatment. Conversely, in cells exposed to exogenous iron for 30, 60 and 180 minutes the phosphorylation levels of ERK 1/2 progressively decreased, reaching basal values after 24 hours of treatment [Fig. 33].

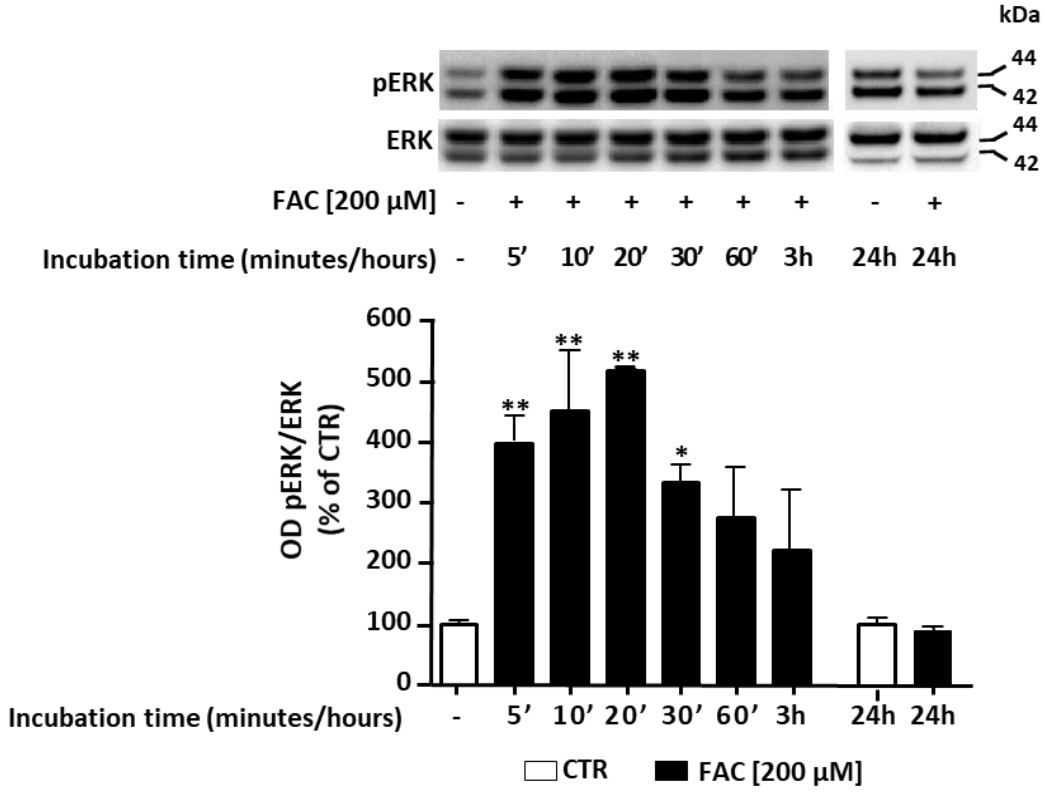

Fig. 33. *Effect of iron treatment on extracellular signal-regulated kinases 1 and 2 (ERK1/2) phosphorylation (pERK1/2) in GN11 cells. All experiments and statistical analysis described in this figure were performed as follows: cells were serum starved for 15 hours and then exposed to FAC 200 µM for 5 – 60 minutes, 3 and 24 hours. 20 µg of protein extract was analyzed by Western Blotting. One representative blot and the densitometric analysis corresponding to three independent experiments are shown. pERK1/2 levels were normalized to total ERK1/2. Data are expressed as percentage of control (mean ± SEM). White bars are controls and black ones are FAC-treated. Differences between treatments were assessed by one-way ANOVA, *p < 0.05, **p < 0.01.*

Since, in the present model, ERK 1/2 phosphorylation was modulated by exogenous iron, the possible involvement of this pathway in the FAC-inhibited chemotaxis was evaluated. To this

purpose a Boyden chamber-based microchemotaxis assay was performed, treating GN-11 cell with 200 µM FAC and a selective inhibitor of MEK 1/2 (U0126, 10 µM). In detail, cells were pretreated with U0126 for 30 minutes, treated with 200 µM FAC with or without U0126 for 1 hour and, finally, exposed for 1.5 hours to 1% FBS in Boyden's chamber. As a result, the exposure to the ERK 1/2 inhibitor reduced the 1% FBS-induced chemotaxis (-30% vs CTR, $p < 0.0001$) as obtained treating cells with FAC (-39% vs CTR, $p < 0.0001$). Similarly, the association of U0126 and FAC significantly inhibited the GN-11 migratory capacity (-39% vs CTR, $p < 0.0001$) [Fig. 34].

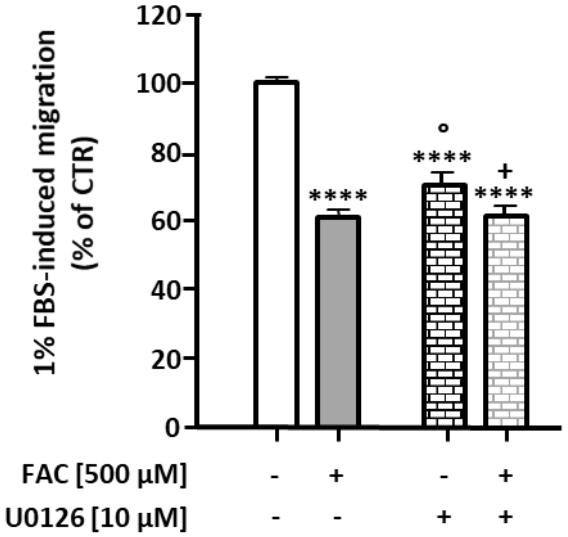

Fig. 34. *Involvement of ERK 1/2 in the FAC-inhibited GN-11 migration. n = 6 per group. Data are expressed as percentage of control (mean ± SEM). White bar is representative of control (CTR, without FAC and U0126) and grey bar is representative of FAC-treated cells. Differences between treatments were assessed by one-way ANOVA, ****p < 0.0001 vs CTR; ° p < 0.05 vs FAC; + p < 0.05 vs U0126.*

7. DISCUSSION

This study addressed the issue of the possible contribution of hypothalamic derangement to the impairment of the hypothalamus-pituitary-gonadal (HPG) axis induced by dietary iron overload.

First of all, to study the effect of iron overload on the reproductive axis, a murine model fed with iron-enriched diet (IED) was used. Briefly, Dongiovanni P. *et al.* [113], in 2013, demonstrated that serum iron and hepatic iron content were higher in IED mice compared to controls (+49% and +95%, respectively) and iron overload caused hepatocellular and non-parenchymal siderosis. IED was associated to an increased release of hepcidin, one of the main regulators of iron homeostasis decreasing plasma iron concentrations. Thus, these data support the validity of IED as a tool to induce iron overload in a murine model. Moreover, in these mice, hepcidin up-regulation affected visceral adipose tissue metabolism decreasing the gene expression of lipoprotein lipase and increasing that of suppressor of cytokine signaling-3 (SOCS3), the latter being involved in insulin resistance and hypertriglyceridemia.

Hypogonadism in men can be defined as a clinical syndrome that results from failure of the testis to produce physiological levels of testosterone (T) and normal number of spermatozoa. This defect is caused by the disruption of one or more levels of the HPG axis [75]. According to the site of the HPG axis primarily affected, hypogonadism can be classified as primary or secondary. The first one is a condition characterized by a testicular failure usually known as hypergonadotropic hypogonadism. The level of T is low, but, because the negative feedback to the HPG axis is usually not functional, luteinizing hormone (LH) and follicle-stimulating hormone (FSH) concentrations are elevated. Instead, the main feature of secondary hypogonadism is a defect in the hypothalamus or pituitary, which results in low T levels because of insufficient stimulation of the Leydig cells, with low or low-normal FSH and LH levels. It is usually called hypogonadotropic hypogonadism [79, 143].

Hypogonadism is the second most common endocrine abnormality, after diabetes mellitus, in iron overload syndromes, such as hemochromatosis and β-thalassemia [81]. Although a testicular origin of this type of hypogonadism has been suggested, a central involvement cannot be excluded [81]. Indeed, a possible iron accumulation at the hypothalamic-pituitary level may impair GnRH neurons and/or pituitary cells leading to hypogonadotropic hypogonadism. Accordingly, focusing on the pituitary involvement, experimental data suggest that, although

iron deposition at this level can occur in gonadotroph, somatotroph, lactotroph, corticotroph and thyrotroph cells, it is more pronounced in the first cellular subtype leading to a defect of FSH and LH production that explains hypogonadism [144]. Moreover, patients affected by hemochromatosis are characterized by low basal serum T, FSH and LH concentrations which do not increase after chronic pulsatile GnRH administration, highlighting a pituitary unresponsiveness [84].

Overall, the findings of this thesis are concordant with those reported in the literature [82, 144]. Indeed, in the *in vivo* model employed, dietary iron overload affected both the testes and the pituitary. Relative to testes, IED determined a phenotypical impairment, as shown by significantly reduced weight and length with a concomitant local iron accumulation. However, the mRNA levels of both the transferrin receptor (TfR) and ferritn (Ft) proteins, involved in internalization and storage of iron, respectively, were not affected by iron overload. Subsequently, possible impairments at the structural level were studied. In particular, seminiferous tubules play important roles hosting spermatogenesis and assuring sperm transport to the efferent duct [145]. Therefore, they were analyzed to evaluate whether iron overload could have negative effects at this level. Eosin and hematoxylin revealed a reduced number of seminiferous tubules as a consequence of IED, suggesting a possible defect in the reproductive function. A possible limitation in these findings lies in the technique used since fibrosis and hyalinization of the seminiferous tubules as well as the hyperplasia of the interstitium would have been analyzed. These data were in line with those obtained analyzing the iron overload effect on pituitary gland. First of all, the increment in the gene expression of FtH suggested an iron accumulation at this site. Indeed, the atomic absorption spectrometry (AAS) could not be performed due to methodological limitations, namely the reduced size of the gland and, therefore, FtH was used a surrogate biomarker of iron content [134]. Following the finding of this accumulation, levels of gonadotropins secreted by pituitary were evaluated. In particular, FSH and LH were taken into consideration because of their involvement in reproductive process and since in hypogonadic patients their level can be altered [75]. Specifically, their β subunit was quantified, given that the α one is common to other gonadotropins, such as human chorionic gonadotropin (hCG) and thyroid-stimulating hormone (TSH) [146]. In pituitary, iron accumulation did not affect FSHβ gene expression, whereas reduced that of LHβ even without reaching a statistical significance.

To further investigate whether iron overload could impact the reproductive system, circulating level of T and LH were evaluated. They were significantly lower in IED mice compared to the control group, confirming the negative effect of iron overload on the HPG axis. These data suggest that, at least in a murine model, IED impairs HPG with the specific involvement of gonads and the pituitary gland.

Conversely, data relative to the involvement of hypothalamus in iron-driven hypogonadism are still controversial. In 1992 Piperno *et al*. evaluated the endocrine alterations in patients in early stage of genetic hemochromatosis. Regarding the analysis of the HPG axis, these subjects showed low levels of serum T compared to controls, but, after hCG stimulation test, these levels return to the normal range, indicating the absence of a gonadal defect. To investigate whether there was an impairment at the central level, basal FSH and LH levels were measured and resulted significantly reduced in patients with hemochromatosis. These findings suggested either the presence of a pituitary or a hypothalamic damage; thus, a LHRH stimulation test was performed. As such, LH levels were increased proving a correct functionality of pituitary and suggesting a possible hypothalamic impairment which could be the cause of the gonadal dysfunction found in patients in early stage of hemochromatosis [147]. Similarly, Siminoski *et al.* hypothesized a possible role for hypothalamus in the onset of hypogonadism in the context of idiopathic hemochromatosis. The intact functionality of Leydig cells was tested demonstrating the increment of T level following the hCG administration. Conversely, although the pituitary secretion of LH was normal in response to GnRH stimulation, LH and FSH levels did not increased after administration of clomiphene, an antagonist of estrogen receptors in hypothalamus and pituitary [83, 148]. This test is used to verify the central functionality because clomiphene is thought to stimulate pituitary gonadotropin release by excluding estradiol from hypothalamic and pituitary receptor sites. This interaction neutralizes the normal negative feedback control of estrogen and results in enhanced secretion of LH and FSH [149]. Therefore, the negative response to clomiphene administration, in presence of a normal pituitary secretion of gonadotropins, let the authors hypothesize a possible defect in the hypothalamic GnRH response [83].

Recently, Rossi *et al*. investigate whether acute iron overload could interfere on the HPG axis of female rats. Although this study is quite different from the current project, the purpose of the investigation was similar. Specifically, differences lay in the way in which iron overload was induced (intraperitoneal injection of iron-dextran *vs* dietary iron overload), in the duration of

the treatment (acute *vs* chronic iron overload) and in the animal model employed (female rats *vs* male mice) [23]. In line with data presented in this thesis, Rossi *et al*. showed a dose-dependent iron accumulation at the pituitary and gonadal levels. Interestingly, hypothalamus was also mainly involved in this deposit. Differently from this evidence, in the *in vivo* model presented in the current thesis, IED did not cause a hypothalamic accumulation of iron, as shown by AAS performed on whole hypothalamus of IED mice compared to control mice. Accordingly, at the hypothalamic level also the regulating mechanisms of iron homeostasis were not affected by iron overload; TfR and FtH mRNA levels did not change between control group and iron-fed mice. A possible explanation could be the presence of blood-brain barrier (BBB) which protects the hypothalamus against iron accumulation. However, the analysis of this compartment continued, moving to the evaluation of genes controlling reproductive function. Interestingly, the gonadotropin-releasing hormone (GnRH) gene expression, which regulates the secretion of FSH and LH, was significantly increased in iron overloaded-mice. This change was not accompanied by variations in the upstream GnRH regulator Kisspeptin (KISS1) and its related G protein-coupled receptor 54 (GPR54). Based on the increased mRNA expression of GnRH, GnRH neurons were further evaluated. Physiologically, GnRH axons extend to the external zone of the median eminence (ME) where they release GnRH peptide close to the fenestrated capillary bed of the pituitary portal blood; this allows GnRH to be transported to the pituitary gland [150]. In IED mice, the ME was much more innervated by GnRH-positive neurites when compared to mice fed a standard diet. This increment was comparable with that one obtained in $HFE^{-/-}$ mice, a model of human hemochromatosis. This evidence suggests that, in IED mice, low levels of circulating LH and T are related to primary defects downstream of the hypothalamus. Moreover, the increased hypothalamic gene expression of GnRH and presence of GnRH neurons projections at the ME are likely to be primarily due to the lack of a selective negative feedback driven by T. Thus, our findings seem to rule out the involvement of the hypothalamus in iron-driven hypogonadism.

In the context of reproduction, an important role is played by leptin. This is a polypeptide hormone that is secreted primarily by adipose tissue and it is involved in several processes, such as mediation of food intake, suppression of lipogenesis in adipose tissue, modulation of immune response, but, also, of gonadotropin secretion. Indeed, it was proposed that reduced pulsatility of LH during the night may be related to low leptin levels present during this time-frame [151]. Moreover, leptin-deficient ob/ob mice are characterized by a morbid obesity with

sterility in males and females that is corrected by continuous leptin injection [152]. In particular, leptin-treated males had significantly elevated serum levels of FSH, increased testicular and seminal vesicle weights and elevated sperm counts compared to controls [153]. These results corroborate the suggestion that leptin may serve as a permissive signal to the reproductive system, acting as a signal of energy reserve essential for normal reproductive function. Regarding iron overload, it was shown that patients affected by β thalassemia failed to maintain adequate leptin production [110] and that hypogonadotropic hypogonadism in this disease could be also due to iron toxicity in adipose tissue, associated to an impairment of leptin levels [154].

Upon IED, mice showed a significant decrement of serum leptin levels with associated reduced amount of perigonadal fat pad. This latter evidence could be probably due, at least in part, to the reduced food intake of IED mice, which, in turn, may be the cause of their reduced body weight. A possible reason for the reduced food intake could be the low palatability of the iron enriched diet. Moreover, IED resulted associated to the onset of insulin resistance, as detected by the increased Homeostatic Model Assessment of Insulin Resistance (HOMA-IR) index and basal glycemia. Since the orexigenic signal neuropeptide Y (NPY) and the anorexigenic pro-opiomelanocortin (POMC) are involved in the integration of energy homeostasis and reproduction, their mRNA levels were evaluated. Iron overload led to significant increase of NPY gene expression and decrement of that of POMC. Although the role for NPY on food intake is well investigated, the effects of NPY on GnRH neurosecretion are probably dual, involving both negative and positive feedback [155]. However, experimental evidence suggested a major inhibitory action of NPY, as demonstrated by Catzeflis *et al*., who showed that chronic administration of NPY inhibited gonadotropin secretion and sexual function in female rats [156]. Accordingly, infusion of NPY to lean control animals leads to a reduction in GnRH and LH release and a disturbed reproductive function [157]. Given this important role of NPY further investigations are necessary to understand whether the observed increase in hypothalamic NPY expression may play a role in the suppression of LH levels in IED male mice.

Furthermore, excess iron is thought to have a pro-oxidant activity in promoting hydroxyl radical generation. Thus, to study the effect of dietary iron overload on the onset of oxidative and endoplasmic reticulum stress, superoxide dismutase (SOD), CAAT/enhancer binding protein (C/EBP) homologous protein (CHOP) and the X-box Binding Protein-1 (XBP-1) transcription factor were evaluated at the central level. As a result, gene expression of these markers did not

change between control and IED group, suggesting that IED did not activate hypothalamic oxidative and endoplasmic reticulum stress. Similarly, iron overload did not induce the mRNA expression of pro-inflammatory cytokine interleukin- (IL-6), although those of tumor necrosis factor α (TNFα) were significantly increased at the hypothalamic level. Moreover, it should be underlined that hypothalamus is an extremely heterogeneous tissue comprised of astrocytes, oligodendrocytes, microglia, endothelial cells, ependymal cells as well as numerous neuronal subgroups and, therefore, the identification of the exact site, in which TNFα is activated, becomes fundamental [158].

Overall these *in vivo* data suggest that dietary iron overload could impair the HPG axis with a possible involvement of pituitary and testes, without a relevant contribution of the hypothalamic compartment. One of the possible reason for this extrahypothalamic mechanism could be the presence of BBB as a protection of hypothalamus from iron accumulation.

To further confirm that iron overload effects were not mediated by hypothalamus, two *in vitro* models of GnRH neurons were used. Indeed, these cell lines, obviously lacking BBB, represented a useful tool to reproduce *in vivo* results, excluding the functional protective role of BBB. These consist of immortalized murine GN-11 cells, representative of immature GnRH neurons, and GT1-7, a model of mature GnRH neurons. Furthermore, GN-11 cells were specifically employed to investigate whether iron overload could affect the cell migration [159] and, eventually, whether the extracellular signal-regulated kinase (ERK) 1/2 cell signaling could be involved.

To induce iron overload in these cell lines, ferric ammonium citrate (FAC) was used [160] showing that in GN-11 cells the iron content was the double compared to GT1-7.

As in the *in vivo* model, the main proteins involved in iron homeostasis were analyzed. In response to exogenous iron overload, the mRNA levels of TfR in GN-11 and GT1-7 cells were decreased whereas that of FtH were increased. These data indicate that both the cell lines are a valid tool to study iron overload given their ability to modulate expression of their genes in order to counteract the effects of the metal accumulation. Indeed, the reduction of TfR could be explained as an attempt of cells to minimize the cellular iron uptake, while increasing FtH could increase intracellular iron storage.

Interestingly, in contrast to data obtained *in vivo*, the evaluation of main regulators of reproductive system revealed that cellular GnRH gene expression was not modified by massive iron deposit.

Also in the *in vitro* models, the possible activation of oxidative and endoplasmic reticulum stress, as well as, of the pro-inflammatory pathway by iron overload was investigated. The experimental condition used to mimic iron overload did not impact the expression of TNFα, whereas, conversely to what obtained in vivo, the only evidence of a possible activation of inflammation, was given by increased mRNA levels of IL-6.

Exogenous iron overload also induced oxidative stress in vitro, as shown by the increased gene expression of SOD2, without involving the endoplasmic reticulum.

Moreover, the GnRH neurons migration was also analyzed since, physiologically, this process is essential for a correct reproductive function. It occurs during the embryonic development, when GnRH neurons migrate from the forebrain to the hypothalamus at the preoptic area level and in more caudal areas in the mediobasal hypothalamus [67]. Interestingly, FAC treatment resulted in inhibition of the fetal bovine serum (FBS)-induced chemomigration. This evidence was confirmed by using the iron chelator deferoxamine mesylate (DFO). Indeed, when cells were cotreated with this compound associated to FAC, the basal migration was restored. Interestingly the neuronal migration was drastically reduced when cells were exposed to DFO alone, maybe because DFO deprived cells of the martial content required for normal biological functions.

Finally, the activation of ERK 1/2 pathway was analyzed in the presence of exogenous iron overload, given its involvement in GN-11 cell migration [142]. Iron significantly induced phosphorylation of ERK 1/2 after short (5 and 10 minutes) FAC treatments. The involvement of ERK 1/2 on GN-11 cell migration was confirmed by using a selective ERK 1/2 inhibitor, the compound U0126. This latter determined an inhibition of FBS-induced chemomigration, even if the effect was less to what obtained with FAC treatment. Conversely, when GN-11 cells were treated with both U0126 and FAC, the inhibition of neuronal migration was comparable to that produced by FAC.

8. CONCLUSIONS

Our results demonstrated that, in male mice, iron overload can lead to a severe impairment of the hypothalamic-pituitary-gonadal (HPG) axis possibly resulting in an hypogonadal condition, a feature possibly deriving from iron deposition in pituitary and/or gonads via extrahypothalamic mechanisms. This finding represents a further step in understanding how iron overload leads to this endocrinopathy. Indeed, controversial data are present in the literature regarding the possible involvement of hypothalamus, pituitary or both the sites in the pathophysiology of iron-driven hypogonadism. The results of this thesis confirm that, at least in a mouse model, iron overload could lead to pituitary changes, associated to a direct impairment of testicular function, excluding the contribution of hypothalamus to the massive HPG axis suppression caused by IED. In particular, pituitary and gonads were directly affected due to iron accumulation at both these organs. This resulted in an impairment of reproductive function, as suggested by decreased levels of LH and T, which can be associated to the onset of hypogonadism [75].

At the testicular level, iron overload led to macro- and microscopic alterations suggesting a possible role of gonads, in the onset of hypogonadism. Conversely, the hypothalamus seemed to be protected from systemic iron overload; iron did not accumulate at this level and genes involved in iron homeostasis were not affected. Interestingly, the low levels of circulating T may account for the lack of a selective negative feedback driven by T; this condition could explain the increment in both GnRH mRNA levels and GnRH neurons projections at the median eminence. In this context, the use of *in vitro* GnRH neurons, which functions were impaired by iron accumulation, leaves open questions relative to the role of BBB in the protection of the central region (hypothalamus).

Trying to translate these findings in humans, it is important to highlight that Farmaki K. *et al.* demonstrated how intensive iron chelation therapy, using combined desferrioxamine and deferiprone, which leads to the reduction of total body iron concentration, improves hypogonadism in adult thalassemic patients [161]. These results are in line with other studies suggesting that the iron chelator deferasirox can reverse endocrinopathies in adults with β-thalassemia major [162]. Based on this evidence, the effect of a chelation therapy in the *in vivo* model used in the current project should be evaluated.

In addition, from a metabolic point of view, the IED animal model showed *(i)* increased basal glycemia and HOMA-IR index, *(ii)* reduced amount of perigonadal fat pad, *(iii)* decreased serum leptin levels, *(iv)* increased NPY gene expression and reduced POMC mRNA levels. Thus, further studies are required to clarify possible mechanisms linking this metabolic impairment to alterations of the reproductive system.

9. FUTURE PERSPECTIVES

One of the major user of cellular iron is the mitochondrion, which, in turn, plays a central role in iron metabolism. Since iron can promote the formation of hydroxyl radicals, the mitochondrial iron level must be tightly regulated to avoid iron-dependent damage and maintain mitochondrial functionality [163]. Defects in mitochondrial function may have deleterious consequences, given the fundamental role for cell life of this organelle. In iron overload disorders, iron could accumulate into mitochondria, agglomerate and/or precipitate within the organelle [164]. Mitochondrial iron burden is responsible for damage to Fe/S cluster as well as mitochondrial DNA that encodes proteins critical for oxidative phosphorylation [163]. In this context, it should be interesting evaluate whether in both the *in vivo* and *in vitro* models presented in this thesis, iron overload could affect mitochondrial functionality. To this purpose, some of the parameters that could be evaluated are *(i)* mitochondrial DNA content, *(ii)* expression of genes controlling the mitochondrial fusion and fission, *(iii)* the OXPHOS subunits, and *(iv)* cellular oxygen consumption.

- To further investigate the metabolic impairment driven by iron overload, body composition of IED and control mice could be analyzed through the dual-energy X-ray absorptiometry (DEXA), which provides a noninvasive approach to assess body fat and lean tissue contents [165]. Moreover, several parameters, such as oxygen consumption, carbon dioxide production, respiratory exchange ratio, activity level and caloric heat production could be studied by using the Comprehensive Laboratory Animal Monitoring System (CLAMS).

In particular, during my PhD program I spent 15 months in the laboratory of Prof. Patti Mary-Elizabeth, at Joslin Diabetes Center, affiliate of Harvard Medical School, Boston, MA, USA, where I learnt the assays listed in the above reported points.

10. REFERENCES

1. Muhlenhoff, U., et al., *Compartmentalization of iron between mitochondria and the cytosol and its regulation.* Eur J Cell Biol, 2015. **94**(7-9): p. 292-308.
2. Pantopoulos, K., et al., *Mechanisms of mammalian iron homeostasis.* Biochemistry, 2012. **51**(29): p. 5705-24.
3. JR, H., *Iron.* Encyclopedia of Human Nutrition, 2005.
4. Gulec, S., G.J. Anderson, and J.F. Collins, *Mechanistic and regulatory aspects of intestinal iron absorption.* Am J Physiol Gastrointest Liver Physiol, 2014. **307**(4): p. G397-409.
5. West, A.R. and P.S. Oates, *Mechanisms of heme iron absorption: current questions and controversies.* World J Gastroenterol, 2008. **14**(26): p. 4101-10.
6. Celotti, F., *Patologia generale e fisiopatologia*. 2002: EdiSES.
7. Shayeghi, M., et al., *Identification of an intestinal heme transporter.* Cell, 2005. **122**(5): p. 789-801.
8. Daher, R. and Z. Karim, *Iron metabolism: State of the art.* Transfus Clin Biol, 2017. **24**(3): p. 115-119.
9. Papanikolaou, G. and K. Pantopoulos, *Systemic iron homeostasis and erythropoiesis.* IUBMB Life, 2017. **69**(6): p. 399-413.
10. Drakesmith, H., E. Nemeth, and T. Ganz, *Ironing out Ferroportin.* Cell Metab, 2015. **22**(5): p. 777-87.
11. Loreal, O., et al., *Iron, hepcidin, and the metal connection.* Front Pharmacol, 2014. **5**: p. 128.
12. Ganz, T. and E. Nemeth, *Hepcidin and iron homeostasis.* Biochim Biophys Acta, 2012. **1823**(9): p. 1434-43.
13. Muckenthaler, M.U., *Fine tuning of hepcidin expression by positive and negative regulators.* Cell Metab, 2008. **8**(1): p. 1-3.
14. Recalcati, S., et al., *Molecular regulation of cellular iron balance.* IUBMB Life, 2017. **69**(6): p. 389-398.
15. Gozzelino, R. and P. Arosio, *Iron Homeostasis in Health and Disease.* Int J Mol Sci, 2016. **17**(1).
16. Cairo, G. and S. Recalcati, *Iron-regulatory proteins: molecular biology and pathophysiological implications.* Expert Rev Mol Med, 2007. **9**(33): p. 1-13.
17. Merono, T., et al., *High risk of cardiovascular disease in iron overload patients.* Eur J Clin Invest, 2011. **41**(5): p. 479-86.
18. Siddique, A. and K.V. Kowdley, *Review article: the iron overload syndromes.* Aliment Pharmacol Ther, 2012. **35**(8): p. 876-93.
19. Pietrangelo, A., *Hereditary hemochromatosis.* Biochim Biophys Acta, 2006. **1763**(7): p. 700-10.
20. Alexander, J. and K.V. Kowdley, *HFE-associated hereditary hemochromatosis.* Genet Med, 2009. **11**(5): p. 307-13.
21. Siah, C.W., et al., *Normal iron metabolism and the pathophysiology of iron overload disorders.* Clin Biochem Rev, 2006. **27**(1): p. 5-16.
22. Kohgo, Y., et al., *Iron overload and cofactors with special reference to alcohol, hepatitis C virus infection and steatosis/insulin resistance.* World J Gastroenterol, 2007. **13**(35): p. 4699-706.
23. Rossi, E.M., et al., *Acute iron overload leads to hypothalamic-pituitary-gonadal axis abnormalities in female rats.* Toxicol Lett, 2016. **240**(1): p. 196-213.
24. Piperno, A., *Classification and diagnosis of iron overload.* Haematologica, 1998. **83**(5): p. 447-55.
25. Origa, R., et al., *Liver iron concentrations and urinary hepcidin in beta-thalassemia.* Haematologica, 2007. **92**(5): p. 583-8.
26. Leecharoenkiat, K., et al., *Iron dysregulation in beta-thalassemia.* Asian Pac J Trop Med, 2016. **9**(11): p. 1035-1043.

27. Ohba, R., et al., *Clinical and genetic characteristics of congenital sideroblastic anemia: comparison with myelodysplastic syndrome with ring sideroblast (MDS-RS).* Ann Hematol, 2013. **92**(1): p. 1-9.
28. Cazzola, M. and L. Malcovati, *Diagnosis and treatment of sideroblastic anemias: from defective heme synthesis to abnormal RNA splicing.* Hematology Am Soc Hematol Educ Program, 2015. **2015**: p. 19-25.
29. Lecube, A., C. Hernandez, and R. Simo, *Glucose abnormalities in non-alcoholic fatty liver disease and chronic hepatitis C virus infection: the role of iron overload.* Diabetes Metab Res Rev, 2009. **25**(5): p. 403-10.
30. Datz, C., E. Muller, and E. Aigner, *Iron overload and non-alcoholic fatty liver disease.* Minerva Endocrinol, 2017. **42**(2): p. 173-183.
31. Aigner, E., G. Weiss, and C. Datz, *Dysregulation of iron and copper homeostasis in nonalcoholic fatty liver.* World J Hepatol, 2015. **7**(2): p. 177-88.
32. Pietrangelo, A., *Iron and the liver.* Liver Int, 2016. **36 Suppl 1**: p. 116-23.
33. Dongiovanni, P., et al., *Iron in fatty liver and in the metabolic syndrome: a promising therapeutic target.* J Hepatol, 2011. **55**(4): p. 920-32.
34. Barros, R.K., et al., *Hyperferritinemia in patients with nonalcoholic fatty liver disease.* Rev Assoc Med Bras (1992), 2017. **63**(3): p. 284-289.
35. Milic, S., et al., *The Role of Iron and Iron Overload in Chronic Liver Disease.* Med Sci Monit, 2016. **22**: p. 2144-51.
36. Fargion, S., L. Valenti, and A.L. Fracanzani, *Beyond hereditary hemochromatosis: new insights into the relationship between iron overload and chronic liver diseases.* Dig Liver Dis, 2011. **43**(2): p. 89-95.
37. Ryan Caballes, F., H. Sendi, and H.L. Bonkovsky, *Hepatitis C, porphyria cutanea tarda and liver iron: an update.* Liver Int, 2012. **32**(6): p. 880-93.
38. Badat, M., B. Kaya, and P. Telfer, *Combination-therapy with concurrent deferoxamine and deferiprone is effective in treating resistant cardiac iron-loading in aceruloplasminaemia.* Br J Haematol, 2015. **171**(3): p. 430-2.
39. Pietrangelo, A., A. Caleffi, and E. Corradini, *Non-HFE hepatic iron overload.* Semin Liver Dis, 2011. **31**(3): p. 302-18.
40. Majore, S., et al., *Type 3 hereditary hemochromatosis in a patient from sub-Saharan Africa: is there a link between African iron overload and TFR2 dysfunction?* Blood Cells Mol Dis, 2013. **50**(1): p. 31-2.
41. Mobarra, N., et al., *A Review on Iron Chelators in Treatment of Iron Overload Syndromes.* Int J Hematol Oncol Stem Cell Res, 2016. **10**(4): p. 239-247.
42. Avrin, W.F. and S. Kumar, *Noninvasive liver-iron measurements with a room-temperature susceptometer.* Physiol Meas, 2007. **28**(4): p. 349-61.
43. Sharma, S.D., et al., *MRI-based quantitative susceptibility mapping (QSM) and R2* mapping of liver iron overload: Comparison with SQUID-based biomagnetic liver susceptometry.* Magn Reson Med, 2017. **78**(1): p. 264-270.
44. Franca, M., et al., *Tissue iron quantification in chronic liver diseases using MRI shows a relationship between iron accumulation in liver, spleen, and bone marrow.* Clin Radiol, 2017.
45. Bollig, C., et al., *Deferasirox for managing iron overload in people with thalassaemia.* Cochrane Database Syst Rev, 2017. **8**: p. CD007476.
46. Bayanzay, K. and L. Alzoebie, *Reducing the iron burden and improving survival in transfusion-dependent thalassemia patients: current perspectives.* J Blood Med, 2016. **7**: p. 159-69.
47. Burfeind, K.G., V. Yadav, and D.L. Marks, *Hypothalamic Dysfunction and Multiple Sclerosis: Implications for Fatigue and Weight Dysregulation.* Curr Neurol Neurosci Rep, 2016. **16**(11): p. 98.
48. Xie, Y. and R.I. Dorsky, *Development of the hypothalamus: conservation, modification and innovation.* Development, 2017. **144**(9): p. 1588-1599.
49. Ambrosi, G., et al., *Anatomia dell'uomo*. Second ed. 2008.

50. Asa, S.L., *Pituitary Histopathology in Man: Normal and Abnormal*, in *Endotext*, L.J. De Groot, et al., Editors. 2000: South Dartmouth (MA).
51. Davis, S.W., et al., *Pituitary gland development and disease: from stem cell to hormone production.* Curr Top Dev Biol, 2013. **106**: p. 1-47.
52. Perez-Castro, C., et al., *Cellular and molecular specificity of pituitary gland physiology.* Physiol Rev, 2012. **92**(1): p. 1-38.
53. de Moraes, D.C., et al., *Pituitary development: a complex, temporal regulated process dependent on specific transcriptional factors.* J Endocrinol, 2012. **215**(2): p. 239-45.
54. O'Donnell, L., P. Stanton, and D.M. de Kretser, *Endocrinology of the Male Reproductive System and Spermatogenesis*, in *Endotext*, L.J. De Groot, et al., Editors. 2000: South Dartmouth (MA).
55. Sedes, L., et al., *Bile acids and male fertility: From mouse to human?* Mol Aspects Med, 2017. **56**: p. 101-109.
56. Caroppo, E., *Male reproductive medicine: anatomy and physiology*. 2011: Cambridge University Press.
57. Wang, P. and Y.G. Duan, *The role of dendritic cells in male reproductive tract.* Am J Reprod Immunol, 2016. **76**(3): p. 186-92.
58. Li, N., E.I. Tang, and C.Y. Cheng, *Regulation of blood-testis barrier by actin binding proteins and protein kinases.* Reproduction, 2016. **151**(3): p. R29-41.
59. Mruk, D.D. and C.Y. Cheng, *The Mammalian Blood-Testis Barrier: Its Biology and Regulation.* Endocr Rev, 2015. **36**(5): p. 564-91.
60. Stanton, P.G., *Regulation of the blood-testis barrier.* Semin Cell Dev Biol, 2016. **59**: p. 166-173.
61. Mathur, P.P. and S.C. D'Cruz, *The effect of environmental contaminants on testicular function.* Asian J Androl, 2011. **13**(4): p. 585-91.
62. Shalet, S.M., *Normal testicular function and spermatogenesis.* Pediatr Blood Cancer, 2009. **53**(2): p. 285-8.
63. Amory, J.K. and W.J. Bremner, *Regulation of testicular function in men: implications for male hormonal contraceptive development.* J Steroid Biochem Mol Biol, 2003. **85**(2-5): p. 357-61.
64. Frungieri, M.B., R.S. Calandra, and S.P. Rossi, *Local Actions of Melatonin in Somatic Cells of the Testis.* Int J Mol Sci, 2017. **18**(6).
65. Abreu, A.P. and U.B. Kaiser, *Pubertal development and regulation.* Lancet Diabetes Endocrinol, 2016. **4**(3): p. 254-64.
66. Fraietta, R., D.S. Zylberstejn, and S.C. Esteves, *Hypogonadotropic hypogonadism revisited.* Clinics (Sao Paulo), 2013. **68 Suppl 1**: p. 81-8.
67. Plant, T.M., *60 YEARS OF NEUROENDOCRINOLOGY: The hypothalamo-pituitary-gonadal axis.* J Endocrinol, 2015. **226**(2): p. T41-54.
68. Constantin, S., *Progress and Challenges in the Search for the Mechanisms of Pulsatile Gonadotropin-Releasing Hormone Secretion.* Front Endocrinol (Lausanne), 2017. **8**: p. 180.
69. Bernard, D.J., et al., *Mechanisms of FSH synthesis: what we know, what we don't, and why you should care.* Fertil Steril, 2010. **93**(8): p. 2465-85.
70. Stephens, S.B.Z. and A.S. Kauffman, *Regulation and Possible Functions of Kisspeptin in the Medial Amygdala.* Front Endocrinol (Lausanne), 2017. **8**: p. 191.
71. Terasawa, E., K.A. Guerriero, and T.M. Plant, *Kisspeptin and puberty in mammals.* Adv Exp Med Biol, 2013. **784**: p. 253-73.
72. Choi, J. and J. Smitz, *Luteinizing hormone and human chorionic gonadotropin: distinguishing unique physiologic roles.* Gynecol Endocrinol, 2014. **30**(3): p. 174-81.
73. O'Hara, L. and L.B. Smith, *Androgen receptor roles in spermatogenesis and infertility.* Best Pract Res Clin Endocrinol Metab, 2015. **29**(4): p. 595-605.
74. Basaria, S., *Male hypogonadism.* Lancet, 2014. **383**(9924): p. 1250-63.
75. Bhasin, S., et al., *Testosterone therapy in men with androgen deficiency syndromes: an Endocrine Society clinical practice guideline.* J Clin Endocrinol Metab, 2010. **95**(6): p. 2536-59.
76. Corona, G., A. Sforza, and M. Maggi, *Testosterone Replacement Therapy: Long-Term Safety and Efficacy.* World J Mens Health, 2017. **35**(2): p. 65-76.

77. Khera, M., et al., *Adult-Onset Hypogonadism.* Mayo Clin Proc, 2016. **91**(7): p. 908-26.
78. Corona, G., et al., *How to recognize late-onset hypogonadism in men with sexual dysfunction.* Asian J Androl, 2012. **14**(2): p. 251-9.
79. Rey, R.A., et al., *Male hypogonadism: an extended classification based on a developmental, endocrine physiology-based approach.* Andrology, 2013. **1**(1): p. 3-16.
80. Wang, C., et al., *Investigation, treatment and monitoring of late-onset hypogonadism in males.* Int J Androl, 2009. **32**(1): p. 1-10.
81. El Osta, R., et al., *Hypogonadotropic hypogonadism in men with hereditary hemochromatosis.* Basic Clin Androl, 2017. **27**: p. 13.
82. Kelly, T.M., et al., *Hypogonadism in hemochromatosis: reversal with iron depletion.* Ann Intern Med, 1984. **101**(5): p. 629-32.
83. Siminoski, K., M. D'Costa, and P.G. Walfish, *Hypogonadotropic hypogonadism in idiopathic hemochromatosis: evidence for combined hypothalamic and pituitary involvement.* J Endocrinol Invest, 1990. **13**(10): p. 849-53.
84. Duranteau, L., et al., *Non-responsiveness of serum gonadotropins and testosterone to pulsatile GnRH in hemochromatosis suggesting a pituitary defect.* Acta Endocrinol (Copenh), 1993. **128**(4): p. 351-4.
85. Siemons, L.J. and C.H. Mahler, *Hypogonadotropic hypogonadism in hemochromatosis: recovery of reproductive function after iron depletion.* J Clin Endocrinol Metab, 1987. **65**(3): p. 585-7.
86. Chatterjee, R. and M. Katz, *Reversible hypogonadotrophic hypogonadism in sexually infantile male thalassaemic patients with transfusional iron overload.* Clin Endocrinol (Oxf), 2000. **53**(1): p. 33-42.
87. Angelopoulos, N.G., et al., *Reversibility of hypogonadotropic hypogonadism in a patient with the juvenile form of hemochromatosis.* Fertil Steril, 2005. **84**(6): p. 1744.
88. Fernandez-Real, J.M., A. Lopez-Bermejo, and W. Ricart, *Cross-talk between iron metabolism and diabetes.* Diabetes, 2002. **51**(8): p. 2348-54.
89. Backe, M.B., et al., *Iron Regulation of Pancreatic Beta-Cell Functions and Oxidative Stress.* Annu Rev Nutr, 2016. **36**: p. 241-73.
90. Fernandez-Real, J.M., D. McClain, and M. Manco, *Mechanisms Linking Glucose Homeostasis and Iron Metabolism Toward the Onset and Progression of Type 2 Diabetes.* Diabetes Care, 2015. **38**(11): p. 2169-76.
91. Wang, X., X. Fang, and F. Wang, *Pleiotropic actions of iron balance in diabetes mellitus.* Rev Endocr Metab Disord, 2015. **16**(1): p. 15-23.
92. Swaminathan, S., et al., *The role of iron in diabetes and its complications.* Diabetes Care, 2007. **30**(7): p. 1926-33.
93. Mehdad, A., et al., *Iron Deprivation May Enhance Insulin Receptor and Glut4 Transcription in Skeletal Muscle of Adult Rats.* J Nutr Health Aging, 2015. **19**(8): p. 846-54.
94. Cooksey, R.C., et al., *Oxidative stress, beta-cell apoptosis, and decreased insulin secretory capacity in mouse models of hemochromatosis.* Endocrinology, 2004. **145**(11): p. 5305-12.
95. Ferri, N. and M. Ruscica, *Proprotein convertase subtilisin/kexin type 9 (PCSK9) and metabolic syndrome: insights on insulin resistance, inflammation, and atherogenic dyslipidemia.* Endocrine, 2016. **54**(3): p. 588-601.
96. Chen, L., et al., *Association of serum ferritin levels with metabolic syndrome and insulin resistance in a Chinese population.* J Diabetes Complications, 2017. **31**(2): p. 364-368.
97. Avila, F., et al., *Serum Ferritin Is Associated with Metabolic Syndrome and Red Meat Consumption.* Oxid Med Cell Longev, 2015. **2015**: p. 769739.
98. Padwal, M.K., et al., *Association of Serum Ferritin Levels with Metabolic Syndrome and Insulin Resistance.* J Clin Diagn Res, 2015. **9**(9): p. BC11-3.
99. Deng, Y. and P.E. Scherer, *Adipokines as novel biomarkers and regulators of the metabolic syndrome.* Ann N Y Acad Sci, 2010. **1212**: p. E1-E19.
100. Ruscica, M., et al., *Translating the biology of adipokines in atherosclerosis and cardiovascular diseases: Gaps and open questions.* Nutr Metab Cardiovasc Dis, 2017. **27**(5): p. 379-395.

101. Zachariah, J.P., et al., *Prospective Relation of Circulating Adipokines to Incident Metabolic Syndrome: The Framingham Heart Study.* J Am Heart Assoc, 2017. **6**(7).
102. Yamamoto, K., et al., *Interplay of adipocyte and hepatocyte: Leptin upregulates hepcidin.* Biochem Biophys Res Commun, 2018. **495**(1): p. 1548-1554.
103. Patel, S.B., et al., *Leptin: linking obesity, the metabolic syndrome, and cardiovascular disease.* Curr Hypertens Rep, 2008. **10**(2): p. 131-7.
104. Tena-Sempere, M., *Interaction between energy homeostasis and reproduction: central effects of leptin and ghrelin on the reproductive axis.* Horm Metab Res, 2013. **45**(13): p. 919-27.
105. Hellstrom, L., et al., *Mechanisms behind gender differences in circulating leptin levels.* J Intern Med, 2000. **247**(4): p. 457-62.
106. Mechanick, J.I., S. Zhao, and W.T. Garvey, *Leptin, An Adipokine With Central Importance in the Global Obesity Problem.* Glob Heart, 2017.
107. Munzberg, H. and C.D. Morrison, *Structure, production and signaling of leptin.* Metabolism, 2015. **64**(1): p. 13-23.
108. Yun, J.E., et al., *Serum leptin is associated with metabolic syndrome in obese and nonobese Korean populations.* Metabolism, 2010. **59**(3): p. 424-9.
109. Lee, S.W., et al., *Association between metabolic syndrome and serum leptin levels in postmenopausal women.* J Obstet Gynaecol, 2012. **32**(1): p. 73-7.
110. Gao, Y., et al., *Adipocyte iron regulates leptin and food intake.* J Clin Invest, 2015. **125**(9): p. 3681-91.
111. Al-Naama, L.M., M.K. Hassan, and M.M. Abdul Karim, *Evaluation of Serum Leptin Levels and Growth in Patients with beta-Thalassaemia Major.* Anemia, 2016. **2016**: p. 8454286.
112. Kimura, Y., et al., *Circulating ferritin concentrations are differentially associated with serum adipokine concentrations in Japanese men and premenopausal women.* Eur J Nutr, 2017. **56**(8): p. 2497-2505.
113. Dongiovanni, P., et al., *Dietary iron overload induces visceral adipose tissue insulin resistance.* Am J Pathol, 2013. **182**(6): p. 2254-63.
114. Park, H.K., et al., *Linking resistin, inflammation, and cardiometabolic diseases.* Korean J Intern Med, 2017. **32**(2): p. 239-247.
115. Rak, A., et al., *Adiponectin and resistin: potential metabolic signals affecting hypothalamo-pituitary gonadal axis in females and males of different species.* Reproduction, 2017. **153**(6): p. R215-R226.
116. Lee, J.H., et al., *Circulating resistin levels are not associated with obesity or insulin resistance in humans and are not regulated by fasting or leptin administration: cross-sectional and interventional studies in normal, insulin-resistant, and diabetic subjects.* J Clin Endocrinol Metab, 2003. **88**(10): p. 4848-56.
117. Park, H.K. and R.S. Ahima, *Resistin in rodents and humans.* Diabetes Metab J, 2013. **37**(6): p. 404-14.
118. Malo, E., et al., *Resistin is an indicator of the metabolic syndrome according to five different definitions in the Finnish Health 2000 survey.* Metab Syndr Relat Disord, 2011. **9**(3): p. 203-10.
119. Anderson, G.J. and D.M. Frazer, *Current understanding of iron homeostasis.* Am J Clin Nutr, 2017.
120. Macchi, C., et al., *Iron overload induces hypogonadism in male mice via extrahypothalamic mechanisms.* Mol Cell Endocrinol, 2017. **454**: p. 135-145.
121. Italia, K., R. Colah, and K. Ghosh, *Experimental animal model to study iron overload and iron chelation and review of other such models.* Blood Cells Mol Dis, 2015. **55**(3): p. 194-9.
122. Bacon, B.R., et al., *Hepatic lipid peroxidation in vivo in rats with chronic iron overload.* J Clin Invest, 1983. **71**(3): p. 429-39.
123. Das, S.K., et al., *Iron-overload injury and cardiomyopathy in acquired and genetic models is attenuated by resveratrol therapy.* Sci Rep, 2015. **5**: p. 18132.
124. Das, S.K., et al., *Resveratrol mediates therapeutic hepatic effects in acquired and genetic murine models of iron-overload.* Liver Int, 2016. **36**(2): p. 246-57.

125. Frydlova, J., et al., *Effect of Erythropoietin, Iron Deficiency and Iron Overload on Liver Matriptase-2 (TMPRSS6) Protein Content in Mice and Rats.* PLoS One, 2016. **11**(2): p. e0148540.
126. Rausa, M., et al., *Bmp6 expression in murine liver non parenchymal cells: a mechanism to control their high iron exporter activity and protect hepatocytes from iron overload?* PLoS One, 2015. **10**(4): p. e0122696.
127. Baum, P., et al., *The role of nerve inflammation and exogenous iron load in experimental peripheral diabetic neuropathy (PDN).* Metabolism, 2016. **65**(4): p. 391-405.
128. Salgado, A.L., et al., *Insulin resistance index (HOMA-IR) in the differentiation of patients with non-alcoholic fatty liver disease and healthy individuals.* Arq Gastroenterol, 2010. **47**(2): p. 165-9.
129. Adachi, S.I., F. Yoshizawa, and K. Yagasaki, *Hyperuricemia in type 2 diabetic model KK-A(y)/Ta mice: a potent animal model with positive correlation between insulin resistance and plasma high uric acid levels.* BMC Res Notes, 2017. **10**(1): p. 577.
130. Zhou, X.Y., et al., *HFE gene knockout produces mouse model of hereditary hemochromatosis.* Proc Natl Acad Sci U S A, 1998. **95**(5): p. 2492-7.
131. Pineda, R., et al., *Characterization of the inhibitory roles of RFRP3, the mammalian ortholog of GnIH, in the control of gonadotropin secretion in the rat: in vivo and in vitro studies.* Am J Physiol Endocrinol Metab, 2010. **299**(1): p. E39-46.
132. Cariboni, A., et al., *Dysfunctional SEMA3E signaling underlies gonadotropin-releasing hormone neuron deficiency in Kallmann syndrome.* J Clin Invest, 2015. **125**(6): p. 2413-28.
133. Pigeon, C., et al., *Carbonyl-iron supplementation induces hepatocyte nuclear changes in BALB/CJ male mice.* J Hepatol, 1999. **30**(5): p. 926-34.
134. Li, J., et al., *Association between serum ferritin levels and risk of the metabolic syndrome in Chinese adults: a population study.* PLoS One, 2013. **8**(9): p. e74168.
135. Ishihara, Y., et al., *Dual role of superoxide dismutase 2 induced in activated microglia: oxidative stress tolerance and convergence of inflammatory responses.* J Biol Chem, 2015. **290**(37): p. 22805-17.
136. Cnop, M., et al., *Endoplasmic reticulum stress and eIF2alpha phosphorylation: The Achilles heel of pancreatic beta cells.* Mol Metab, 2017. **6**(9): p. 1024-1039.
137. Dunys, J., E. Duplan, and F. Checler, *The transcription factor X-box binding protein-1 in neurodegenerative diseases.* Mol Neurodegener, 2014. **9**: p. 35.
138. Giacobini, P., et al., *Hepatocyte growth factor/scatter factor facilitates migration of GN-11 immortalized LHRH neurons.* Endocrinology, 2002. **143**(9): p. 3306-15.
139. Maggi, R., et al., *Immortalized luteinizing hormone-releasing hormone neurons show a different migratory activity in vitro.* Endocrinology, 2000. **141**(6): p. 2105-12.
140. Messner, D.J., B.H. Rhieu, and K.V. Kowdley, *Iron overload causes oxidative stress and impaired insulin signaling in AML-12 hepatocytes.* Dig Dis Sci, 2013. **58**(7): p. 1899-908.
141. Scheiber-Mojdehkar, B., et al., *Differential response of non-transferrin bound iron uptake in rat liver cells on long-term and short-term treatment with iron.* J Hepatol, 1999. **31**(1): p. 61-70.
142. Ruscica, M., et al., *Role of the energy sensor adenosine monophosphate-activated protein kinase in the regulation of immature gonadotropin-releasing hormone neuron migration.* J Endocrinol Invest, 2011. **34**(10): p. e362-8.
143. Tajar, A., et al., *Characteristics of secondary, primary, and compensated hypogonadism in aging men: evidence from the European Male Ageing Study.* J Clin Endocrinol Metab, 2010. **95**(4): p. 1810-8.
144. Bergeron, C. and K. Kovacs, *Pituitary siderosis. A histologic, immunocytologic, and ultrastructural study.* Am J Pathol, 1978. **93**(2): p. 295-309.
145. Hermo, L., et al., *Surfing the wave, cycle, life history, and genes/proteins expressed by testicular germ cells. Part 2: changes in spermatid organelles associated with development of spermatozoa.* Microsc Res Tech, 2010. **73**(4): p. 279-319.
146. Bousfield, G.R. and J.A. Dias, *Synthesis and secretion of gonadotropins including structure-function correlates.* Rev Endocr Metab Disord, 2011. **12**(4): p. 289-302.

147. Piperno, A., et al., *Preclinical hypogonadism in genetic hemochromatosis in the early stage of the disease: evidence of hypothalamic dysfunction.* J Endocrinol Invest, 1992. **15**(6): p. 423-8.
148. McCullough, A., *Alternatives to testosterone replacement: testosterone restoration.* Asian J Androl, 2015. **17**(2): p. 201-5.
149. Patankar, S.S., et al., *Effect of clomiphene citrate on sperm density in male partners of infertile couples.* Indian J Physiol Pharmacol, 2007. **51**(2): p. 195-8.
150. Constantin, S., *Physiology of the gonadotrophin-releasing hormone (GnRH) neurone: studies from embryonic GnRH neurones.* J Neuroendocrinol, 2011. **23**(6): p. 542-53.
151. Fenichel, R.M., et al., *Leptin levels and luteinizing hormone pulsatility in normal cycling women and their relationship to daily changes in metabolic rate.* Fertil Steril, 2008. **90**(4): p. 1161-8.
152. Ewart-Toland, A., et al., *Effect of the genetic background on the reproduction of leptin-deficient obese mice.* Endocrinology, 1999. **140**(2): p. 732-8.
153. Barash, I.A., et al., *Leptin is a metabolic signal to the reproductive system.* Endocrinology, 1996. **137**(7): p. 3144-7.
154. Kyriakou, A. and N. Skordis, *Thalassaemia and aberrations of growth and puberty.* Mediterr J Hematol Infect Dis, 2009. **1**(1): p. e2009003.
155. Manfredi-Lozano, M., J. Roa, and M. Tena-Sempere, *Connecting metabolism and gonadal function: Novel central neuropeptide pathways involved in the metabolic control of puberty and fertility.* Front Neuroendocrinol, 2017.
156. Catzeflis, C., et al., *Neuropeptide Y administered chronically into the lateral ventricle profoundly inhibits both the gonadotropic and the somatotropic axis in intact adult female rats.* Endocrinology, 1993. **132**(1): p. 224-34.
157. Teerds, K.J., D.G. de Rooij, and J. Keijer, *Functional relationship between obesity and male reproduction: from humans to animal models.* Hum Reprod Update, 2011. **17**(5): p. 667-83.
158. Thaler, J.P., et al., *Hypothalamic inflammation and energy homeostasis: resolving the paradox.* Front Neuroendocrinol, 2010. **31**(1): p. 79-84.
159. Maggi, R., et al., *Factors involved in the migration of neuroendocrine hypothalamic neurons.* Arch Ital Biol, 2005. **143**(3-4): p. 171-8.
160. Chen, Y.T., et al., *Iron dysregulates APP processing accompanying with sAPPalpha cellular retention and beta-secretase inhibition in rat cortical neurons.* Acta Pharmacol Sin, 2017.
161. Farmaki, K., et al., *Normalisation of total body iron load with very intensive combined chelation reverses cardiac and endocrine complications of thalassaemia major.* Br J Haematol, 2010. **148**(3): p. 466-75.
162. Poggi, M., et al., *Longitudinal changes of endocrine and bone disease in adults with beta-thalassemia major receiving different iron chelators over 5 years.* Ann Hematol, 2016. **95**(5): p. 757-63.
163. Levi, S. and E. Rovida, *The role of iron in mitochondrial function.* Biochim Biophys Acta, 2009. **1790**(7): p. 629-36.
164. Berdoukas, V., T.D. Coates, and Z.I. Cabantchik, *Iron and oxidative stress in cardiomyopathy in thalassemia.* Free Radic Biol Med, 2015. **88**(Pt A): p. 3-9.
165. Brommage, R., *Validation and calibration of DEXA body composition in mice.* Am J Physiol Endocrinol Metab, 2003. **285**(3): p. E454-9.